Master Thesis

# Sophisticated ESP Sensor Data Analysis and Failure Classification

**Written by:**
Michael Nirtl, BSc
m00927450

**Advisor:**
Univ.-Prof. Dipl.-Ing. Dr.mont. Herbert Hofstätter
Dipl.-Ing. Dr.mont. Rudolf Fruhwirth
Dipl.-Ing. Bernd Kometer

Leoben, 20.09.2017

# EIDESSTATTLICHE ERKLÄRUNG

Ich erkläre an Eides statt, dass ich die vorliegende Diplomarbeit selbständig und ohne fremde Hilfe verfasst, andere als die angegebenen Quellen und Hilfsmittel nicht benutzt und die den benutzten Quellen wörtlich und inhaltlich entnommenen Stellen als solche erkenntlich gemacht habe.

# AFFIDAVIT

I hereby declare that the content of this work is my own composition and has not been submitted previously for any higher degree. All extracts have been distinguished using quoted references and all information sources have been acknowledged.

# Kurzfassung

Das sich entwickelnde digitale Ölfeld eröffnet viele neue Möglichkeiten für neue auf Daten gestützte Methoden zur Pumpenüberwachung. Elektrische Tauchkreiselradpumpen sind mit Untertagesensoren ausgestattet und liefern Daten welche für automatische Fehlererkennung verwendet werden können. Die vorgestellte Methode der automatischen Dateninterpretation mittels neuronaler Netze kann die Pumpenüberwachung erleichtern und ermöglicht effektivere Datenintegration.

In dieser Arbeit wird eine Methode zur Datenanalyse und Fehlerklassifizierung beruhend auf dem Konzept der Heuristik vorgestellt. Dabei werden neuronale Netze verwendet um geeignete Dateninterpretationsmodelle zu entwickeln.

Die extrahierten Datensätze wurden analysiert und gefiltert um verschiedenste Probleme bezüglich Datenkonsistenz während der Messung und des Speicherns in der Datenbank zu beheben. Dabei wurden messbedingte Ausreißer entfernt, Zeitstempel bearbeitet, logische Filter implementiert und ein Filter zur Bearbeitung fehlender Werte angewandt.

Die Untertagedaten wurden mit Obertagedaten kombiniert um Bruttoproduktionsraten während messungsfreier Zeiten zu modellieren. Die Genauigkeit bei der Berechnung dieser Raten mittels neuronaler Netze beträgt 3 - 6 $m^3$/d. Es wurden verschieden manipulierte Daten verwendet um den Effekt des Beobachters der während der Messung der Produktionsraten via Separator auftritt zu eliminieren.

Zur Fehlerklassifizierung wurden neben echten Daten auch mittels Sensordaten künstlich erzeugte Datensätze verwendet. Die Evaluierung der mittels künstlich erzeugter Daten trainierten neuronalen Netze wurde mit echten Daten von Pumpenausfällen durchgeführt. Die verschiedenen Datensätze der Produktionsstätten wurden separat und in Kombination zum Trainieren der neuronalen Netze verwendet um eine Sensitivitätsanalyse durchzuführen und deren Leistung zu vergleichen. Die automatische Fehlerklassifizierung mittels Daten von Tauchkreiselradpumpen ist mit einer Genauigkeit von über 80% möglich. Abschließend wird ein Ausblick für zukünftige Forschungsarbeiten im Bereich der Fehlerklassifizierung und Früherkennung diskutiert.

# Abstract

The evolving digital oilfield offers new possibilities for data based approaches to pump monitoring. Electrical submersible pumps equipped with downhole sensors provide data which can be used for automatic malfunction detection. The proposed method of intelligent interpretation facilitates pump monitoring and integrates data more effectively.

In this thesis, an approach based on data driven model builders was chosen to create neural networks which are capable of classifying ESP conditions and modelling operating parameters.

In order to obtain a clean data set for machine learning, data cleansing including different types of filtering operations was applied. Techniques included: outlier removal, time stamp handling, missing values treatment and plausibility checks.

The downhole sensor data in combination with surface data was used to model gross production rates during measurement gaps with an accuracy of 3 - 6 $m^3$/d. Different ways of data manipulation and data arrangements are presented to overcome difficulties related to the observer effect when using surface separator measurements for production rate determination.

Sensor data was also applied to generate realistic artificial data sets for failure classification. Real life examples of pump failures were then used to evaluate the capability of feed forward neural networks for failure classification. Individual and combinatorial training data sets were investigated to analyze sensitivities. Classification of pump failure with artificial neural networks can be carried out with an accuracy of greater than 80%. To conclude, a brief outlook for future research regarding failure classification and prediction is given.

# List of Tables

# List of Figures

# Abbreviations

| | |
|---|---|
| AI | Artificial intelligence |
| ANN | Artificial neural network |
| CBT | Bottom hole temperature |
| CCP | Completely connected perceptron |
| CCR | Correct classification rate |
| CSP | Casing pressure |
| FF | Feed-forward |
| FRE | Frequency |
| GOR | Gas oil ratio |
| ESP | Electrical submersible pump |
| LWD | Logging while drilling |
| MOC | Motor current |
| MOP | Motor power |
| MWT | Motor winding temperature |
| NN | Neural network |
| PDP | Pump discharge pressure |
| PIP | Pump intake pressure |
| RT | Real time |
| SCADA | Supervisory control and data acquisition |
| SFS | Sequential forward selection |
| SRP | Sucker rod pump |
| TBP | Tubing pressure |
| TH | Torton horizon |
| VIB | Vibration |
| VSD | Variable speed drive |
| WC | Water cut |

# Table of content

**Page**

# 1 Introduction

Electrical submersible pumps (ESP) are commonly used in petroleum industry for artificial lift system applications. Those pumps are typically equipped with various sensors to observe and monitor the pump to ensure proper functionality. An ESP itself consists mainly of a multistage centrifugal pump, a seal-chamber section as well as a driving motor and therefore offers a variety on failure possibilities. This thesis provides an overview about the principles of ESPs as well as their design. Additionally failure mechanisms are covered in detail. Furthermore, sensor data which is acquired downhole in order to analyze and predict the pumps behavior by using artificial intelligence is discussed.

The field, where the investigated pumps are located, is called the Austrian Matzen field. It can be found about 25km northeast of Vienna and is one of the largest onshore oil fields in Europe. The deployed wells are operated by OMV Austria E&P and were mainly implemented during the re-development project of the 16$^{th}$ Torton horizon. The project was started in 2011 with the objective of doubling the gross production rate. Therefore, sucker rod pumps (SRP) were replaced by ESPs after a candidate screening process to increase production and optimize the reservoir potential. Additionally, new wells were drilled horizontally and equipped with ESPs. In total, 46 electrical submersible pumps are contributing to the production of the Matzen field [1]. An increase of about 62% in total oil production was obtained by re-development measures. Currently, 16% of the produced oil in Austria is lifted by ESPs.

Each of the installed pumps is equipped with sensor technology and a variable speed drive (VSD). Measuring certain parameters allows monitoring, optimization and improved control of ESPs. The downhole sensor allows pressure, temperature, vibration and current related metering. Additionally, surface sensors are installed to measure and record casing and tubing pressure as well as frequency. The data is transmitted and fed into the Austrian OMV process control network. The measurements are recorded and stored by the use of software provided by Weatherford. This computer program is called life-of-well information software (LOWIS) and allows also accessing and visualizing data.

The recorded data shall be used to create a model, which analyses the operating mode of the pump to indicate proper functionality or malfunctions. In order to build a reliable model, artificial intelligence (AI) in terms of artificial neural networks (ANN) is used. The objective of the model is to classify the operating mode of the ESPs and allow prediction of upcoming failure or malfunction events. Therefore, the model is built by learning from historical data sets which are including different examples of failure and malfunction. Before the data can be used for machine learning, data cleansing and quality control must be performed to result in a reliable and accurate model.

# 2 Problem Description

At the current situation, the pumps are observed and monitored remotely by using a software tool which accesses a data base continuously fed by the pump sensors. Additionally, measurements on production rates of the wells are taken in the field. The warning system which is currently used to inform the engineer about malfunction is reliable but gives many false alarms due to a simple lower and upper threshold value alarm system. In order to ease and simplify pump monitoring, a new approach for sensor data interpretation will be introduced and tested.

## 2.1 Scope

The scope of this thesis includes model building for pump status classification as well as for pump failure prediction. Therefore, artificial neural networks shall be used to build those models. Since the tasks of the two desired models are different, different model architectures will be used and tested. Additionally, production rate modeling will be conducted since the production rate measurements are performed discontinuously via separator measurements.

The objective of this proof of concept is to build a model which can be used to classify the current operation mode of the pump in order to give an indication on proper functionality or malfunction.

## 2.2 Problem Solution

To solve the previous described tasks of this work, data extraction and acquisition will be done by accessing different available databases. The data sources which are incorporated are subsurface ESP sensor data, surface measurements at the wellhead and separator measurements at metering stations. The obtained data will be checked in order to meet appropriate data quality control (QC) standards. To avoid problems with data leaks, time stamps or measurement errors, data cleansing will be performed by applying different filtering techniques and time series operations. After reviewing the cleaned data in terms of quality assurance (QA), it can be used for training and building models.

For classification and production rate modeling, the data is fed to feed forward neural networks and many different models of different configurations are generated. Those models are evaluated and tested to identify the best one. For computing the models, cVision, a software tool from Neuro Genetic Solutions GmbH is used.

# 3 Literature Review

In this section, an investigation regarding the Austrian Matzen field, recent field development activities as well as pump monitoring and automatization is described in order to point out important background information as well as similar research work.

## 3.1 Austrian Matzen Field

The Austrian Matzen field is a mature oil field, which is situated 25km northeast of Vienna (Figure 1). It is located in the center of the tertiary pull-apart structure in the Vienna Basin. The 16th Torton horizon (TH) is part of this onshore oil field giant and consists mainly out of Badenian aged sandstone, also called Matzen sand. It is the most important reservoir in the Matzen field. With a maximum thickness of 70m, the horizon shows excellent reservoir properties and contains the bulk volumes of hydrocarbons of the Matzen field. Nonconformities which are causing reservoir heterogeneity in terms of vertical flow barriers are thin, fine grained layers in a range of 0.1 to 1m thickness. Those small-scale heterogeneities have a strong impact on field development and well placement and are typically linked to abnormal production behavior [2].

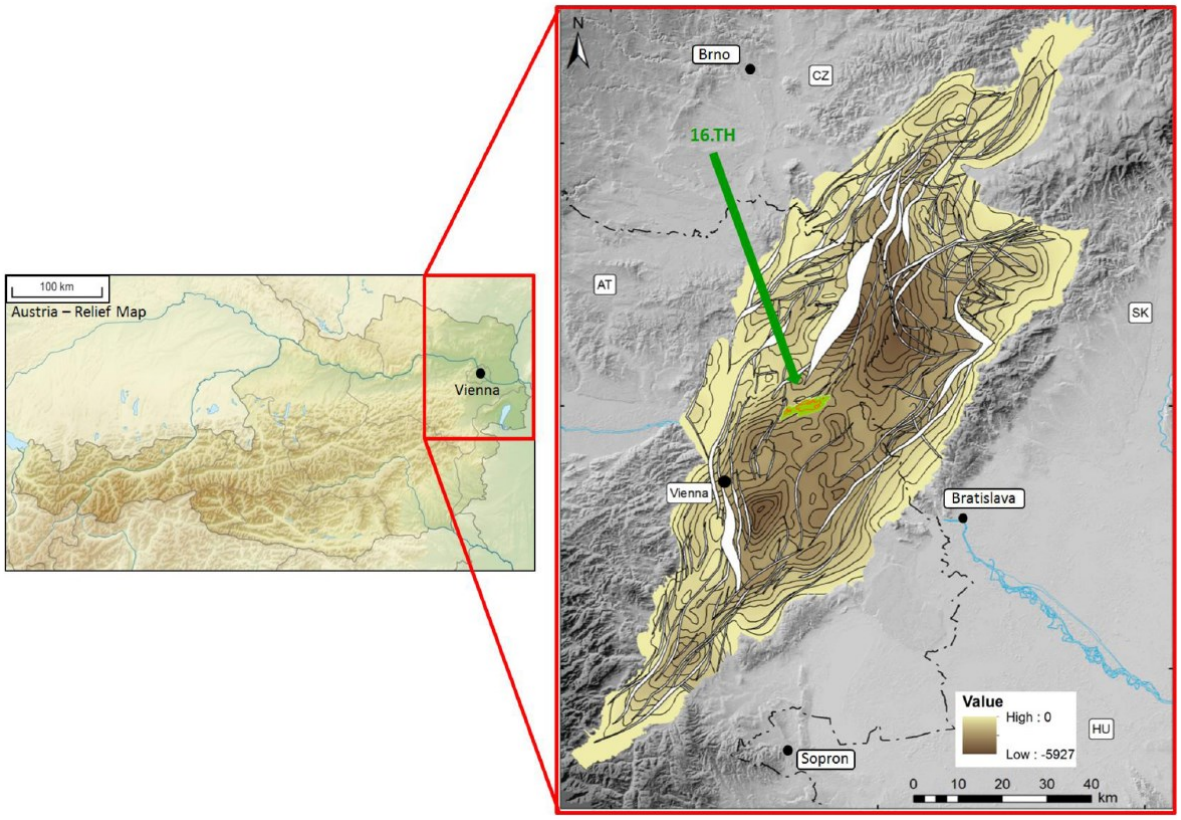


Figure 1 - 16th Torton horizon on the Vienna Basin depth structure map [3], [4]

The Matzen sand was discovered in 1949 and covers an area of about 26km$^2$. The initial gas in place was found to be 17.6 million m$^3$. The oil in place was estimated to be 94.6 million m$^3$ originally. Since a gas cap was already in place, the reservoir conditions were considered saturated. From core analysis an average net porosity of 27% and an average permeability of

1190mD were derived. The boundaries limiting the permeability distribution are 18mD on the lower and 10D on the upper end point. The oil in the field is asphalt based and owns a specific gravity of 0.905 which is corresponding to 24.9°API. The oil water contact (OWC) was determined by electrical measurements and production tests at an average depth of 1490m. The reservoir pressure was calculated via mass balance at a depth of 1490m resulting in 120bar. This reservoir pressure level could be stabilized since 1971. The drive mechanism of the reservoir is mainly governed by water drive and was identified and qualitatively proven in 1957. About 80% of the energy driving the reservoir is contributed from a huge aquifer. The other 20% are shared by gas cap drive and solution gas drive with 10% each [2].

Overall, OMV operates about 1,100 wells in the Gänserndorf area, whereas 438 are accessing the 16$^{th}$ TH. Around 80 of those wells are located in the Bockfliess area, which is from special interest since the data for this thesis is derived from ESP wells and facilities in this area [5].

The cumulative production from the 16$^{th}$ TH is about 283 MM bbl of oil. The peak production of 50,000 barrels per day was reached in 1954. Today the amount of liquid which is produced per day is approximately 85,500 barrels. With a water cut (WC) of about 97% the oil production results in about 2,400 barrels per day. The gas oil ratio (GOR) of 737 scf per barrel indicates rather small amounts of associated gas. The entire production history of the 16$^{th}$ TH is illustrated in Figure 2 below [5].

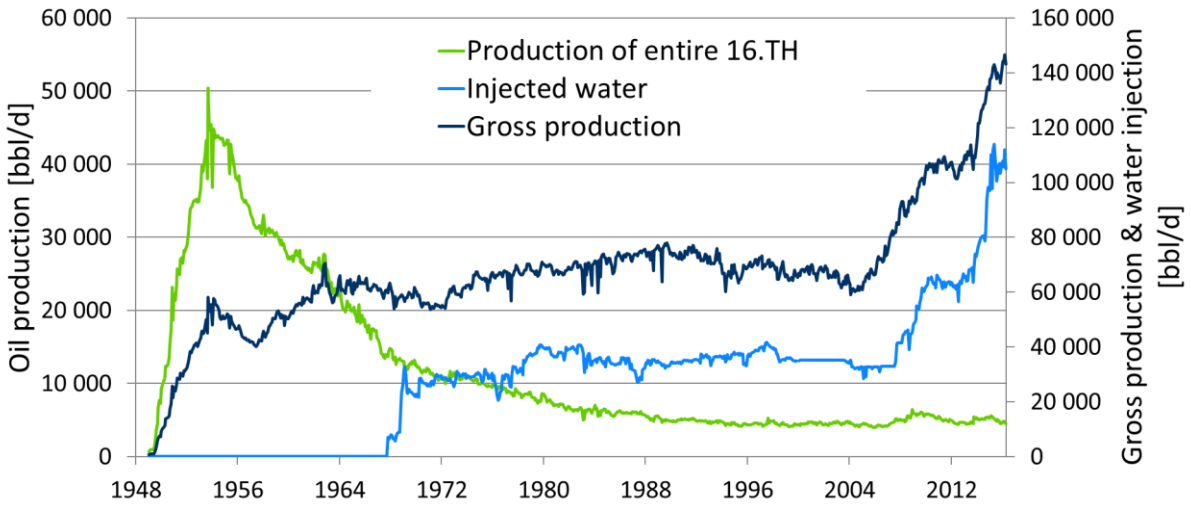


Figure 2 - Production and injection history of the 16$^{th}$ TH [6]

In Figure 2, the start of water injection using a flank water injection strategy can be identified in the end of 1967. The implementation of this pressure maintaining measure reduced the slope of the production decline by the half.

## 3.2 Re-Development of the Matzen Field

In 2011, a campaign with the objective of doubling the gross production in the Matzen field started. The project involved a re-development of the existing measures and infrastructure and was applying the basic concept of water injection to maximize oil displacement. Moreover new wells were drilled in order to achieve improved reservoir penetration. Those wells were drilled horizontally and are placed in the upper as well as lower parts of the reservoir. In terms of subsurface operations, several additional perforations were added. Drilling and perforating was done in order to allow production of the so called attic oil. Furthermore, pump units were exchanged to increase production rates using high-rate artificial lift systems. The injection strategy was adjusted to sweep as much oil as possible from the reservoir [5].

### 3.2.1 Measures & Production Increase

After the planning phase, the first actions were about quick wins in production realized with additional perforations and bean-ups. Therefore, 19 SRPs were upgraded by exchanging beam pumping units, equipped with more powerful electric motors and switched to higher pumping speeds. Additionally, 13 wells were perforated in higher intervals to gain additional reservoir access and also to identify sweet spots for planned horizontal wells of the project.

In order to achieve the declared goal of doubling the gross production rate, a high-rate artificial lift system had to be designed and tested. For this reason, ESPs were installed in two pilot wells and evaluated whether the high production rates with accompanying effects such as possible sand production and lower dynamic liquid levels are feasible or not. The experiment was successful and the lessons learnt were used as valuable input for completion design and material selection. Run-life optimization of the pumps was from main interest concerning the design specifications. As a result, ESP strings were installed consisting of a compression pump, intake gas separator, two protectors, a motor and a sensor. Additionally, the pumps were upgraded with tungsten carbide bearings and the carbon steel housing was coated with Monel to enhance corrosion resistance of the material.

For SRP to ESP conversion, a life cycle cost analysis was conducted to get an idea about the optimum artificial lift system for usage. The result of the investigation was that at a production rate of about 1500 bbl/d, the total cost of ownership is lower when using an ESP instead of a SRP. Taking into account the newly won knowledge as well as certain reservoir and production parameters, candidates were selected and sensor equipped ESPs were installed. The measured sensor data is transmitted via the ESP cable to the surface and then fed into the process control system.

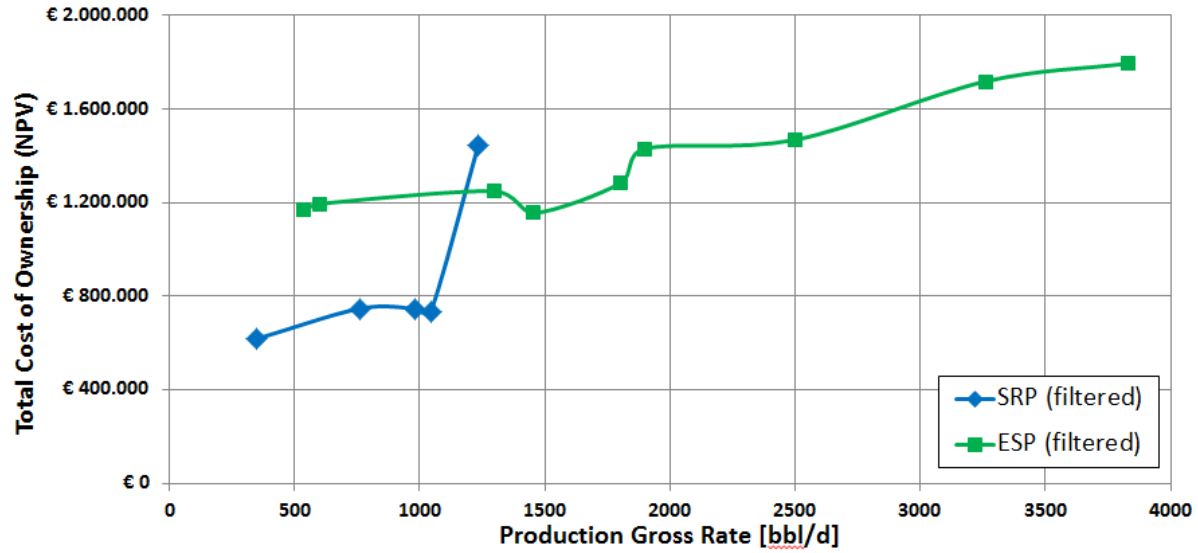


Figure 3 - Life cycle cost analysis of ESP and SRP systems [6]

As part of the re-development project 5 new wells were drilled horizontally. Three of those 5 wells were planned as producer and two as injector wells. The well placement was chosen in a way that more attic oil is accessed to increase recovery. During the drilling operations, real time (RT) logging while drilling (LWD) measurements were required to update the geological model built by offset well data and also to support potential well placement decisions. For drilling the wells, a geo-steering system was used to avoid permeability degradation as well as early water production. Therefore, a target corridor was defined in a range of 0.5 to 3 m TVD below the top of the sandstone. In Figure 4, a geological cross section along planned and drilled trajectories is shown.

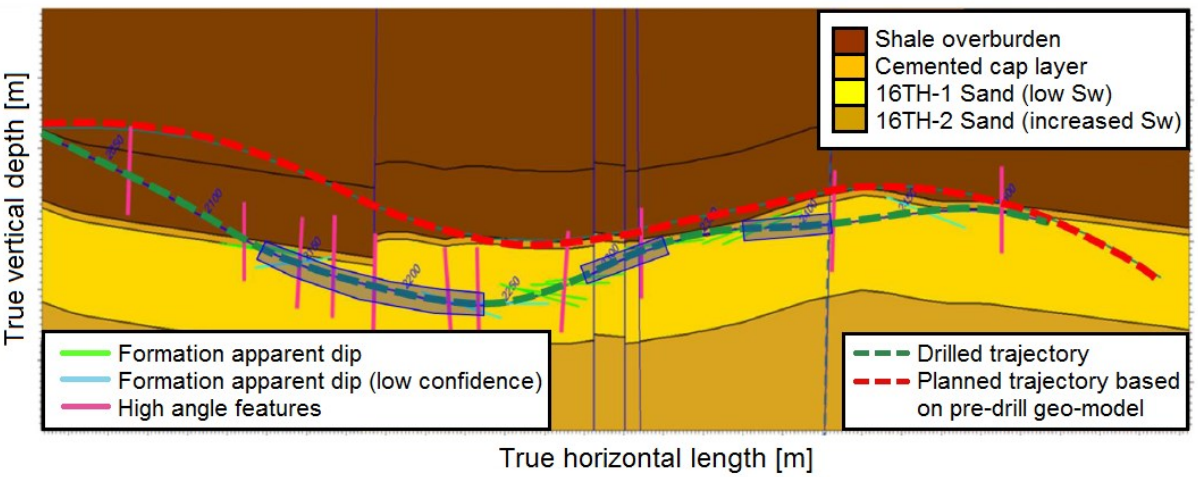


Figure 4 - Geological cross section along a planned and drilled well trajectory [5]

To allow optimal production via ESP systems, a completion design consisting of a 9 5/8'' production casing and a 7'' liner was selected. The large diameter was chosen to enable the placement of a high performance ESPs and to fulfill the requirements for the expected high production rates. For an optimal operation in terms of increased run life, a 100 m MD long

straight section was required within the build section, where the ESP was planned to be placed. The straight section is necessary to keep bending stresses in the equipment low and thus decrease chances for pump failure. The horizontal penetrated reservoir sections were about 400 to 500 m MD long and only partially kept open for production to avoid producing from unfavorable reservoir parts. Moreover, autonomous inflow control devices (AICD) were implemented in the completion design of the production string for improved sweep efficiency. Those devices are sensitive to fluid viscosity and impose an additional pressure drop to highly watered-out zones [5].

The highly increased production profile of the reservoir required additional pressure maintaining measures. Before the re-development project six injection wells were used to support the aquifer in maintaining the reservoir pressure. Due to the production increase a new injection strategy had to be developed. After evaluation of several possibilities, a compromise between drilling new injector wells and converting old producer wells was found. Two horizontal injector wells were drilled at the southern flank and nine production wells were converted for injection purposes. All of the new converted injector wells are located at the northern and northwestern flanks of the Bockfliess area. Additionally, a high quality water treatment plant for the injection water was implemented in order to avoid formation damage or fracturing. The treatment facilities, also called gas-oil-separation plant is located downstream of the separator stations and consists out of a slug catcher, separators, hydro-cyclones and oil tanks for separated residual oil [5].

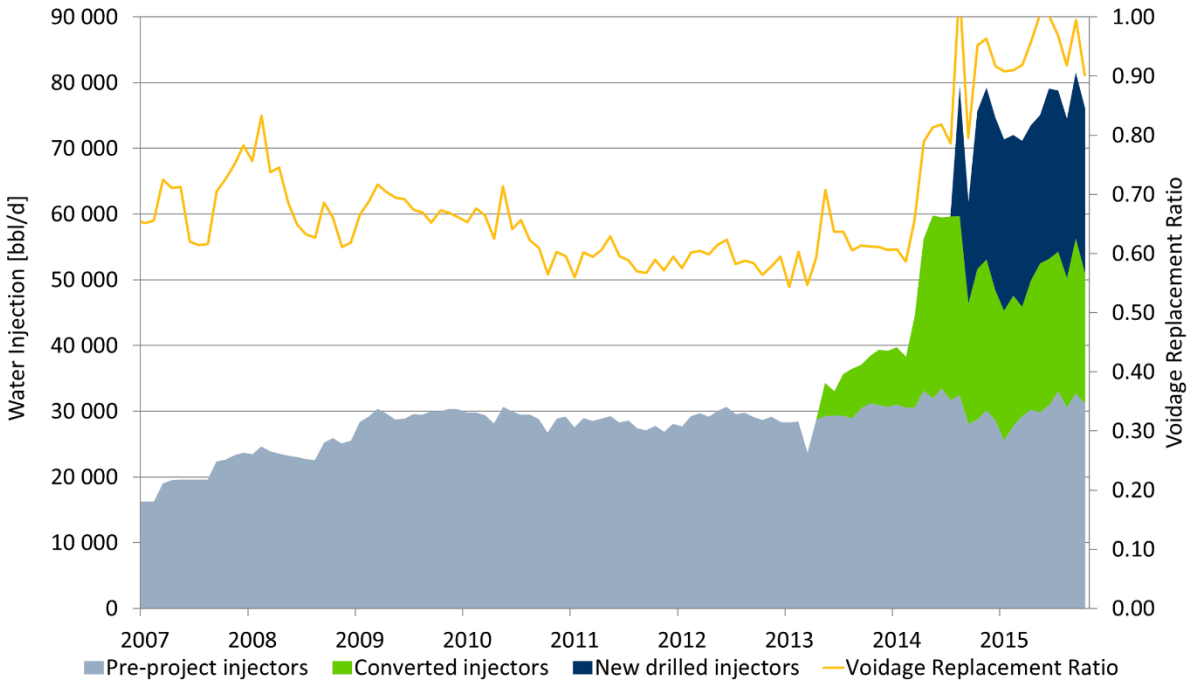


Figure 5 - Injection profile of the 16th TH [5]

In Figure 5, the injection profile and the contributions of old and new measures over the last years is illustrated. Next to the significant amount of injection volume by new drilled horizontal

injectors, it can be seen, that the voidage replacement ratio (VRR) is increased from 0.6 to about 1. The obtained ratio is necessary to maintain the reservoir pressure at the current level [5].

### 3.2.2 Outcome

By the end of 2016, 32 ESPs were deployed by replacing already existing sucker rod pumping units. Additionally, the three new drilled horizontal wells were equipped with ESPs. The results of the project can be seen in Figure 6 below.

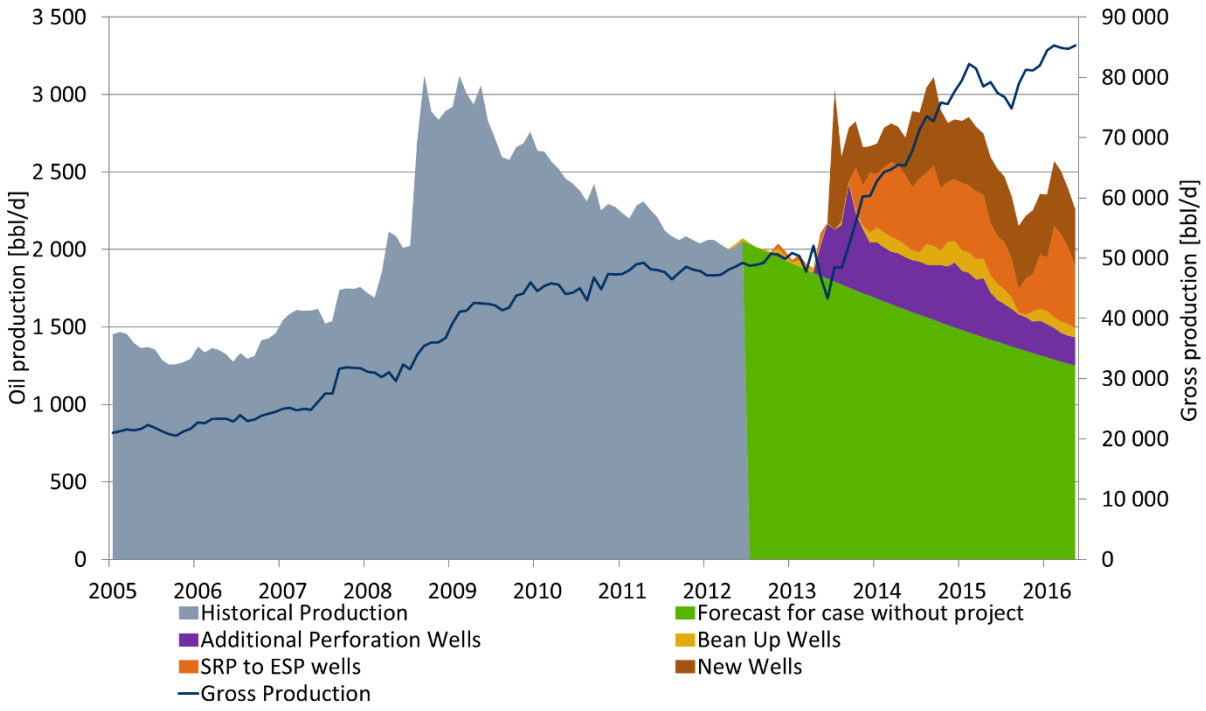


Figure 6 - Production profile of the 16th TH [5]

The undertaken actions during the re-development project of the 16th Torton horizon resulted in a significant incremental oil production. The major contribution to the production increase is coming from converted wells as wells as from the three high-rate ESP wells. At the end of 2015, a steep decline in oil production can be seen. This decline is resulting from postponed activities due to investment constraints after the oil price crash in 2015 [5].

During the campaign, 32 SRP wells were converted to ESP wells and three new wells were drilled for ESP installations. The gain in oil production of 62% is composed of 43% from converted wells and 19% from new wells. Currently, there are 46 ESPs operated, producing around 17% of the total oil production. The majority of the oil is still produced via conventional SRPs [5].

## 3.3 Monitoring & Diagnosis of ESPs

In order to achieve efficient run time and operations of ESPs, potential problems need to be detected early and remedied immediately. Therefore, pump monitoring and sensor data analysis is crucial and a powerful contributor for maintaining optimum production and extending pump life of downhole installations. Moreover, it is very important that by extending the pump life, repair costs as well as production losses due to downtime are reduced. Today it is very common for upstream operating companies to deploy web-based monitoring platforms for real time sensor data surveillance. The data therefore is gathered from various sources and combined to build models, which are able to identify abnormal pump behavior and other types of failure in the production system [7].

Typical failures which can occur are discussed by *Gupta et al. (2016)* and are presented below. For this thesis, especially the orange colored text is from interest.

**Mechanical failure**

- Leaking
- Failed pressure test
- Stuck
- Burst
- Bent
- Broken
- Disconnected

**Material related failure**

- Burn
- Corroded
- Worn
- Melted
- Overheated

**Electrical failure**

- Short circuit
- Open circuit
- Faulty power

**Other**

- Plugged with solids
- Contaminated fluid

The causes, which are leading to failure according to *Gupta et al. (2016)*, can be classified into six categories. For this thesis, especially the orange colored text is from interest.

**Design related**

- Equipment capacity
- Material selection
- System configuration

**Fabrication**

- Manufacturing problem
- Improper QC

**Storage/Transport**

- Improper storage
- Improper transportation

**Installation**

- Assembly procedure
- Installation procedure

**Operational**

- Normal wear and tear
- Inadequate training

**Reservoir**

- Reservoir fluids
- Reservoir performance

Since many failure possibilities are offered within the category of mechanical failure, it is very important to minimize incidents related to it. In previous studies it is revealed, that excessive trips (condition which makes the motor controller to shut down the pump) and pump shutdowns can have strong influence on the run life of an ESP. Therefore, it is very important to distinguish between real failure events and false alarms triggered during operations [8].

During the last decades, more and more data has been gathered in the E&P industry. The traditional approach of using static data (structural and lithological maps, well trajectories, logs, seismic data, production history, etc.), which is measured infrequently with low quality and lacks of integration, is very likely leading to high uncertainty in the decision process. Nowadays, it is very common to gather data from various sources in real time allowing the incorporation of dynamic behavior. This new trend in data collection enables data scientists and engineers to use complex analytics and models to extract more meaningful information and ease decision making with regards to further actions and problem solving [7].

In the following subchapters, different approaches and models for failure classification and prediction are presented and discussed. This literature review shall provide an insight of similar research work.

### 3.3.1 Principal Component Analysis for Failure Prediction

The model introduced by *Gupta et al. (2016)* is using principal component analysis (PCA), a statistical method which is used for dimensionality reduction. This linear dimensionality reduction technique allows extraction of important features while removing correlated variables and revealing strong patterns.

The PCA model which is used in their approach was introduced by *Eriksson, Byrne et al. (2013)*:

$$X = TP^T + E \qquad (1)$$

| | | |
|---|---|---|
| Where | X | Input matrix |
| | T | Scores matrix |
| | P | Loading matrix |
| | E | Residual matrix |

PCA is a purely data driven method which is employing multivariate statistics to find representative data in reduced dimensional space. By applying this technique, the first principal component captures the highest possible variance, while any additional component is orthogonal to its preceding components and captures the next highest possible variance. The covariance between a pair of principal components is zero. This ensures that all dependencies within the selected variables are gone and only the uncorrelated variables that best explain variance in the data are kept [7].

Additionally, the Hotelling T-square statistic was used to introduce a measure representing the collective variation of all variables at each time step. The Hotelling T square statistic is described by the following equation (*Westerhuis, Gurden et al. in 2000*):

$$Hotelling\ T_i = t_i \lambda^{-1} t_i^T \qquad (2)$$

Where $t_i$ Timestamp of T

$\lambda^{-1}$ Inverse of the covariance matrix of T

For training the PCA model, a training data set was created from historical data. For this set, only data from stable operation times was included. The training data was normalized and configured before it was fed into the PCA model as input. The number of principal components was chosen in a way that the proportion of variance captured by the remaining principal components is insignificant. As it can be seen it Figure 7 below, six principal components were able to capture more than 96% of variance in the data and thus considered as sufficient. The result was obtained in the form of the corresponding T, P and E matrices as well as the $T_{stable}$ matrix and Hotelling $T_{stable}$ square for the stable operations. The latter ones were stored for comparison [7].

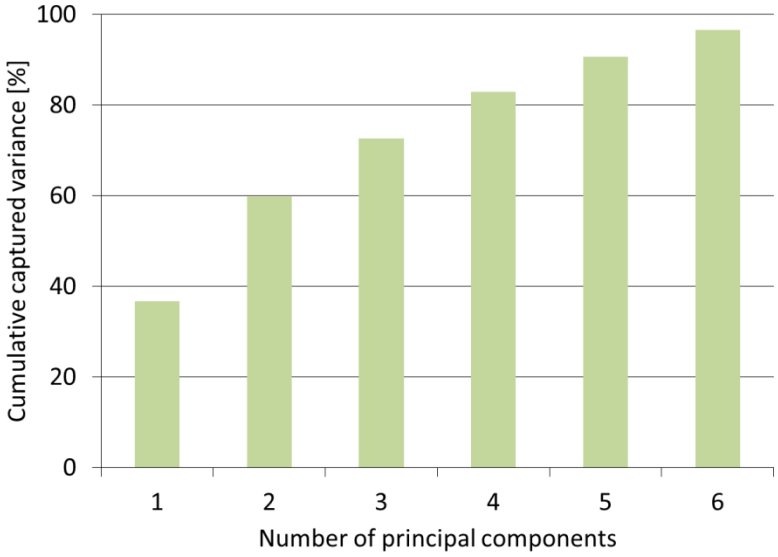


Figure 7 - Cumulative captured variance over number of principal components [7]

As the next step, the derived model in terms of matrices was tested and used for prediction. Different data sets which are representing unstable operation corresponding to a later pump trip or failure were used as testing data. The obtained $T_{unstable}$ and Hotelling $T_{unstable}$ square were used for comparison. Furthermore, ESP health maintenance key performance indicators (KPIs) were introduced to describe normal and abnormal behavior. The two presented KPIs are based on Scores of principal components and on the Hotelling T square statistic. Both indicators can be used to identify abnormal behavior which is going to give a trip or failure with a high likelihood in the future [7].

In Figure 8, a scatter plot of principal component 1 and 2 is illustrated. In green, the stable operation conditions are indicated. The unstable operation points are colored in blue. It can be seen, that for stable operations, all points are located close to zero, while for unstable operation the points can be found scattered in another region of the plot.

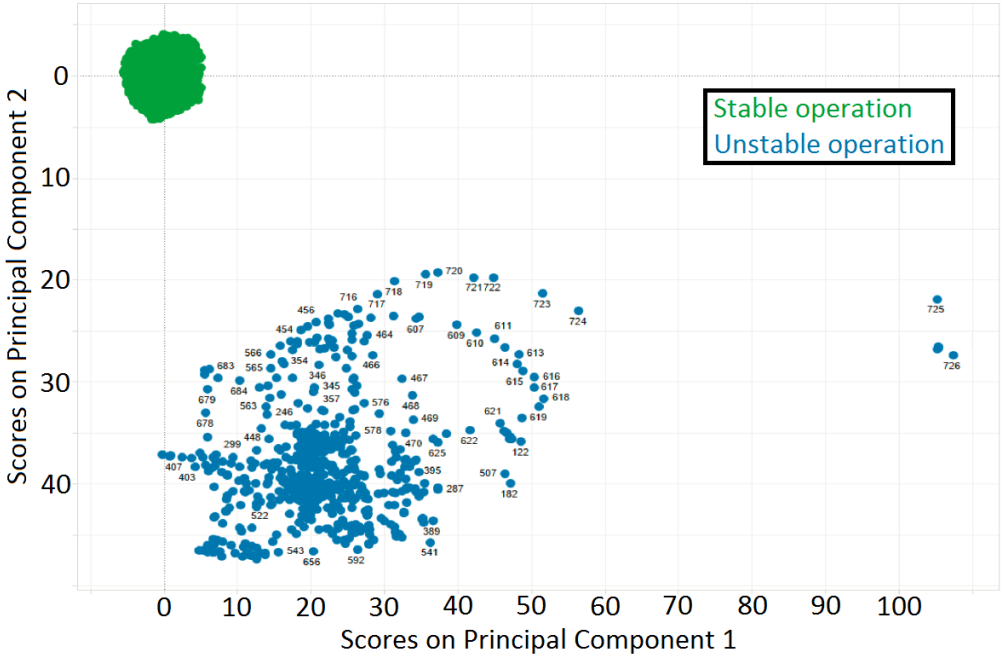


Figure 8 - Scatter plot of principal components [7]

Additionally, a prescriptive model has been built. Based on model diagnostics and prescriptive analytics the appropriate measures and actions are identified and given as recommendation for action. In case of an alarm due to an abnormal pump behavior, the system allows the engineer in charge to act immediately by getting information about which adjustable parameter to trigger to restore proper pump conditions. In Figure 9, the workflow of the presented approach is illustrated [7].

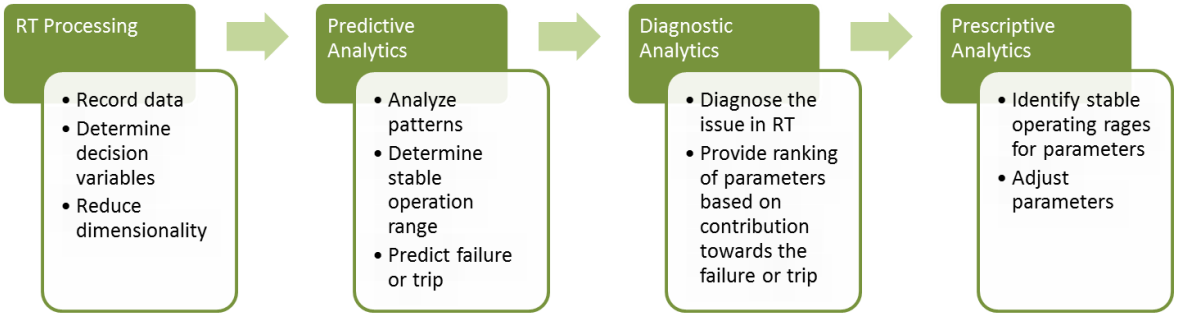


Figure 9 - ESP analytics workflow [7]

### Conclusion

The approach which is introduced by *Gupta et al. (2016)* is showing a data driven analytical solution derived from a database with failure and trip events. The obtained model can be reliably used for failure or trip prediction and additionally gives recommendations in terms of parameter selection for corrective adjustments. It can be integrated into supervisory control and data acquisition (SCADA) systems for RT analysis resulting in minimization of downtime and possible losses of production.

## 3.3.2 Advanced ESP Ammeter Card Analysis

In ESP monitoring, ammeter cards obtained from current measurements are a fast troubleshooting method for engineers. The interpretation of such cards requires a certain level of experience to be able to draw the correct conclusions. This requirement makes it difficult to allow consistent results with this approach, since each engineer brings her or his personal contribution. For illustrative purpose, different types of ammeter card measurements are shown in Figure 10 below.

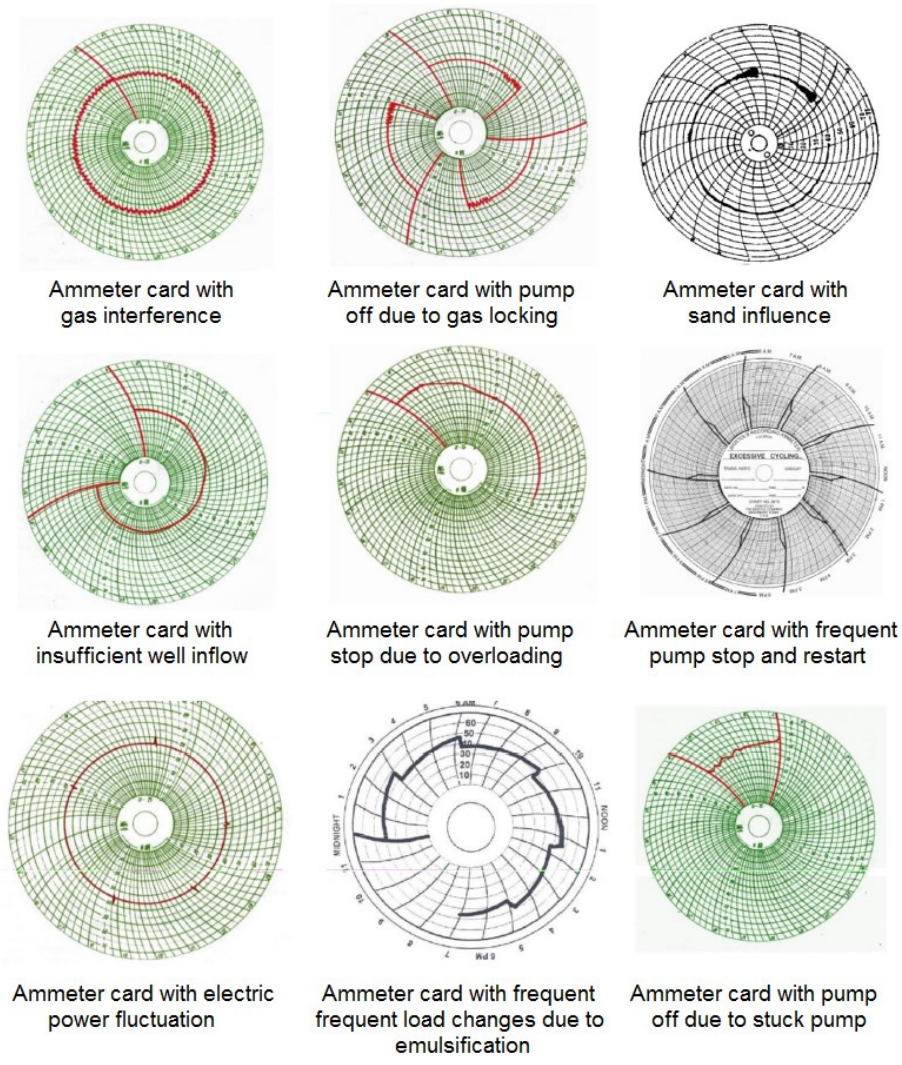


Figure 10 - Ammeter card examples [9]

In a study carried out by *Han et al. (2015)*, 10 different working modes were investigated for classification. The different modes were shown below:

- Frequent stop and restart
- Sand influence
- Pump off by gas locking
- Pump off by stuck pump
- Insufficient reservoir inflow
- Emulsification
- Electric power fluctuation
- Gas interference
- Pump off by overloading
- Normal operation

For this classification or interpretation task, a feed forward neural network with error back propagation was chosen. This machine learning tool allows automation of card interpretation based on a heuristic model approach. The input consisted out of 45 different features, which were hand-crafted such as number of pump stops or number of current fluctuations. The architecture of the net was built by 45 neurons in the input layer, 45 neurons in the hidden layer and 10 neurons in the output layer, since the output units in the last layer are corresponding to the operation modes. In Figure 11 below, the network and its main components are illustrated [9].

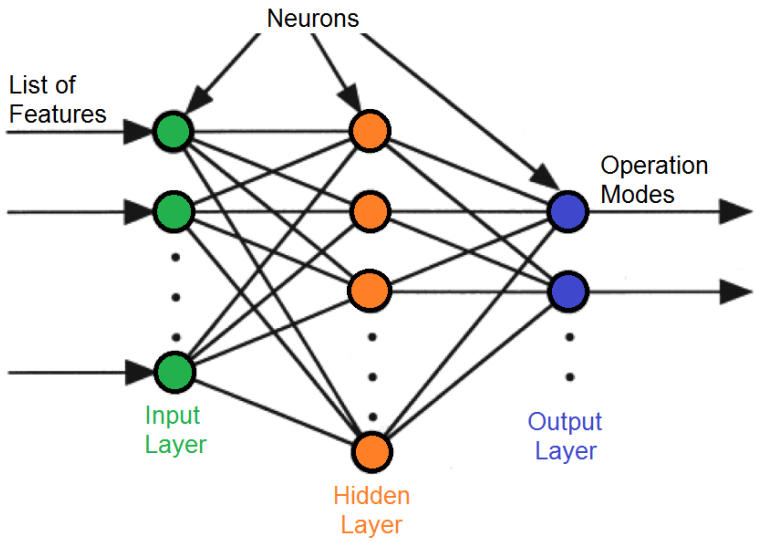


Figure 11 - Feed forward neural network

To train the network appropriately, many different cards were analyzed and features were extracted. In order to cover all ten named operation modes, a certain number of training examples was required. Therefore, ammeter cards were generated via simulation to ensure that all different categories are captured in the training data set. For each operation mode, about 50 different feature sets from ammeter cards were used [9].

A more detailed description of neural networks and their working principle is given in Chapter 5 (Introduction to Artificial Neural Networks).

After training, the derived model was tested against a data set from an offshore well, were constant current measurements together with a sharp decline in production were observed. According to *Han et al. (2015)*, the test failed, since the model was not able to classify the status appropriately. It has to be mentioned, that there is no similar case mentioned to be used during training, which makes a positive classification by the derived model nearly impossible, since a neural network is a data driven tool based on historical data.

### Analytical Model

In order to support the previously described model, *Han et al. (2015)* derived an analytical model based on pressure build up data. The supportive model aims to detect different types of malfunction or problems such as gas interference, equipment leakage downstream of the pump, emulsification or viscosity changes, pump wear or shaft break. The proposed model is using wellhead pressure data from surface sensors [9].

In Figure 12 below, a pressure build up curve for a well shut-in procedure is illustrated. Figure A, is showing the well before it is put on production. In Figure B, a constant production rate is indicated and the liquid level is reduced before the well is shut in (Figure C). In Figure D, equilibrium is reached, which means that the wellhead pressure reaches a static level.

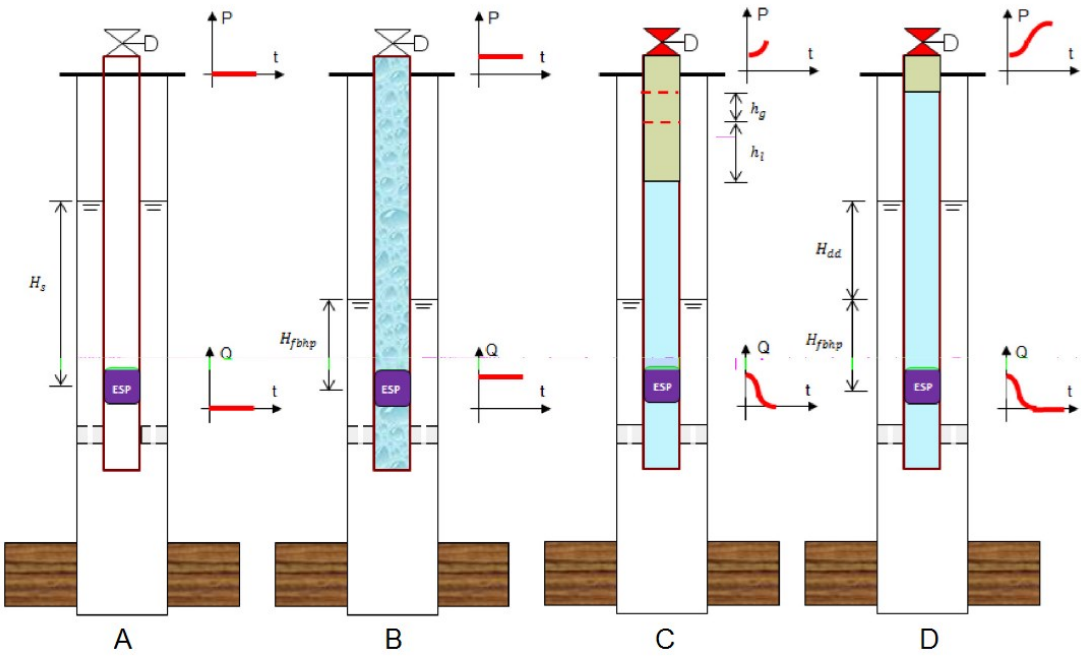


Figure 12 - Pressure build up schematics [9]

The model uses the measured data to compute certain decision variables which are fed to a decision tree. These variables are calculated via an analytical approach. For the computation, the measured time period is split up into two halves. This step is necessary to differentiate between different pressure build up gradients during the shut-in operation. As a result, the model identifies the reason for malfunction without giving a further ranking of other possible failing mechanisms [9].

The analytical model was evaluated and tested for a case where tubing leakage occurs and it manages to give the correct source of malfunction. For further investigations it would be interesting to have broader testing activities to identify limitations and weaknesses of the model.

### Conclusion

The proposed models by *Han et al. (2015)* are using different approaches, which allows smart combination of both to support each other. The neural network based model lacks in testing documentation which doesn't allow further profound evaluation of the performance. Furthermore, the given testing result is misleading and not representative considering the training data which was used to build this model. For further research, an investigation on ammeter cards with deep learning algorithms and image processing would be of high interest, since similar analyses have been done using dynamometer cards of sucker rod pumping units. On the other hand, pressure build up analysis seems to be a valuable tool and indicator to identify malfunction in production technology. It is easy to implement but needs a shut in period in order to obtain the pressure build up curve, which implies a production loss in that time frame.

# 4 Electrical Submersible Pump

The electrical submersible pump as an artificial lift system was invented around 1910. Armais Arutunoff started doing experiments with ESPs in the Baku oilfields near the Caspian sea. Due to his pioneering work in this field of production technology, Arutunoff received about 90 patents related to submersible equipment. Today, around 10% of the world's total crude oil production is lifted via ESP units. Since its invention, those pumping units were improved and developed in order to handle more difficult production conditions such as higher gas liquid ratios, changing liquid production rates or viscous crudes. In recent years, the application of monitoring systems became more and more established and is today a state of the art technology for enhancing lifetime of such downhole equipment. The main applications today are onshore production and injection operations as well as offshore production activities. ESP units are used in cases where electricity is easily available and large amounts of liquids need to be lifted [10].

In the following subchapters, the principles and basic theory as well as the main components of ESPs are explained and discussed.

## 4.1 General

An electrical submersible pump is a downhole used equipment and belongs to the group of impeller or centrifugal pumps. The two most important parts, considering the working principle, are the rotating impellers and the stationary diffusers. Both together are called a stage. When the fluid enters a stage through the impeller eye, it is radially accelerated by centrifugal forces by the rotational movement of the impeller. This process is adding kinetic energy to the production fluid. Next, the fluid is led into the diffuser where it is diffused and the previously gained velocity is converted to pressure. Thereby, kinetic energy is transformed to potential energy according to Bernoulli's principle. An ESP typically consists out of multiple stages, which are arranged serially in order to reach required discharge pressure conditions and pump fluid to the surface.

Other important parts of the ESP are the electric driving motor, the sealing chamber or protector as well as several other smaller components. Additionally to the downhole deployed equipment, surface equipment such as transformers or variable speed drives is necessary to control and monitor ESP production operations. The different components and their specific function are explained in Chapter 4.2 (ESP System Components).

An ESP system is a high rate artificial lift setup. A comparison of similar producing systems is illustrated in Figure 13. The operational range for an ESP can be found between 1,000 bpd for very deep applications and 30,000 bpd for shallower operations. The length of ESP production strings is limited to around 110ft to ensure proper assembly, handling and installation [10].

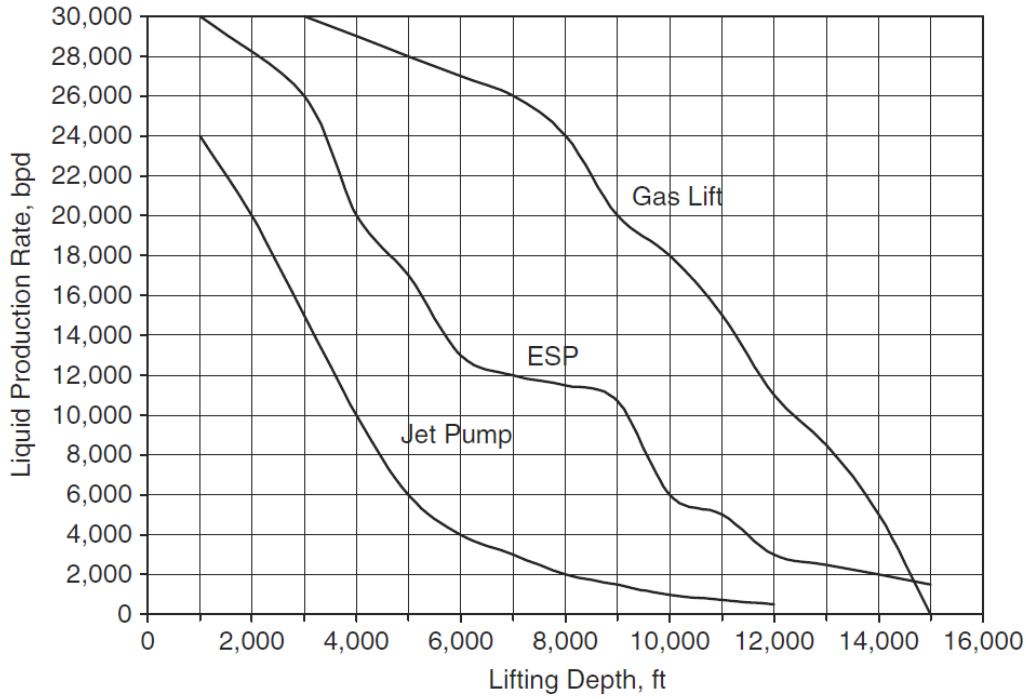


Figure 13 - Comparison of different artificial lift systems [10]

The advantages, disadvantages and limitations of electrical submersible pumps are listed below [10]:

- Wide range of production (100 – 64,000 bpd)
- Operating depth of up to 15,000 ft
- Relatively high energy efficiency at production rates above 1,000 bpd
- Deployment in deviated wells possible
- Low maintenance required
- Small surface footprint (offshore operations)
- Electric power supply must be available and reliable
- Variable speed drive for adapting production rates (additional investment)
- Usage of gas handling devices is required in case of more than 5% of free gas at the pump intake
- Sensitive to wear due sand or other abrasive materials
- Limited temperature ranges for operation (maximum of 120 – 200 °C)
- Problematic for viscous crudes

### 4.1.1 Pump Performance Curves

In this chapter, pump performance curves are discussed. Those curves are typically used to describe the behavior of a pump at different pumping conditions. In general, there are three different types: Head, efficiency and brake horsepower. Since the density of the fluid is increasing when the pressure is increasing, the property head can be calculated by dividing the pressure through the density. This ratio is a constant for a given pumping rate and is usually

used to present performance of a pump, because it is constant for any liquid. It is important to mention here, that only head and efficiency are not influenced by the fluid's density. However, horsepower is changing for fluids with different densities.

In Figure 14, a plot of pump performance curves is illustrated. It can be seen, that the delivered pressure or head is decreasing with increasing flow rates. Moreover, the pump is showing a range of optimum efficiency. Normal ESP operations are designed in a way, which allows the pump to be operated within this range.

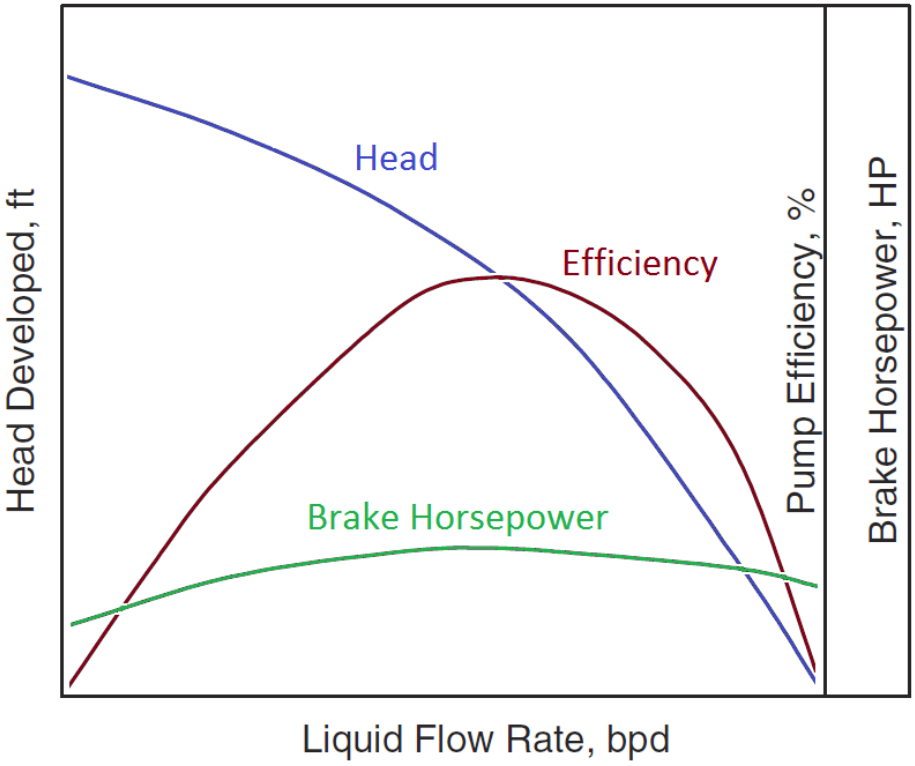


Figure 14 - Pump performance curves [10]

The brake horsepower curve is describing the necessary amount of horsepower to pump fluid at different flow rates. It is the power which is required to drive the pump and has to be delivered by the driving motor. Brake horsepower includes several types of losses which occur in the system. An illustration of those is given in Figure 15. Comparing the different types of losses, especially the friction losses are very interesting since their contribution is depending on the flow rate. The other losses such as bearing losses, disk friction losses and leakage losses are more or less constant or only slightly changing. The turbulence losses are shaping the hydraulic power curve in a way that it looks similar to the efficiency curve. The range where no turbulence losses are occurring is the overlapping with the range of optimal operation [10].

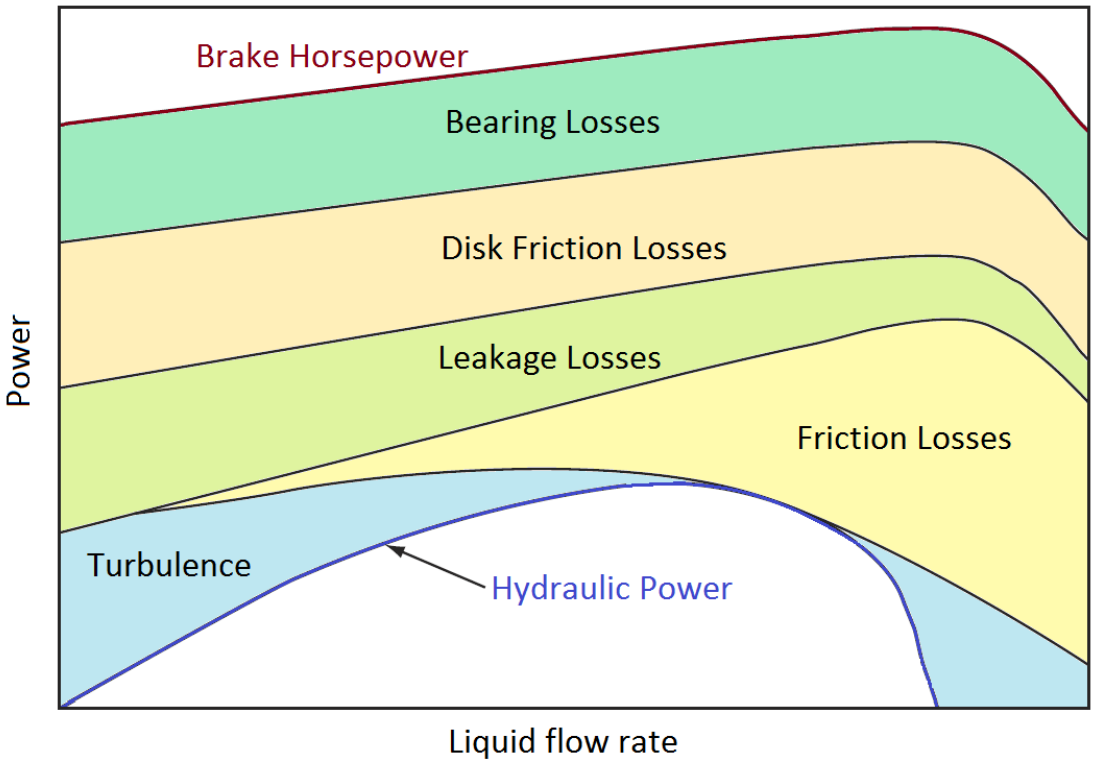


Figure 15 - Power losses in a centrifugal pump stage [10]

### 4.1.2 Affinity Laws

The pump affinity laws are used to demonstrate the relationship between variables in pump performance. They are useful, since centrifugal pumps are very often operated at constant speed because no frequency converters are available. However, the pump performance parameters have been investigated a long time and certain rules, the so-called affinity laws, were found. Below, the three different relationships were presented [10]:

$$Q_2 = Q_1 * \frac{N_2}{N_1} \quad (3)$$

$$H_2 = H_1 * (\frac{N_2}{N_1})^2 \quad (4)$$

$$HP_2 = HP_1 * (\frac{N_2}{N_1})^3 \quad (5)$$

Where
- $N_i$ Pumping speeds [RPM]
- $Q_i$ Pumping rates at $N_i$ [bpd]
- $HP_i$ Required brake horsepower at $N_i$ [hp]

Equation 3, 4 and 5 are showing proportional behavior towards a change in speed. The higher the speed, the higher is the performance parameter. The different laws only differ in the exponent of the speed ratio, which is two for the head-speed relation and three for the

horsepower-speed relation. The fourth rule of the affinity laws is stating that the efficiency of a pump is not changing with speed changes. However, this statement is often not true and can cause some experimental error.

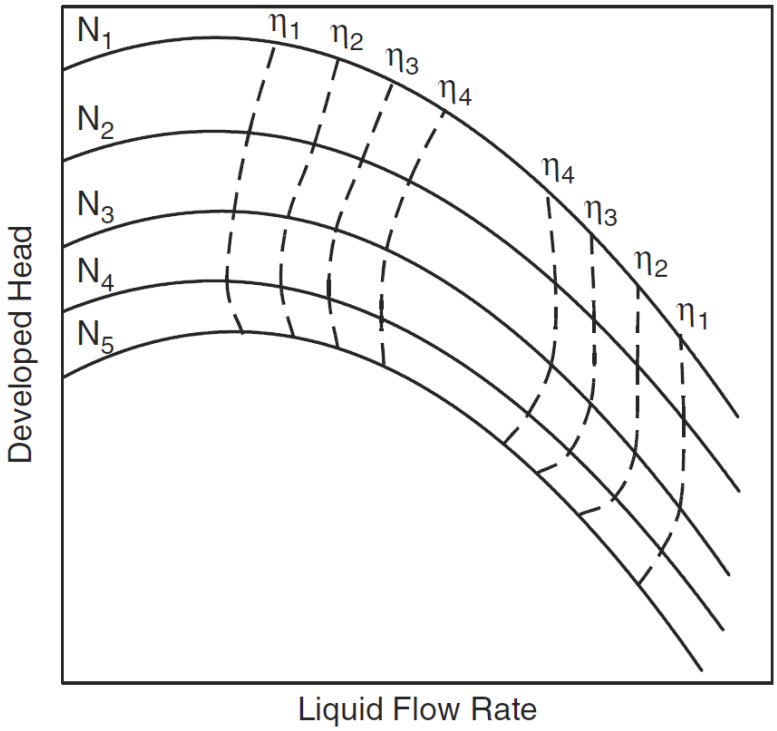


Figure 16 - Pump curves at different speeds [10]

In Figure 16, different pump curves at different pumping speeds are illustrated. The pumping speeds are increasing from $N_5$ to $N_1$. The efficiency ($\eta$) isolines are showing the path of constant efficiencies across different pump curves or pumping speeds. With increasing speed, the efficiency range grows and shifts the optimum range to higher flow rates. Nevertheless, the system represented by the system curve is determining where the operation point is located [10].

## 4.2 ESP System Components

An ESP System is a complex equipment consisting out of multiple different components. In Figure 17, an overview of a complete electrical submersible pump system is illustrated. The main parts of such a system are the centrifugal pump, the protector and the electric motor. The motor is supplied with three-phase AC current from the surface via a special cable, which is mounted on the tubing string. At the surface, different electrical equipment processes electricity to ensure that appropriate voltage and current are provided to the driving motor. In modern systems, a sensor unit is located at the bottom of the production string to allow continuous pump parameter monitoring and gives additional information for troubleshooting in case of malfunction.

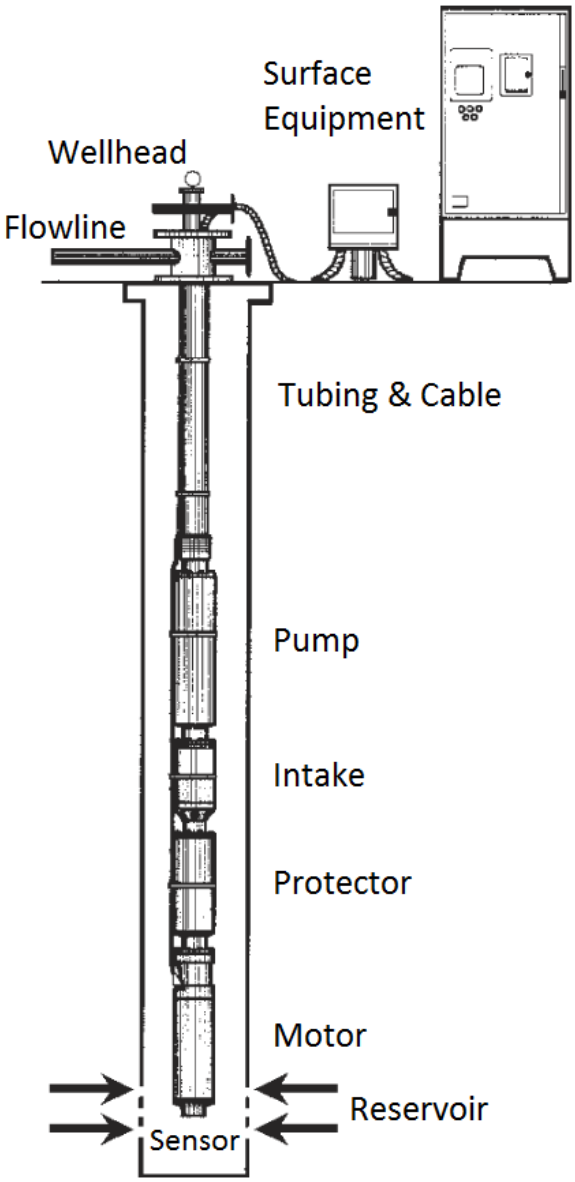


Figure 17 - Overview of an ESP system [10]

The amount of liquid, which is produced with an ESP system, is mainly depending on the following list of factors [10]:

- Rotational speed of the motor
- Impeller diameter
- Impeller type or design
- Actual head which has to be delivered
- Thermodynamic or transport properties of the pumped fluid such as density, viscosity etc.

In the following subchapters, the different components are described and discussed in detail.

### 4.2.1 Centrifugal Pump

The centrifugal pump with its multiple stages is the heart of an ESP system and the most important part in terms of design and planning. The number of stages governs the production rate, the delivered head or pressure and the required power. The stages of an ESP are operating in a vertical position and are operating in a series. During operations, an ESP is submerged in well fluids.

A typical stage is illustrated in Figure 18 below. Arrows in the right half of the picture indicate the fluid flow path. The fluid is entering a stage from the bottom through the impeller's eye (suction side). An impeller operates self-priming and consists out of a set of vanes, which are rotating during operation. First, energy is imparted to the fluid by centrifugal force and the fluid exits the impeller with high velocity. Then added kinetic energy is converted to potential energy in the form of pressure in the diffuser. Therefore, the velocity of the fluid is reduced significantly. The impeller is mounted on the shaft and rotates with it. The diffuser is static and does not move. It is also equipped with a set of vanes to guide the fluid [10].

The maximum number of stages is depending on different factors. Typically, several hundred stages can be installed. The number of those is mainly influenced by the mechanical strength of the pump shaft (shaft's horsepower rating), the burst pressure rating of the pump housing and the maximum allowable load on the main thrust bearing.

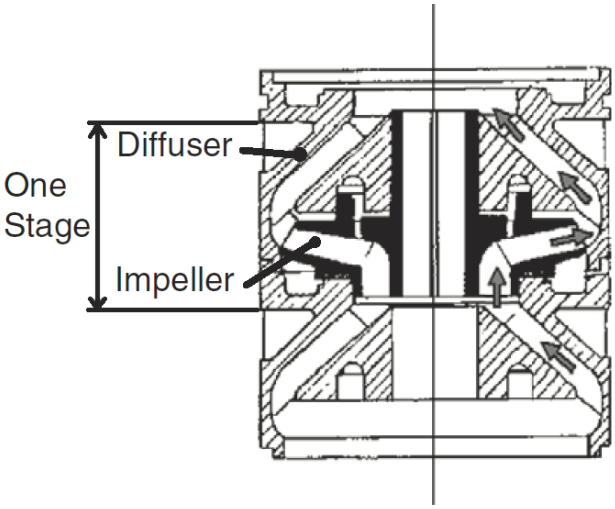


Figure 18 - Single ESP stage [10]

The rotational movement of the shaft is transferred to the impellers via so-called keys. In Figure 18, the key way is shown directly at the line of symmetry. It is also illustrated in Figure 19 below. In case of a free-floating configuration, the impellers are not fixed in axial direction, which allows them to float. Fixed impeller pumps or so-called compression pumps have fixed impeller configurations and are the second type in this regard. The latter ones, are more modern in design and are equipped with additional bearings to compensate for forces [10].

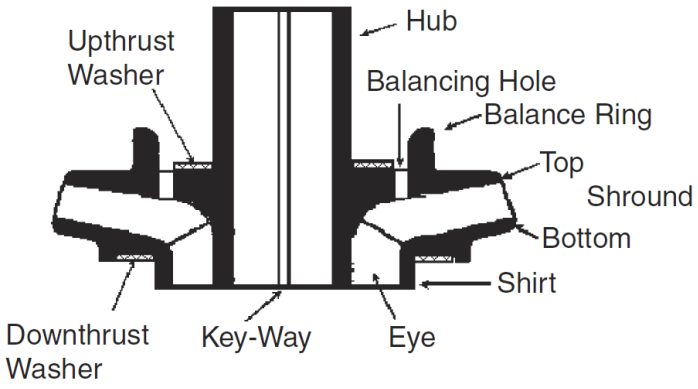


Figure 19 - Nomenclature of ESP impeller parts [10]

During operation, forces develop and push the impellers up or downwards. This so-called axial thrust forces develop due to pressure differences across the impeller and different cross sections on the top and the bottom of the impeller. Balancing holes and rings are used to reduce this effect to a certain degree but not totally [10].

### Floating and Fixed Impeller Pumps

Due to the axial thrust forces, floating impellers are moving at a certain position according to the pumping speed since they are not fixed in axial direction. In case of low pumping rates, low forces occur and the impeller is rotating while contacting the previous diffuser at the bottom. At high rates on the other hand, high axial thrust forces are pushing the impeller upward so that it contacts the diffuser above. To avoid severe material degradation, thrust washers (also called synthetic pads) are located at the points of contact [10].

Figure 20 illustrates different pump operation ranges. The optimal operation range is limited by a minimum and maximum flow rate and gray shaded in the figure above. Outside of this recommended region, a strong decline in efficiency can be observed.

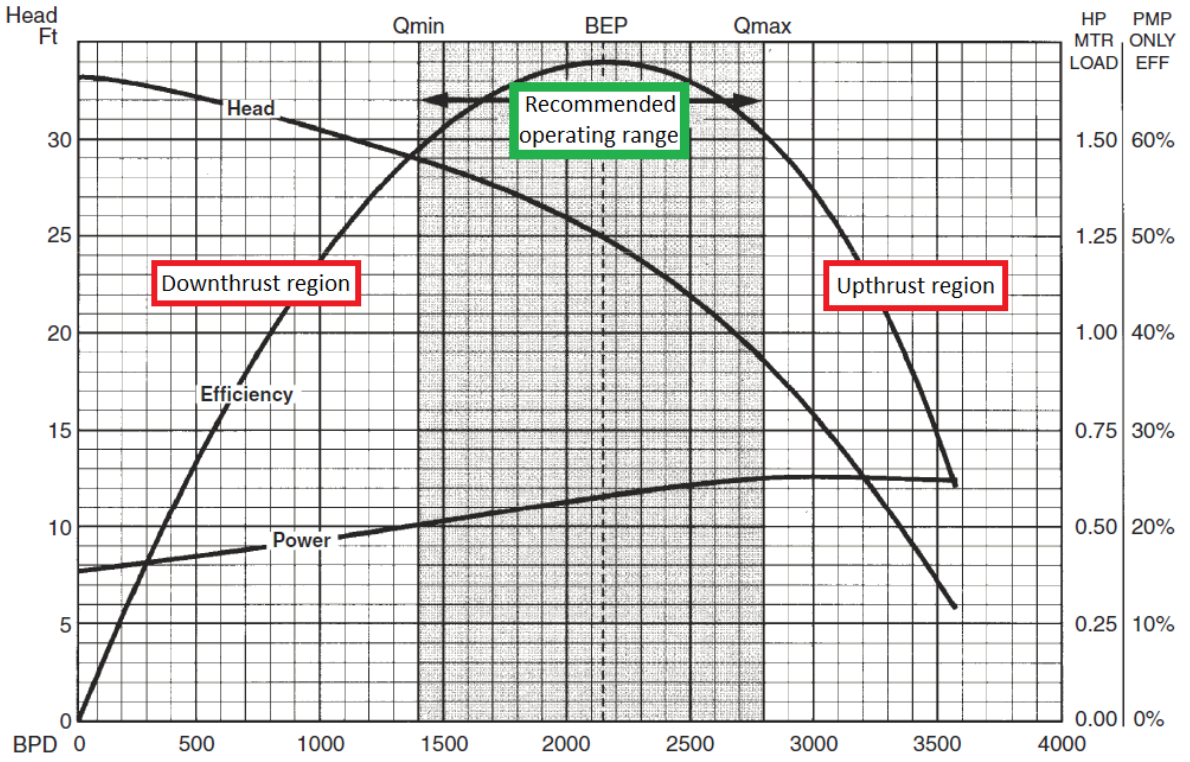


Figure 20 - ESP operation ranges [10]

In case that the pump is operated in up- or downthrust region, most of the forces are compensated by frictional forces arising in the washers at the top or the bottom of the impeller. Thus, thrust bearings with smaller capacity are required since those take less load. When fixed impeller pumps are used, all axial forces are transmitted via the shaft and are balanced by the main thrust bearing, which is located in the protector of the ESP [10].

Both, the compression pumps as well as the floating impeller pumps have their advantages and disadvantages. The benefits of the floating impeller design are listed below:

- No fixing of impellers necessary – time consuming process
- Pumps with several hundred stages possible
- Thrust bearings with smaller capacity needed
- Lower investment cost compared to compression pumps

Compression pumps are typically built in diameters above 6 inches and are capable of producing large volumes of liquids. Fixed impellers allow operating the pump in a wider range and thus add flexibility. The maximum number of stages for compression pumps in one pump is limited to about 80 to 100 [10].

### Main Thrust Bearing

As already mentioned, the main thrust bearing is located in the protector (Chapter 4.2.3) of the ESP string. It is from high importance when the pump is designed in fixed impeller configuration since it is responsible for the elimination of the bulk of the thrust forces. In ESP systems mainly

pad-type plane thrust bearings are used because they show significant advantages compared to bearings with rolling elements. The advantages of this bearing type are listed below [10]:

- Less heat generation during operation
- Not sensitive to solid contaminants in the lubrication oil
- Support higher thrust loads

The main thrust bearing consists out of two shoes and a thrust runner in between. During operations, the bearing is lubricated with oil to ensure a fluid film in between the different parts of the main thrust bearing. In case of lubrication problems, metal-to-metal contact leads to severe damage and typically ends the lifetime of an ESP. Known sources for destruction of the lubrication film are reduction of oil viscosity due to high temperature, misalignment of the thrust runner and shoes, vibrations or solid particles which are scratching contact surfaces [10].

### Impeller Types

As there are different pump configurations, there are also different types of impellers available for ESP application. The two types are radial and mixed flow impellers and an illustration is given in Figure 21.

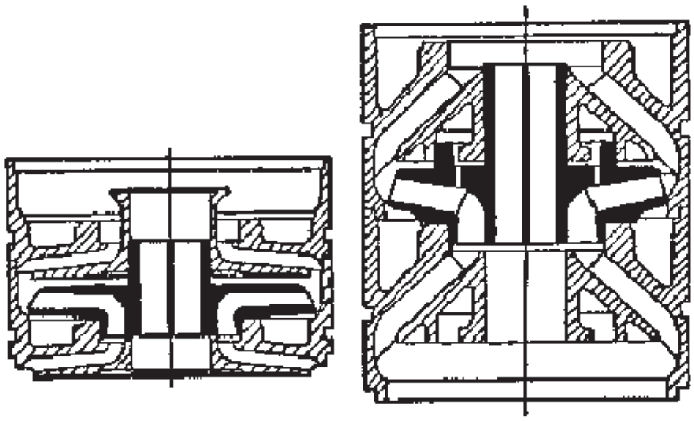

Figure 21 - Radial (left) and mixed flow impeller (right) [10]

The different pump designs can be compared by the concept of specific speed, which was introduced and defined as the rotational speed required to produce a liquid rate of 1 gallon per minute against 1ft of head. The definition is the following [10]:

$$N_S = \frac{N\sqrt{Q}}{H^{0.75}} \qquad (6)$$

Where
- N Pump speed [RPM]
- Q Pumping rate [gpm]
- H Developed head per stage [ft]

The specific speed is only used for comparing different designs and has no practical importance. Characteristic values for radial impeller pumps are ranging between 500 and 1,800. Radial impellers are typically resulting in higher head but lower flow rates compared to mixed flow impeller configurations. Mixed flow impeller pumps can reach a maximum value of specific speed around 4,500 and thus are capable of handling more free gas than radial impeller pumps [10].

In Figure 22 below, the efficiency curves of both impeller types are plotted over the flow rate. It is clearly visible, that mixed flow impellers are more suitable for lifting large volumes of fluids.

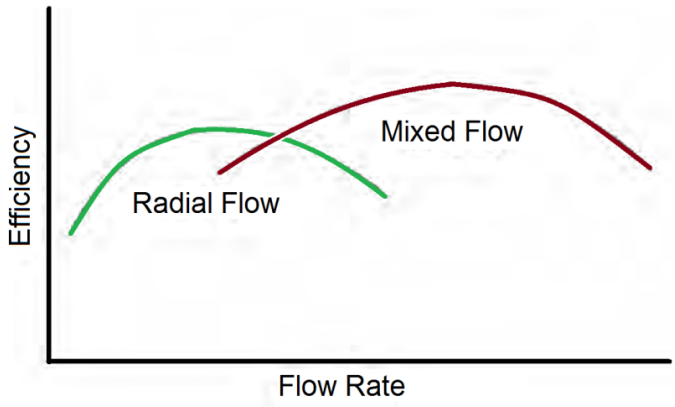


Figure 22 - Comparison of impeller types [11]

### Typical Failures

ESPs are offering a variety of possible failure types. Considering just the pump, the main failure prone parts are the shaft and bearings. Both are exposed to harsh conditions during operations and have to withstand high loads. Table 1 provides an overview of typical failures and associated reasons.

Table 1 - Typical failures of centrifugal pumps [10]

| Failure | Reason |
|---|---|
| Torsional yield failure (shaft) | Torque capacity exceeded |
| Torsional twist (shaft) | Startup inertia |
| Torsional fatigue (shaft) | Repeated torsional vibrations |
| Bearing wear | Abrasive conditions |
| Galling of bearings | Lost lubrication |
| Upthrust wear | Too high flow rates |
| Downthrust wear | Too low flow rates |
| Radial wear (journal bearings) | Abrasive-laden fluids |
| Erosion in pump stages | Abrasive-laden fluids |
| Scale buildup | Chemical composition |

### 4.2.2 Motor

Electrical motors for ESP applications are three-phase, two-pole, squirrel cage induction type electric machines. They are the most reliable motors because the rotor is not connected to the electric power supply. Furthermore, this type shows the best efficiency which explains its popularity in the oil and gas industry.

An alternating current (AC) is flowing through stator windings inducing a current in the rotor. The magnetic field developed by the current in the stator is rotating and interacts with the magnetic field of the induced rotor current. This interaction results in movement of the rotor, which is trying to keep up with the rotating magnetic field developed in the stator. The difference in speed between the two magnetic fields is called slip and plays an important role when it comes to generation of motor torque (Figure 23). The speed of the rotor is determined by the frequency of the AC current. To control the rotational speed of such a motor, a variable speed drive (VSD) or frequency converter is necessary. This type of equipment allows adaption of the frequency to influence the motor towards the desired speed and adds flexibility to operations. Nevertheless, a VSD is rather expensive and thus increases capital expenditure [10].

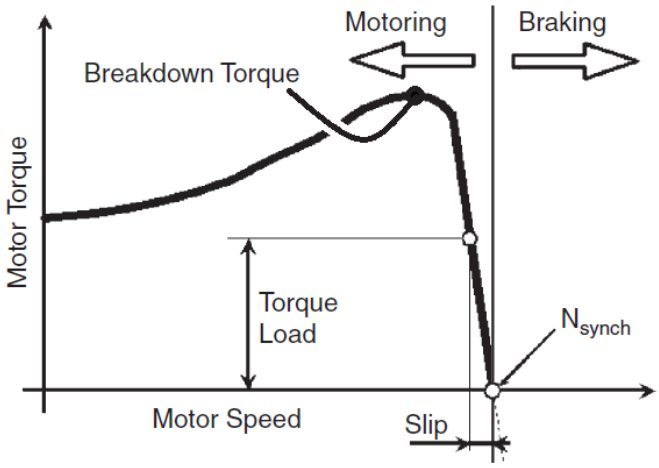


Figure 23 - Torque generation and slip [10]

During operations, the long motor shaft, which can be up to 30ft long, needs to be kept as free of vibrations as possible. This is ensured by radial bearings, so-called journal bearings. They are located at several locations along the shaft and consist out of two parts. The journal part of the bearing is rotating with the shaft while the stationary part of it is fitted between the stator and the journal. The axial load of the rotor and shaft weight is taken by a thrust bearing which is installed at the top of the motor [10].

The lubrication of the motor and all its bearings is provided via highly refined oil with a specific gravity between 0.8 and 0.83. The oil brings the required dielectric strength to prevent short circuit between motor parts, proper lubrication for the bearings and provides good thermal conductivity to transport the generated heat of the motor to the outside [10].

Since the diameter of a borehole is rather small, the ratio of length to motor diameter is large. The most important differences of ESP motors to conventional electric machines (at surface) are listed below [10]:

- High length-diameter ratio
- Motor power increases with length
- Better cooling via oil and wellbore fluids
- Higher electric current density due to better cooling
- Significant voltage drop due to high cable length needs to be considered

The power of a single motor can be up to 300hp. Since the wellbore diameter is constraining the size of the motor, only length can be increased to reach higher power requirements. Therefore, tandem configurations can be used. Tandem motors are assemblies of more than one motor in a series, where each motor has its own electrical supply. Figure 24 illustrates a tandem motor configuration with two independent electrical systems. Such motor assemblies are capable of supplying more than 1,000hp and offer great flexibility since different motors can be combined. The motors thereby are mechanically coupled but operated independently in an electrical sense [10].

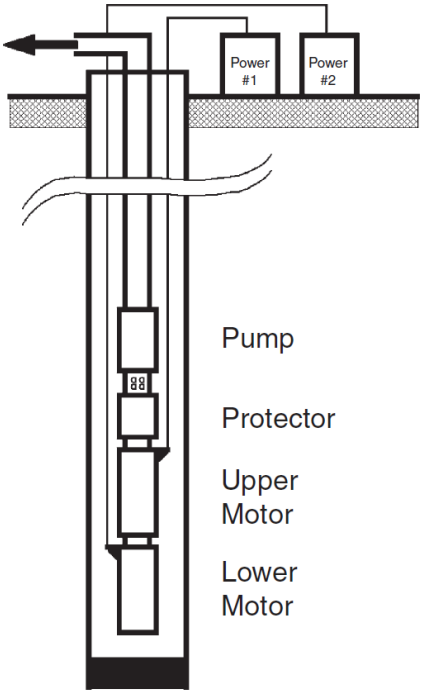


Figure 24 - Tandem motor configuration [10]

In case of VSD application (see Chapter 4.2.7), the frequency of a motor can be changed easily to operate the pump at different rates. Generally, the horsepower rating of a motor is provided at 50 or 60 Hz power. But changing the frequency influences the torque or horsepower rating of a motor, since the horsepower output of a motor is directly proportional to the frequency [10].

This relation is very important to understand since the affinity laws constrain the range of operation due to required pump horsepower. Equation 3 and 5 (Chapter 4.1.2) are showing that when the flowrate is doubled by increasing speed, the required horsepower is 8 times larger. If the speed is increased without considering this fast increasing power demand, the motor is not capable of delivering the required power and will overheat. An illustration of this relationship is given in Figure 25. The intersection point of the power curves is showing the maximum allowable frequency $f_{max}$ for safe operations.

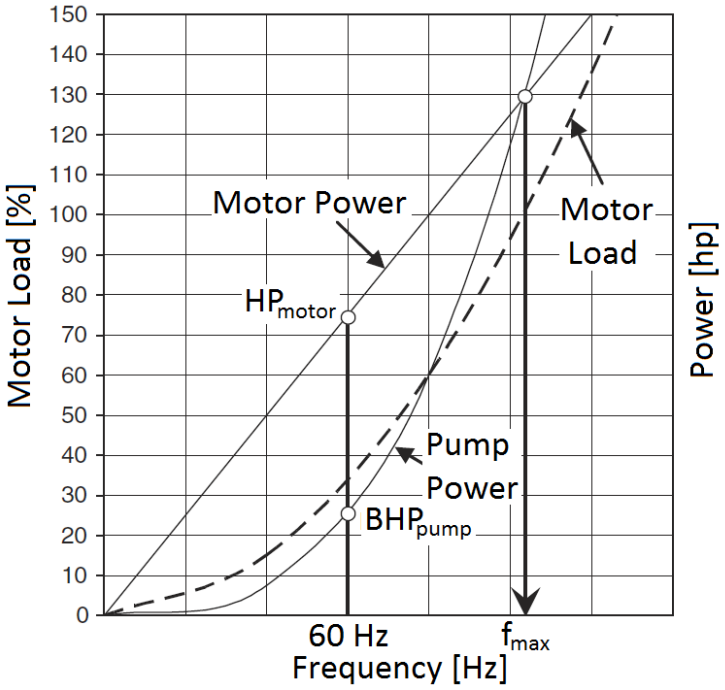


Figure 25 - Motor and pump power curves [10]

### Typical Failures

ESP motors are mostly failing due to electrical reasons. Excessive heating of the motor's wiring by overloading can cause damage or burnout. Thereby, overloading can occur due to several reasons such as undersized motors, changes in total dynamic head, pump failures or irregular voltages (harmonics). Moreover, the protector can leak causing contamination of the dielectric oil and thus short circuit and an eventual burnout. Insufficient cooling can lead to damage of insulating materials due to increased temperatures. Poor heat exchange can be caused by low fluid velocities around the motor or inadequate design [10].

## 4.2.3 Protector

The protector or sealing section is a part of equipment which is located between the pump and the motor. It is used to seal off the motor from conducting well liquids to avoid short circuit or other electric failure. Therefore, the protector is filled with the same high dielectric strength oil as the motor is. Furthermore, the seal section is necessary since the motor cannot be in a closed housing due to expansion of the oil at elevated operating temperatures and risk of burst. Additionally, the main thrust bearing is located at the lower end of the sealing section [10].

The most important functions of a protector are listed below [10]:

- Takes axial thrust load
- Isolation of the motor from well fluids
- Allows motor oil expansion and contraction
- Provides pressure equalization by communication
- Transmits the torque from the motor to the pump shaft

To fulfill all listed tasks and requirements, two types of isolation chambers are available: The labyrinth- and the bag- (or bladder-) type. They differ in the manner of isolation, which is used to prevent communication between motor oil and well fluids [10].

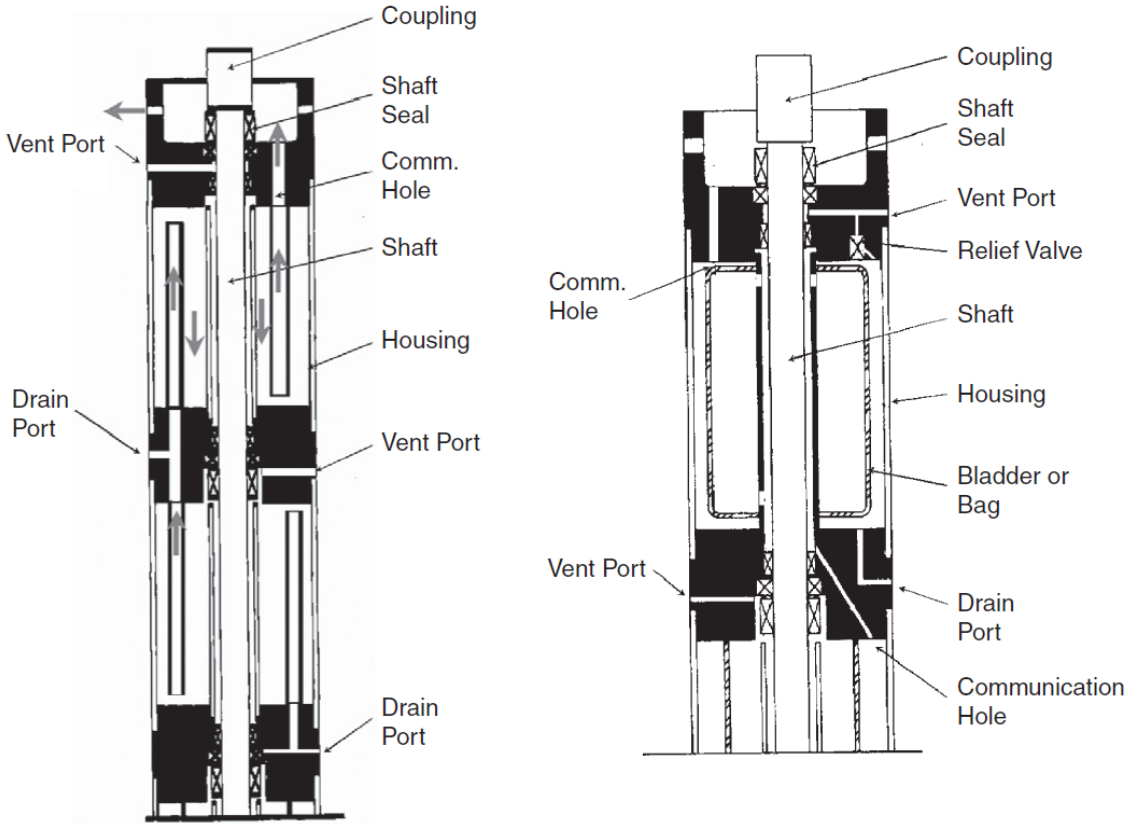


Figure 26 - Labyrinth type (left) and bag type chamber (right) [10]

For labyrinth type chambers it is important, that there is a density difference between the motor oil and well fluids. For motor oils with a specific gravity of 0.8 to 0.83 the minimum value for the SG of the well fluid is 0.9 to ensure proper functionality. Moreover, this chamber type is designed to be operated in vertical position since its ability to absorb expanding oil from the motor decreases as the angle deviates from vertical position [10].

Bag type chambers can be used for applications where the motor density and well fluids densities are quite similar. There is no direct physical contact between the fluids since this type is designed as a closed vessel system. Also the oil storage ability is not influenced by the angle

which enables application of bag type chambers even in wells with 30° deviation or more from vertical position [10].

For proper sealing, at least two chambers are installed in series. For increased safety during operations, protectors with more chambers or tandem protectors are available.

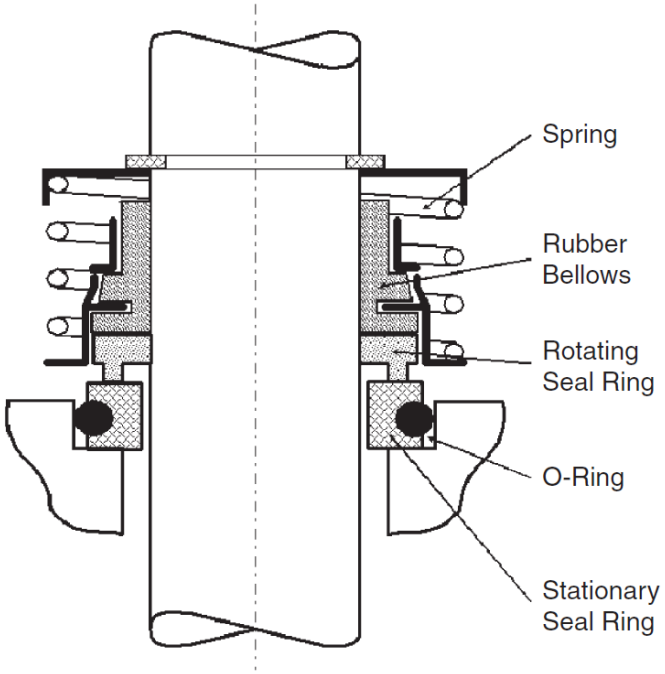


Figure 27 - Shaft seal [10]

The mechanical shaft seal avoids communication between the motor oil and well fluids along the shaft inside the protector. This seal is usually located at the top of each chamber and is rotating during operations. Therefore, it consists out of a stationary seal ring, which is fixed to the protector's housing and a rotating seal ring [10].

### Typical Failures

Protector section failure directly influences motor operations. Typical failures of this protective equipment are listed in Table 2.

Table 2 - Typical failures of protectors [10]

| Failure | Reason |
|---|---|
| Broken or damaged seals | Vibrations, faulty equipment, improper installation |
| Broken main thrust bearing | Excessive down- or upthrust conditions |
| Failed seal (labyrinth type) | Deviation of vertical position > 30° |

### 4.2.4 Measurement Equipment

During operations, several parameters are measured at different locations. To ensure successful monitoring and troubleshooting in case of malfunction, three different measurement positions are available. The measuring is done at the wellhead, the ESP downhole and at the separator. Table 3 lists all measured parameters with their associated position.

Table 3 - Measured Parameters

| Parameter | Position |
|---|---|
| Tubing pressure | Wellhead |
| Casing pressure | Wellhead |
| Motor current | Variable speed drive |
| Motor power | Variable speed drive |
| Frequency | Variable speed drive |
| Pump intake pressure | Downhole |
| Pump discharge pressure | Downhole |
| Bottom hole temperature | Downhole |
| Motor winding temperature | Downhole |
| Vibrations | Downhole |
| Current leakages | Downhole |
| Gross production rate | Separator |

Typical applications for downhole sensors are ESP wells where performance monitoring is required or where instability problems are likely to occur. The usage of such sensors improves the ESP run life, can lower operating costs and reduces early failure rates.

The downhole data used in this thesis is measured with the downhole sensor unit Phoenix XT150 from Schlumberger. It is a high temperature ESP monitoring system and allows surveillance of ESPs by measuring several key parameters as listed in Table 3.

### 4.2.5 Gas Handling

In the following, different gas handling methods are described and discussed.

#### Intake Gas Separator

In order to prevent free gas from entering the pump, intake gas separators are used and installed below the centrifugal pump unit. Gas separation is necessary because free gas reduces pump performance since the pressure increase per stage decreases as free gas is present. Free gas can influence an ESP system in the following ways [10]:

- Decreasing head
- Fluctuating output and possible cavitation
- Gas locking

The most common gas separators are the reverse flow type, the vortex type and the rotary type separator. An overview of all three designs is illustrated in Figure 28. Another possibility of gas separation can be the installation of the pump below perforations to allow natural separation in the annulus.

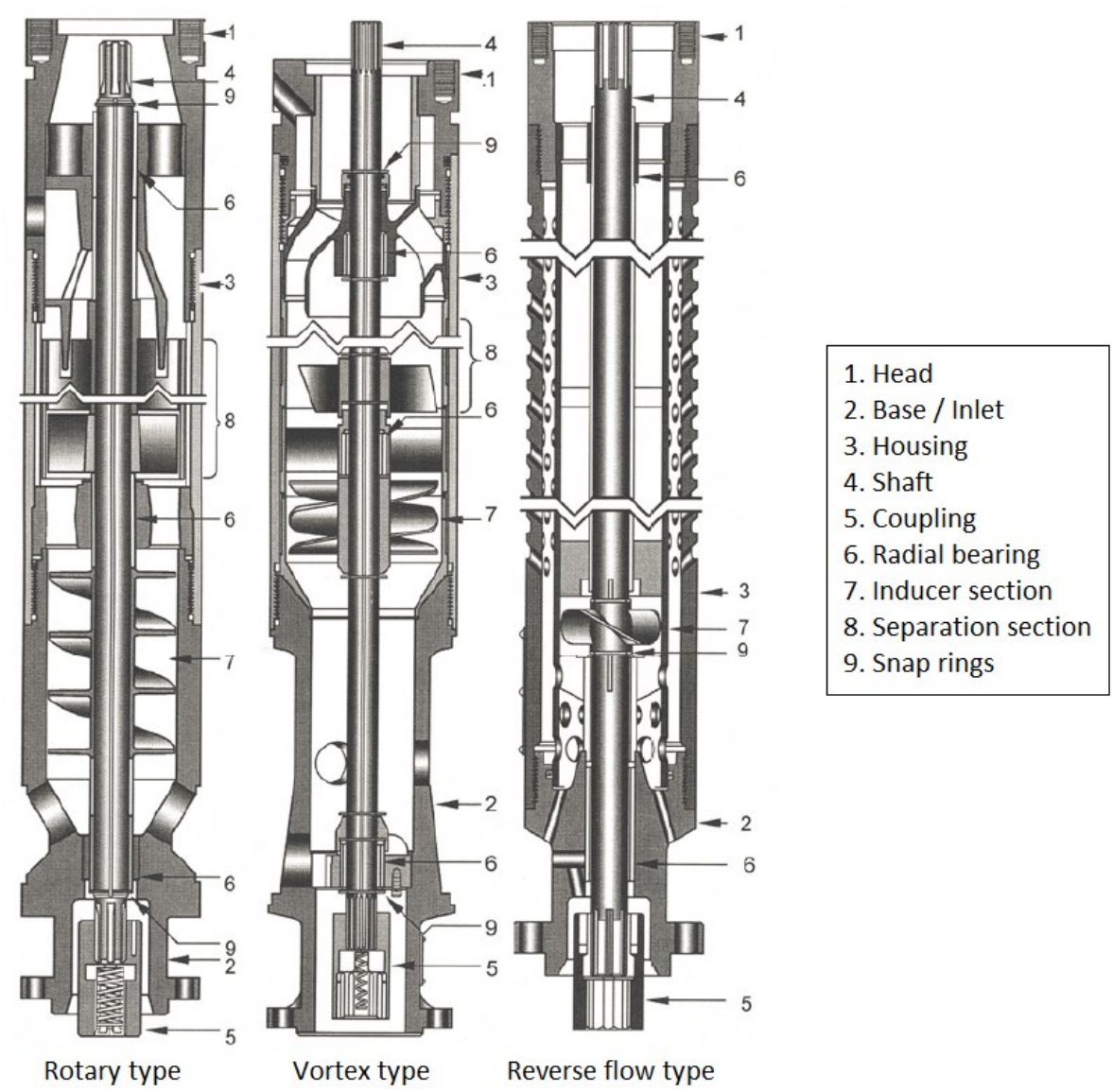


Figure 28 - Separator designs [11]

The simplest type of gas separation units is the reverse flow gas separator or reverse flow intake. This equipment works on the principle of gravitational separation and can be used in wells with low to moderate liquid and gas rates. There are no moving parts (although the inducer section can include rotating parts) inside the separator, which is also a main advantage next to its simplicity [11].

The two other design types for gas separation are the vortex type and rotary centrifuge type separator. The difference between them is that the rotary type has a rotating chamber instead of the vortex generator (Nr. 7 in Figure 28). Both are working on the principal of centrifugal

gas-liquid separation. Since the liquids are pushed outwards, a crossflow after the flow divider is necessary to direct the fluid into the pump. On the other hand, gas is guided to separator outlets to allow gas production through the annulus. Due to the rotating parts, the vortex and rotary type separators are offering additional potential for failure. Nevertheless, both types can handle more free gas compared to the simple reverse flow separator [10].

### Gas Handling Equipment

In case gas cannot be prevented from entering the ESP, appropriate gas handling is crucial to maintain high performance.

Overstaged pumps were the earliest solution for the problem of gas interference. Those pumps are equipped with additional stages to increase the pressure to the desired level and compensate for the first few stages with lower performance due to gas interference [10].

Tapered pumps are another type of equipment, which are a successful and energy efficient for handling free gas. The pumps include at least two different stage designs. The flow rate is decreasing, as the fluid is moving through the pump. The gas is highly compressed and partially dissolved in the lower stages, whereas in the upper ones lower flow rates allow optimal head generation. All stages of such a system should be designed to operate in their optimum range. Therefore, detailed knowledge about the well conditions is required [10].

Another possibility to handle entered gas is stage recirculation (Figure 29). This modification aims to break up gas pockets, which are created in stages. Additionally, a better homogenization of the fluid shall be reached. The recirculation path is formed by holes in the bottom shroud of the diffuser and in the top shroud of the impeller. Although stage recirculation greatly reduces gas locking, it decreases pumping efficiency by 20 to 30% [10].

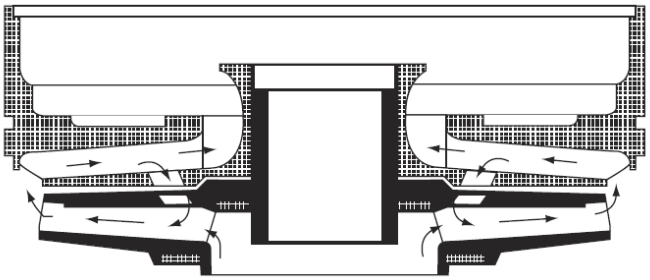

Figure 29 - Gas handling via stage recirculation [10]

Moreover, gas handlers can be installed upstream of the pump to ease pump operation. Pre-compression of the mixture and gas dispersion are improving the ESP’s tolerance to free gas production by reducing the risk of gas locking. Such systems allow well fluids with up to 75% of free gas at the intake to be lifted. Nevertheless, additional horsepower is required to drive gas handling equipment [10].

To conclude gas handling, Figure 30 illustrates gas handling performance of different ESP systems. Mixed flow pumps are already giving good results considering the conventional

design method. Advanced designs such as separator included ones are resulting in significantly improved gas handling performance.

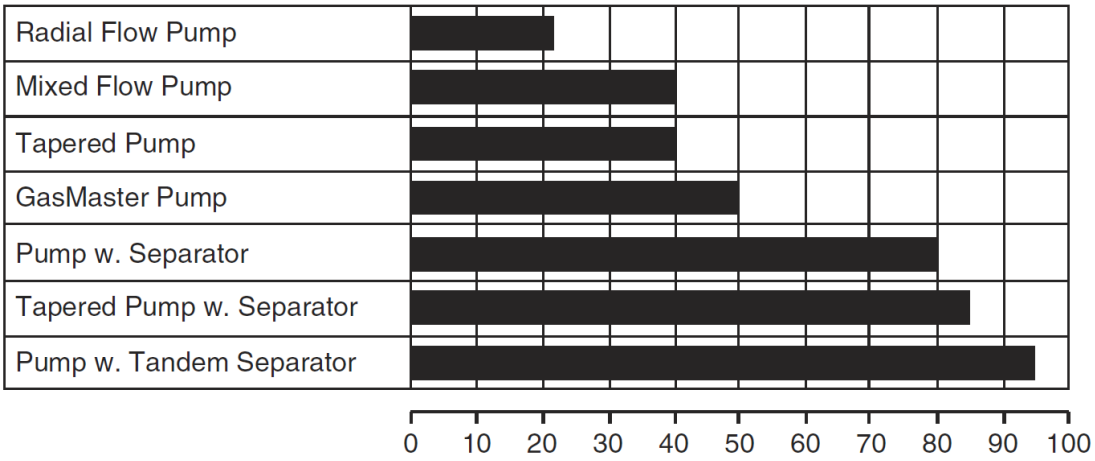


Figure 30 - Gas handling performance of different ESP systems [10]

### Typical Failures

Failure of rotary gas separators often occurs when solids are present in the produced fluid. Abrasives are accelerated by centrifugal forces resulting in severe wear and damage. Additionally, solids or precipitations can plug the intake causing a decrease in flowrate and energy losses. In the worst case, solids are entering and plugging the rotating parts of the separator which can lead to a shaft damage or break.

## 4.2.6 Cable

The electric power, which is required to operate the ESP is transmitted via a special three-phase electric power cable. Due to harsh operating conditions of cables the type and material selection are an important factor and the design procedure.

Copper or aluminum can be used for conducting the electric current. Even though aluminum is less expensive and lighter, copper is used more often since it is easier to splice and provides better conductivity. Insulator materials are used to withstand high temperatures, provide oil resistance and prevent gas from migrating into the cable body. Moreover, insulation prevents short circuits and leakage currents between the different conductors. The insulator material is protected by so-called jackets, which are usually made of nitrile rubber and EPDM (ethylene propylene diene monomer). Additionally, metal armor is used to protect the cable by providing mechanical strength.

ESP cables are available in two different construction designs: Round and flat. The flat type cable is very often used since it offers the advantage of its slim geometry. The cable construction is illustrated in Figure 31.

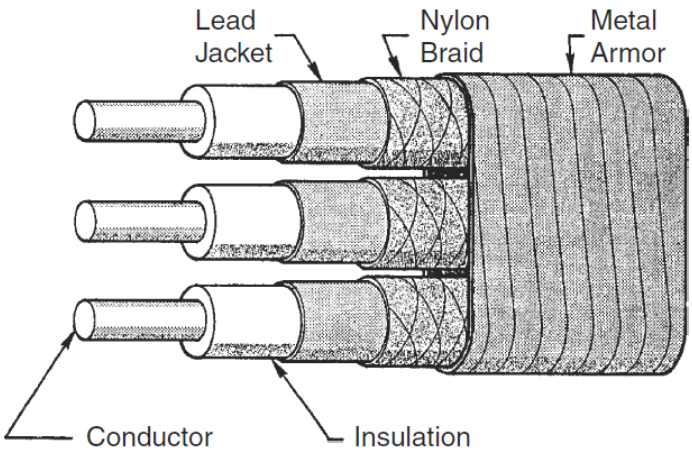


Figure 31 - Flat ESP cable [10]

For the design procedure, the resistance of the cable is a very important parameter since it is directly influencing the occurring voltage drop. For cable selection, voltage drop diagrams are used to identify losses associated to a certain current. The voltage drop can be calculated with the following equation [10]:

$$\Delta U_{Cable} = \sqrt{3} * R_T * I \qquad (7)$$

| | | |
|---|---|---|
| Where | ΔU | Voltage drop [V] |
| | RT | Resistance of the cable [Ohm] |
| | I | Electric Current [A] |

To install the cable, a special wellhead tool is required: A wellhead penetrator is used for feeding the downhole cable through the wellhead. The penetrator and the cable connection is frequently found as a source of malfunction. Therefore, the installation and connection of it needs to be carried out with special attention. On the other end of the cable, a connection to the motor lead extension has to be made. The procedure of joining two cables together is called splicing. Most splices are made by wrapping tape splicing but also others such as molded or vulcanized splicing are known. For integrity reasons, a splice-free cable is always preferred [10].

### Typical Failures

The ESP cable is connecting the motor to the power supply. In case of failure of this component, shut down of the system will follow immediately.

Table 4 gives an overview of typical failures.

Table 4 - Typical failures of ESP cables [10]

| Failure | Reason |
|---|---|
| Mechanical damage | Unwary running or pulling operations |
| Corrosion | Harsh environment, insufficient protection |
| Insulation deterioration | High temperature, gases |
| Insulation breakdown | Increasing current, Temperature increase |
| No connection | Connection problems, improper splicing |

## 4.2.7 Surface Facilities

ESP systems require certain surface facilities. Figure 32 illustrates an overview of surface facilities of an ESP system.

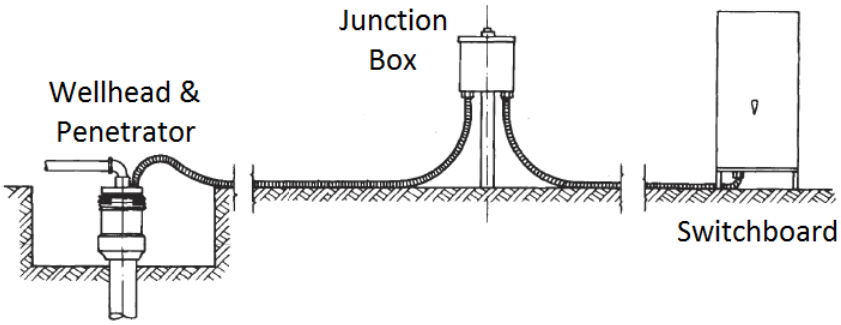


Figure 32 - Surface facilities arrangement [10]

As already discussed, special wellheads with penetrators are used to allow electrical connection. The penetrator allows higher wellhead pressures compared to conventional wellheads with cable feed-through. Additionally, the wellhead is supporting the weight of the production string and maintaining control of the annulus [10].

The junction box, also known as vent box, is the connection point of downhole and surface cable. As the name says, it vents any gas to the atmosphere which might has reached this point by migrating up through the cable. It is also used as measurement station to check for electrical failure and malfunction [10].

The switchbox is used to control the ESP and also protects surface and downhole equipment from a variety of electrical problems. Moreover, it enables monitoring and recording of measured data [10].

In case of insufficient electrical power supply, transformers are delivering required levels of voltage. The transformer design must take the voltage drop in the power cable into account to provide the necessary voltage to the motor downhole [10].

In order to allow a more flexible range of operation, variable speed drives are used. A VSD consists out of three major components. Those are the rectifier section, the DC voltage control section and the inverter section. In ESP applications, voltage source inverters are typically used. These inverters are controlling the voltage output while keeping the current constant. Indeed the current fluctuates due to changing loads on the unit [10].

## 4.3 Design Considerations

Designing an ESP system is a straightforward engineering process, but it can get quite complicated when gassy wells are concerned or VSD units are required. In order to select a proper design, the following input data must be included according to *Takacs (2009)*:

1. Well data
   Casing and liner sizes, weights and setting depths
   Tubing size, weight and thread
   Total well depth
   Depth of perforations or openhole section
   Well inclination data

2. Well performance data
   Tubing head pressure at the desired rate
   Casing head pressure
   Desired liquid production rate
   Static bottom hole pressure or static liquid level
   Flowing bottom hole pressure or dynamic liquid level
   Productivity data
   Producing gas oil ratio (GOR)
   Producing water cut or water oil ratio
   Bottom hole temperature at desired rate

3. Fluid properties
   Specific or API gravity of produced oil
   Specific gravity of water
   Specific gravity of produced gas
   Bubble point pressure
   Viscosity of produced oil
   PVT data of produced fluids

4. Surface power supply data
   Primary voltage available at the wellsite

Frequency of the power supply
Available power supply capacity

5. Unusual operating conditions
   Production of abrasives, especially sand
   Paraffin deposition
   Emulsion formation
   Type and severity of corrosion
   Extremely high well temperatures

A recommended workflow to calculate and design the different components of an ESP system in an appropriate order is provided by API's recommended practice for sizing and selection of electric submersible pump installations. Figure 33 illustrates the design process recommended by API.

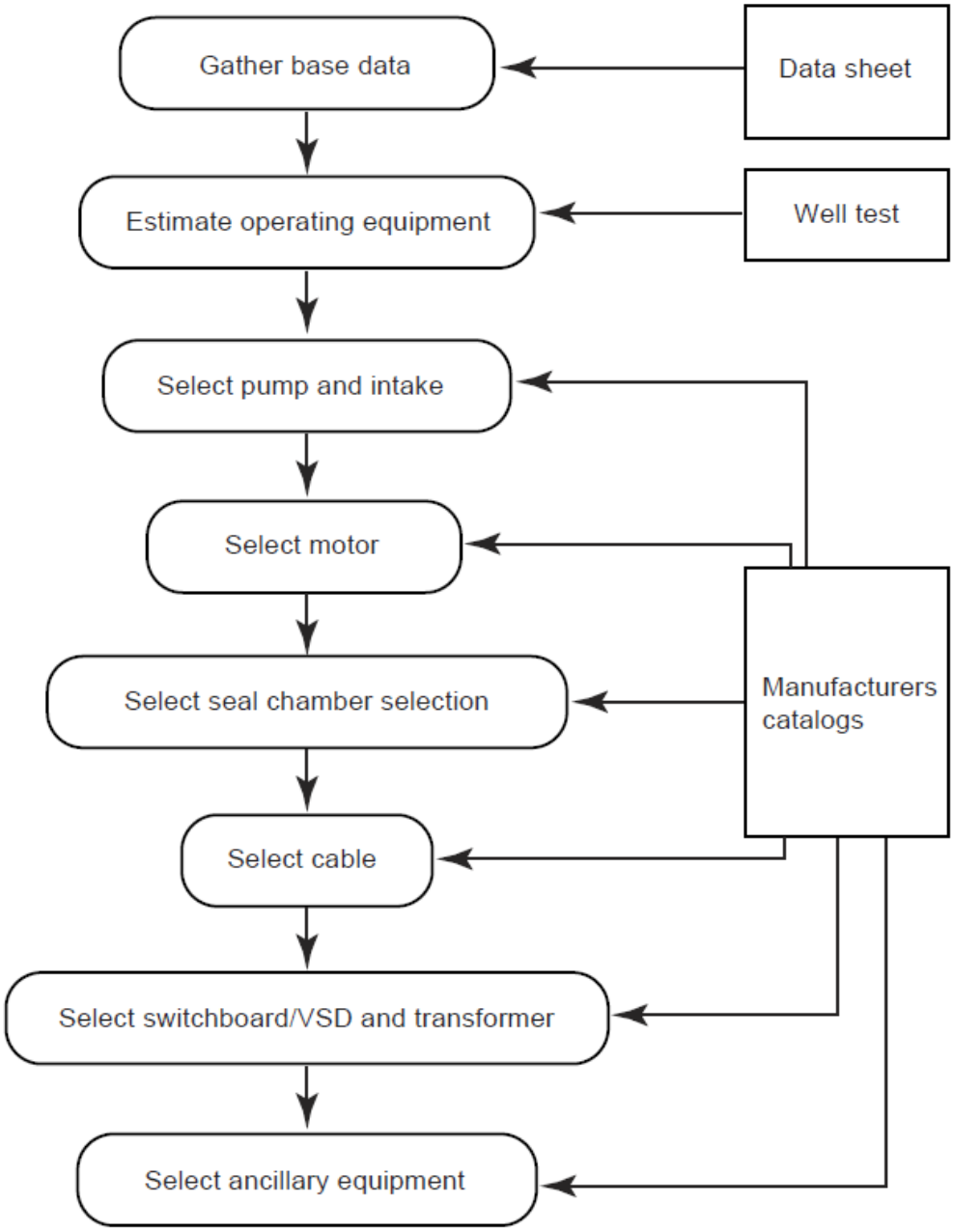


Figure 33 - ESP design process [12]

The pump selection is the first and most important step, since it is the heart of an ESP system. The parameters, which have to be defined are the pump series (outside diameter), pump type, number of stages and the mechanical strength. The number of stages is from main interest since it influences the majority of later design variables. It can be calculated with the following equation [10]:

$$Stages = \frac{Total\ dynamic\ head\ [ft]}{head\ per\ stage\ [ft]} \qquad (8)$$

## 4.4 Troubleshooting

Troubleshooting is the procedure of finding the source in case of failure or malfunction. It is used to obtain a logical and technical explanation for saliences occurring during production operations. Therefore, certain sources of information are necessary. Modern ESP systems are equipped with state of the art sensor technology. Those sensors enable constant monitoring of downhole conditions allowing the engineer in charge to identify problems and set remedial actions accordingly. Additionally, information is gathered at surface facilities which are including wellhead and separator. Data sources used during this thesis are already discussed in Chapter 4.2.4 (Measurement Equipment) and shown in Table 3.

According to *Takacs (2009)*, the most important parameters are the liquid production rate measured at surface, the motor current from an ammeter chart and the pump intake pressure. The last parameter can be obtained either by acoustic dynamic liquid level measurement or downhole measurement. Those three variables allow quite detailed diagnosis to investigate on pump's operation point, wear and leaks, electrical or mechanical damages, pump performance, well inflow, etc. [10].

### 4.4.1 Monitoring

Nowadays, pump monitoring is not just limited to surface sensor measurements. Expensive ESP systems justify additional investment in downhole sensor technology to improve operations and enhance the run life of an ESP. Monitoring systems are usually web-based user interfaces, which allow the engineer to observe and supervise relevant pump parameters. Alarm settings can help to notify and early detect abnormal operation conditions.

During the thesis, Life-of-well information software (LOWIS), a software tool from Weatherford, was used for monitoring of ESP wells. The program allows accessing measured data in tabular or graphical manner. Figure 34 shows a screenshot of the LOWIS user interface.

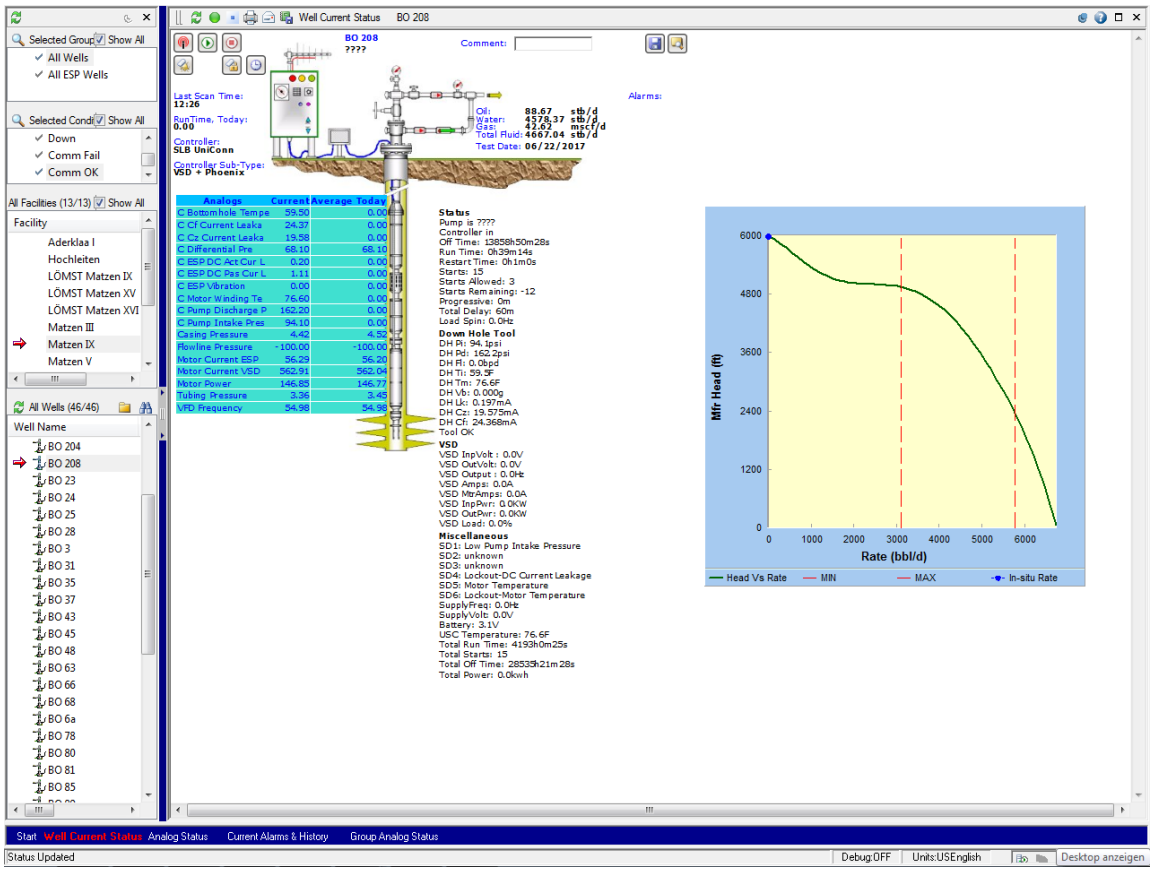


Figure 34 - LOWIS user interface

### 4.4.2 Methodology

In case an ESP failed, troubleshooting is performed to identify the reason and set remedial actions. Troubleshooting requires some experience, since often more different interpretations of sensor data is possible. To ease this procedure, troubleshooting guides from different pump manufacturers are available. These aids typically use the exclusion principle by telling which parameter must change to result in a certain failure. Moreover, remedial actions are recommended to restore optimal operation conditions. A part of a troubleshooting aid for failure or reason identification is shown in Figure 35. The different symbols are indicating small or strong changes. Empty positions are expressing no change in the associated parameter.

Next to different manufacturer's guides, the American Petroleum Institute published their recommended practice 11S with the title "Operation, maintenance and troubleshooting of electric submersible pump installations" in 1994.

| Scenario | Broken Shaft | Reverse Rotation |
|---|---|---|
| Amps | ⇓ | ↑/↓ |
| Hz | | |
| Volts Phase to Ground | | |
| Insulation Resistance | | |
| D/H Flow | ⇓ | –/∪ |
| P. Intake | ∩ | |
| P. Discharge | ⇓ | –/∪ |
| D/H Temperature | | |
| Motor Temperature | ∩ | ∩ |
| Delta Pressure | ∪ | ∪ |
| Vibration | ∩/? | |
| Surface Flow Rate | ⇓ | –/∪ |
| W/H Pressure | ∪ | ∪ |
| Annular Pressure | | |

Figure 35 - Troubleshooting aid

In case of severe pump damage, the pump must be pulled and replaced by a new production string. If the pump is not or just slightly damaged, remedial actions can be performed. A simple example is reverse rotation because the only parameter which must be changed is the direction of rotation.

### 4.4.3 Dismantling and Inspection

To obtain more detailed information about the failing mechanism of a damaged pump, the pulled pump is dismantled and inspected. It is a valuable source of information which adds value to future pump designs and operations. Moreover the inspection allows validation of previous failure identification. A better understanding of the pump failure can be obtained.

One lesson learnt by dismantling and inspection, included the replacement of zirconium based bearings by tungsten carbide bearings. The latter ones are showing higher resistance against abrasive solids due to harder material surface. During operation, the zirconium bearings were damaged and broken leading to a shaft break. Figure 36 shows the dismantled pump and the white broken bearing.


Figure 36 - Broken Zirconium bearing

# 5 Introduction to Artificial Neural Networks

A neural network is the complement of a human brain in computer science. For both, the architecture is very similar and the training procedure is influencing connections between the different neurons to improve the outcome. Figure 37 illustrates the architecture of a single biological neuron and its connections. The input from other units is transmitted by dendrites and summarized before the neuron. Regarding the figure, there are different inputs entering the neuron. In the neuron the inputs are processed and the output is handed over to other neurons by the so-called axon.

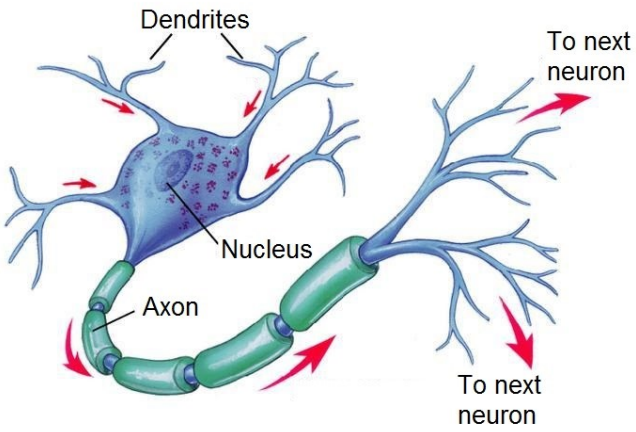


Figure 37 - Structure of a biological neuron [13]

In artificial intelligence, the complement to a biological neuron is the artificial neuron (Figure 38). The input is transmitted by the different connections and multiplied with so-called weights. When entering the neuron, the different inputs are summarized and processed by an activation function, which is sizing the output. Finally, the output is transmitted to the next neuron via another connection with a different weight.

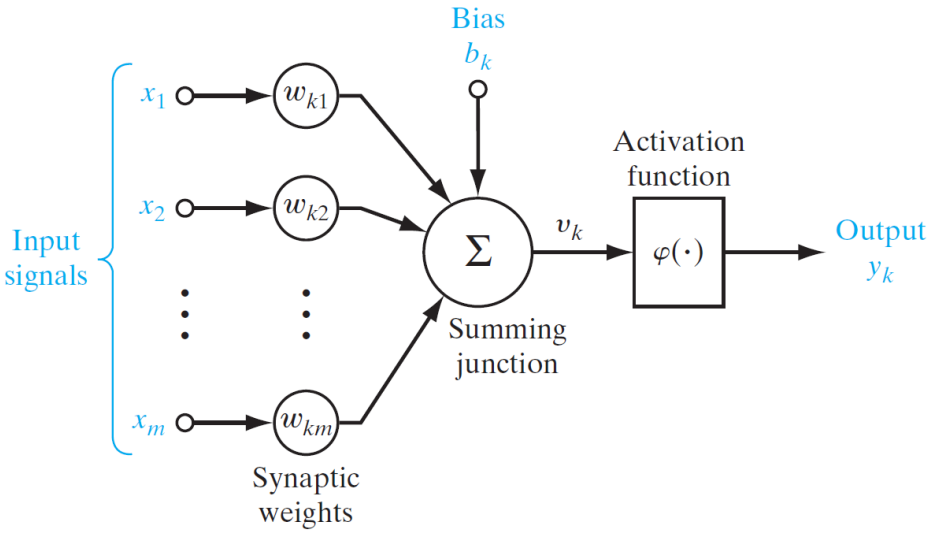


Figure 38 - Principle of an artificial neuron [14]

As in the human brain, an artificial neural network can consist out of many neurons. The number of neurons is directly influencing required computation power of the computing machines to obtain results in appropriate time. The architecture of a simply neural network is illustrated in Figure 11. The main components are the input layer, the hidden layer and the output layer. The number of neurons or units in the input layer is equal the number of inputs fed to the network, the so-called features. The number of output units is equal to the number of outputs. In terms of classification, each class or category is represented by one output neuron. For example, the classification of a motor status to tell whether the motor is turning or not requires two output units. The hidden layer is located between the input and output layer and consists out of hidden neurons, which can be arranged in a layered structure. This means, that instead of ten hidden neurons in one layer, two layers with five hidden neurons each can be in place. As the architecture varies in complexity, the performance may change as well.

### 5.1.1 Feed Forward Neural Network

Feed forward (FF) neural networks are networks where the information is propagating through the network with fixed weights in forward direction resulting in an output. In the backward phase, an error signal which is produced by comparing the actual output to the desired output is propagating backwards through the network, layer by layer. The weights between the neurons are successively adjusted during this process also known as error back propagation [14].

A simple type of a FF neural network is the multi-layer perceptron (MLP). Figure 39 illustrates a MLP with two hidden layers and three output units in the output layer. Moreover, there are also other architectures available, such as the completely connected perceptron (CCP) and recurrent neural networks (RNN).

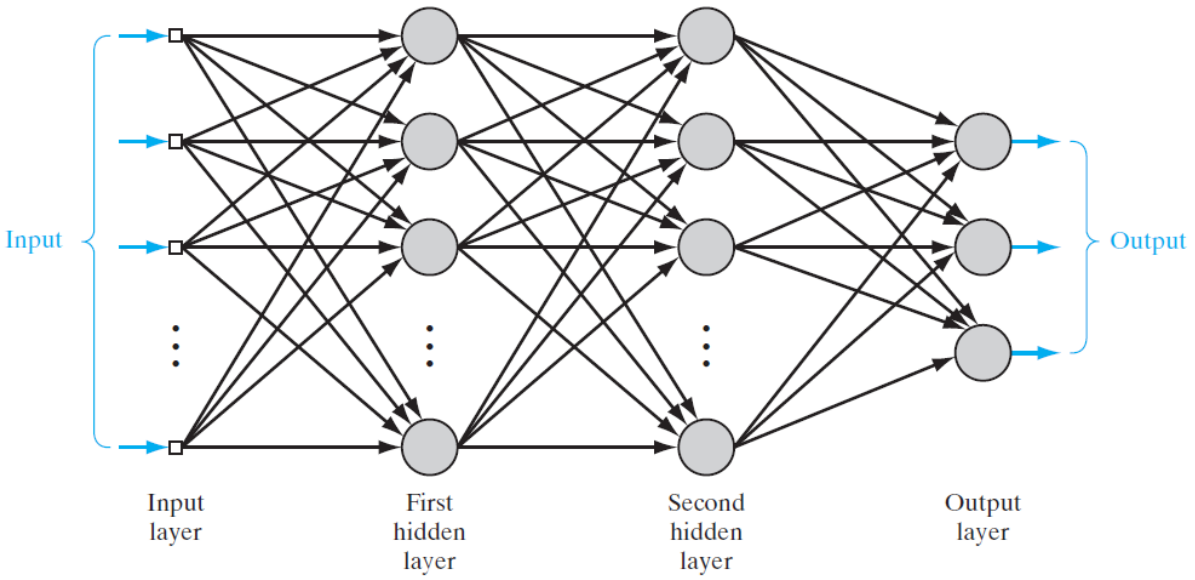


Figure 39 - Multi-layer perceptron [14]

A CCP would additionally have connections between hidden neurons within the hidden layer. This adds performance improvement and increases the complexity of the network architecture.

FF neural networks are capable of handling time independent tasks. For classification, one observation of different measured parameters for each time stamp is fed to the network. By training the network with appropriate examples or so-called labeled data, the network learns to classify as desired.

### 5.1.2 Training, Validation and Testing

In this chapter, the different steps of setting up a model by training of a neural network are explained in detail. Additionally, further features such as sequential forward selection and softmax layer are described.

#### Data Partitioning

The first thing before a data set can be used for machine learning is partitioning of the data set. The reason for this operation is the need of quality control, which allows evaluating a created network. Therefore, the data is split into three different classes: Training, validation and testing data. Training data will be used while the network is learning by examples. Validation data, which is also part of training data is used to judge on each individual trained network to choose the best one. Testing data is a subset, which is unknown to the network. It is fed to the network for further evaluation on network performance.

Table 5 shows a small part of a data set which is already partitioned. The last column of the table includes three different labels for data splitting which is additionally indicated by colors. A typical data partitioning would be 60% of a data set for learning, 20% for validation and 20% for testing. The partitions can be either in series or randomly as shown in Table 5 below.

Table 5 - Example of data set partitioning

| Time stamp | MWT | PIP | PDP | MOC | Status | Data Split |
|---|---|---|---|---|---|---|
| 10.01.2017 06:00 | 60.7 | 88.8 | 143.8 | 205.3 | Normal | T |
| 10.01.2017 06:10 | 61.2 | 88.8 | 143.8 | 206.0 | Normal | V |
| 10.01.2017 06:20 | 60.6 | 88.8 | 143.8 | 206.0 | Normal | L |
| 10.01.2017 06:30 | 61.0 | 88.8 | 143.8 | 205.2 | Normal | L |
| 10.01.2017 06:40 | 60.6 | 88.8 | 143.8 | 206.4 | Wear | V |
| 10.01.2017 06:50 | 60.8 | 88.8 | 143.7 | 205.4 | Wear | T |
| 10.01.2017 07:00 | 61.2 | 88.8 | 143.8 | 206.4 | Wear | L |
| … | … | … | … | … | … | … |
| | Input (features or channels) | | | | Output | |

Where MWT Motor winding temperature
PIP Pump intake pressure

| | |
|---|---|
| PDP | Pump discharge pressure |
| MOC | Motor current |
| L | Learning or training data |
| V | Validation data |
| T | Testing data |

As seen in Table 5, labeled data is used during training, validation and testing. One observation is a set of measurements at a certain time and includes four different channels or features. For classifying the status of an ESP, the status for each observation was given to the network as categorical output as well. This output is used during supervised learning to quantify the error, which is used for weight adjustment and model improvement.

Typically, data set partitioning is performed more often to obtain different subsets for learning, validation and testing. During the training with the learning subset, a validation set is used to evaluate on progress and model performance to find the best model. In order to avoid that, the model which is chosen to be best, is overfitting the validation set, a test set which is different from the validation set is used. This procedure is necessary since the validation set is used for choosing parameters of the model such as network size. This statistical method is known as cross validation [14].

For all machine learning tasks, three to five cross validation families have been used.

### Training and Validation

The training process of a FF neural network is based on quantifying the error followed by weight adjustment. The error is obtained by using supervised learning with labeled data. A so called training epoch includes feeding one observation to the input layer, forward propagation through the network, output calculation, error quantification and weights update. Depending on the amount of data, the number of training epochs can vary.

During the training, a so called supervisor is used to look at the actual result while knowing the desired one and quantifying the error. This error is calculated as an error gradient in order to adjust weighs correctly. As described earlier, error back propagation is used to improve the network performance by distributing the calculated error back throughout the whole network from the output layer to the input layer. This learning method is called supervised learning and is illustrated in Figure 40 below.

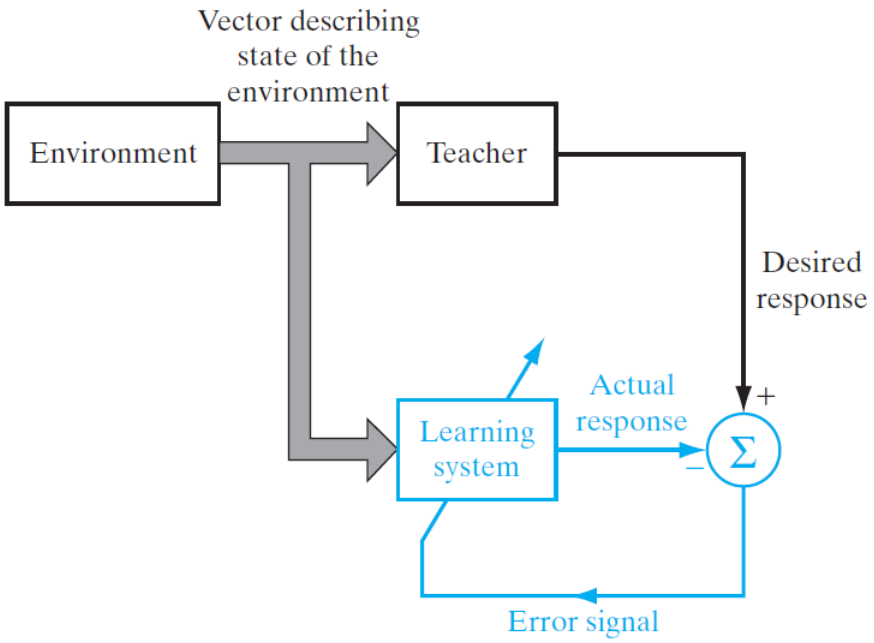


Figure 40 - Supervised learning [14]

Besides supervised learning, there are two other methods: Unsupervised learning and reinforcement learning. Unsupervised learning is used for data clustering which is a similar process to classification. Clustering is the process of grouping unlabeled data in a way that objects within a group are more similar to each other than to objects in other groups.

The backpropagation of the error gradient can be controlled via three main factors: learning rate, backpropagation algorithm and the method of error calculation. Three different possibilities for learning rates are known:

- Global learning $\eta$ = const.
- Local learning $\eta_k$ = const.
- Local adaptive learning $\eta_k = \eta_k(t)$

Especially the last one, local adaptive learning is resulting in good training results. It allows adapting the learning rate locally to react on changes during the training by comparing learning rates and errors of previous epochs with the current one. On the other hand, the initialization of local learning rates is more complex than using global learning. To illustrate the method for calculating a new weight, the Vanilla backpropagation equation is written below:

$$w_{t+1} = w_t - \eta \frac{\delta E}{\delta w} \qquad (9)$$

For calculating the new weight, the old weight is modified by subtracting the product of the error gradient and the learning rate. In case the learning rate is well chosen, the error of the next weight will be lower than the one in the previous epoch. The aim of this procedure is to find the minima of the loss function, which is representing the error over all weights. Figure 41

illustrates the loss function (blue line) of weight $w_i$. The black dot represents the weight configuration at the last epoch and the tangent shows the error gradient at this point. The green dot indicates the next value for the weight in case the learning rate is chosen appropriately as illustrated. In case the learning rate exceeds a certain level, the next weight would result in an higher error compared to the previous epoch. This is indicated by the red dot in Figure 41.

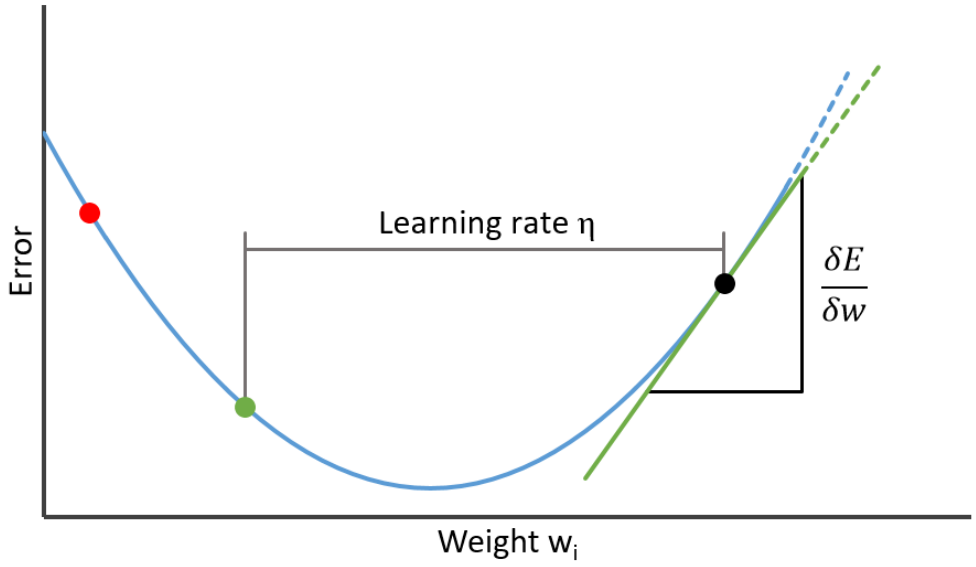


Figure 41 - Learning rate and weight adjustment

Since the loss function owns more than one minima, the goal is to find to global minima. Therefore, different weight initializations are necessary to avoid ending in local minima which would result in a non-optimal solution. These different initializations are realized by using cluster learning. The method uses a cluster of so-called experts which are trained with the same data at same data partitions. Figure 42 illustrates the learning progress of two different experts where Expert 1 (red dots) is ending in a local minima and Expert 2 (green dots) is ending in the global minima of the loss function.

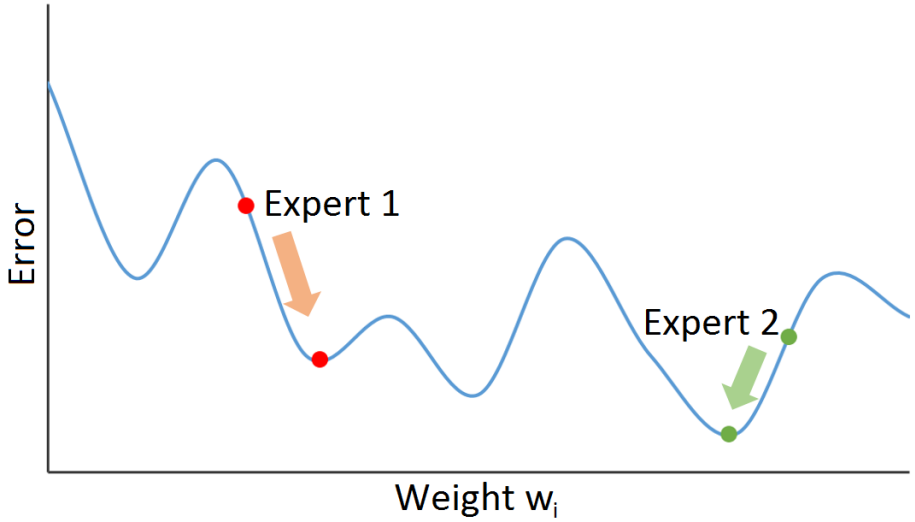


Figure 42 - Cluster learning

During the training, learning and validation errors are calculated to evaluate on error status. This allows to train the network appropriately and avoids overtraining. The effect of overtraining can be identified by comparing learning and validation error as illustrated in Figure 43. The early-stopping point is indicating the validation error minimum. Further training results in exact data modelling and increases the validation error. By comparing the validation error of previous epochs with the current one, an early stopping criteria can be applied to avoid overtraining and achieve time saving. Additionally, the fluctuation of the error can be observed for a certain amount of epochs to stop earlier since no performance improvement can be achieved. In this case, the two error lines of validation and learning would progress in parallel without changing.

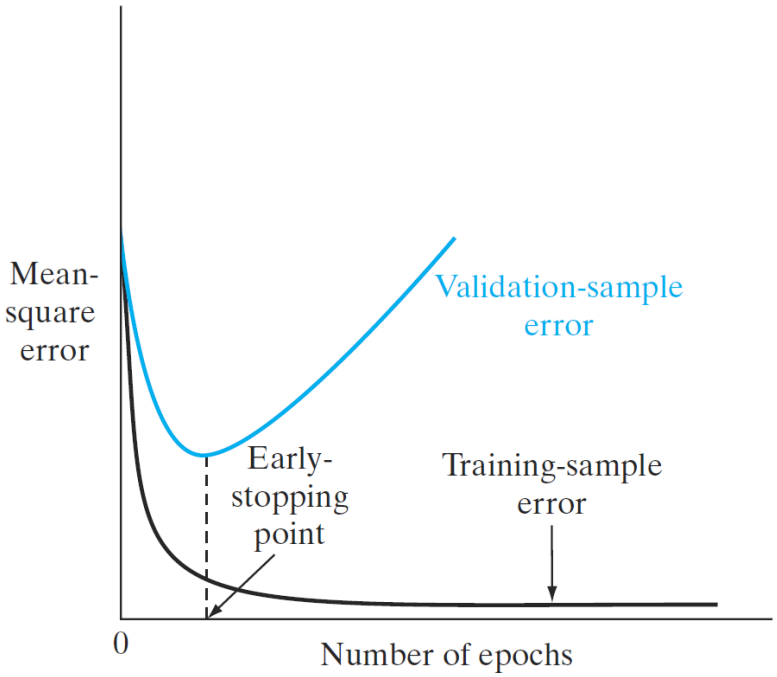


Figure 43 - Training and validation error [14]

To identify the optimal network size of the neural network, different generations are trained, validated and tested. Therefore, the validation error is used to compare the different generations or network sizes. By choosing the network generation with the lowest validation error the effect of overtraining can be avoided in higher generations. Figure 44 illustrates the learning and validation errors of different neural network generations.

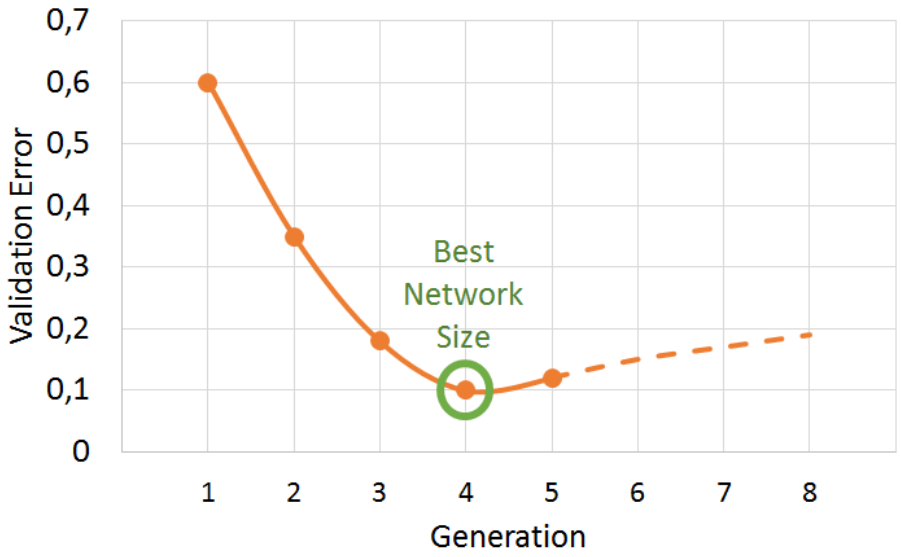


Figure 44 - Evaluation of the network size by validation

### Testing

As described previously, a subset of labeled data is used for testing the performance of the trained and selected model. This allows further evaluation of the performance of the model since the test set is new to the network and statistically independent.

### Sequential Forward Selection

The sequential forward selection is a well known statistical method which allows to identify data channels within the data set which are significant for model performance. During the process, each channel is used to train a neural network individually. The best performing model's channel is selected to be the best and most significant one. This channel is then combined with all the other channels one by one to identify the next more significant data channel. In case of five available channels, 5 + 4 + 3 + 2 + 1 networks have to be trained to obtain a complete ranking.

In Figure 45 below, the first four channels are giving the lowest validation and testing error (yellow bars and blue line). Additional channels are not adding improvement and can be neglected during the training procedure. This saves time due to less data processing.

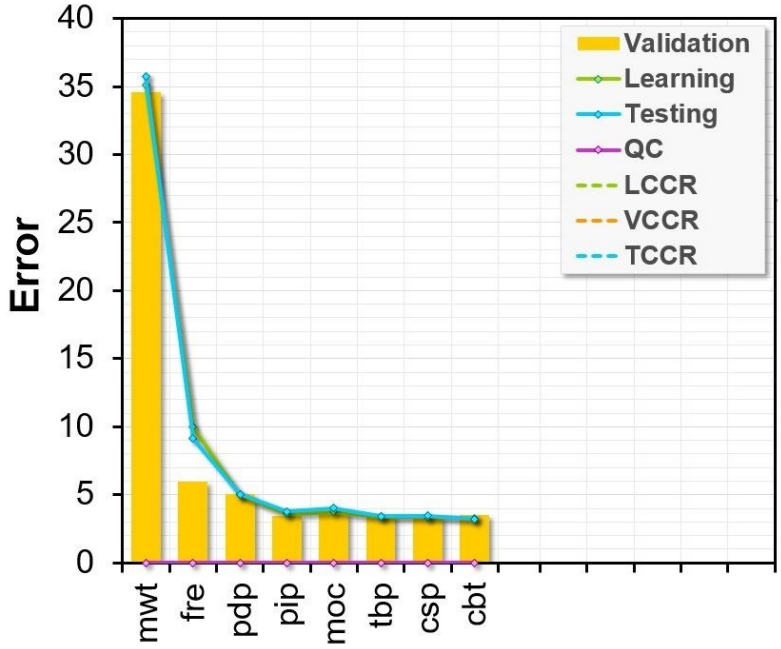


Figure 45 - Sequential forward selection

| | | |
|---|---|---|
| Where | mwt | Motor winding temperature |
| | fre | Frequency |
| | pdp | Pump discharge pressure |
| | pip | Pump intake pressure |
| | moc | Motor current |
| | tbp | Tubing pressure |
| | csp | Casing pressure |
| | cbt | Bottom hole temperature |

### Softmax Layer

A classification problem, where a non-numerical categorical output is used and desired requires the use of a softmax layer. This layer calculates probabilities for each class by using equation 10, which is also known as softmax function or normalized exponential function:

$$Probability\ Wear = \frac{e^{Output\ Wear}}{e^{Output\ Wear} + e^{Output\ Normal} + e^{Output\ Break}} \quad (10)$$

| | | |
|---|---|---|
| Where | Output Wear | Numerical value of the output neuron designated to wear |
| | Output Normal | Numerical value of the output neuron designated to normal |
| | Output Break | Numerical value of the output neuron designated to shaft break |

Due to the properties of the exponential function, the largest positive numerical output of the three different output neurons results in the state with the highest probability. The state with

the highest probability is then selected as the categorical output. Considering all probabilities, the sum of all have to be one.

# 6 Model Building

A model is required in order to process a certain input and produce a desired output of interest. It is the result of a process called model building. When it comes to model building, three different model types are available. Those are:

- Deterministic models
- Statistical models
- Heuristic models

A deterministic model excludes any randomness where the result from a certain input is absolutely reproducible. Perfect examples for deterministic systems are physical laws.

A statistical model is a class of mathematical model and normally specified by mathematical equations which are based on one or more random variables. Also non-random variables can be included. Statistical models typically produce several solutions of equal likelihood which are not entirely reproducible.

Heuristic models are models derived from historical data or observations. These models are built based on data which has been measured or rules which have been observed. A heuristic technique is any approach of problem solving which is sufficient to reach immediate goals. A famous example for such a model is the rule of thumb. The computation or execution of such models is typically very fast.

This thesis is dealing with heuristic, fully data driven models. For model building, artificial intelligence or more precisely, artificial neural networks (ANN) are used.

In the following subchapters, the theoretical approach and procedure of model building with ANNs is discussed. Furthermore, the workflow including data acquisition, quality control, data preparation and data cleansing is described.

## 6.1 Data Acquisition

The data, which is measured during operations is recorded and stored in a database. For classification, surface data measured at the wellhead and downhole sensor data was acquired by accessing LOWIS. The different data channels with associated measurement locations are listed in Table 3 in Chapter 4.2.4 (Measurement Equipment). Figure 46 illustrates the signal schematics of the process network and the data flow. The downhole data is directly collected at the high voltage side of the surface transformer and transferred via transmission control protocol / internet protocol (TCP/IP) to the process network where it is stored in a database.

Within LOWIS, the data is stored in three different time intervals. Those are current, periodic and daily trend. The current trend stores one observation every 10 minutes. The periodic trend is averaging the current trend data over four hours and storing it including statistics such as mean, standard deviation, minimum and maximum value. The daily trend is doing the same averaging procedure for 24 hours and includes statistics over this period.

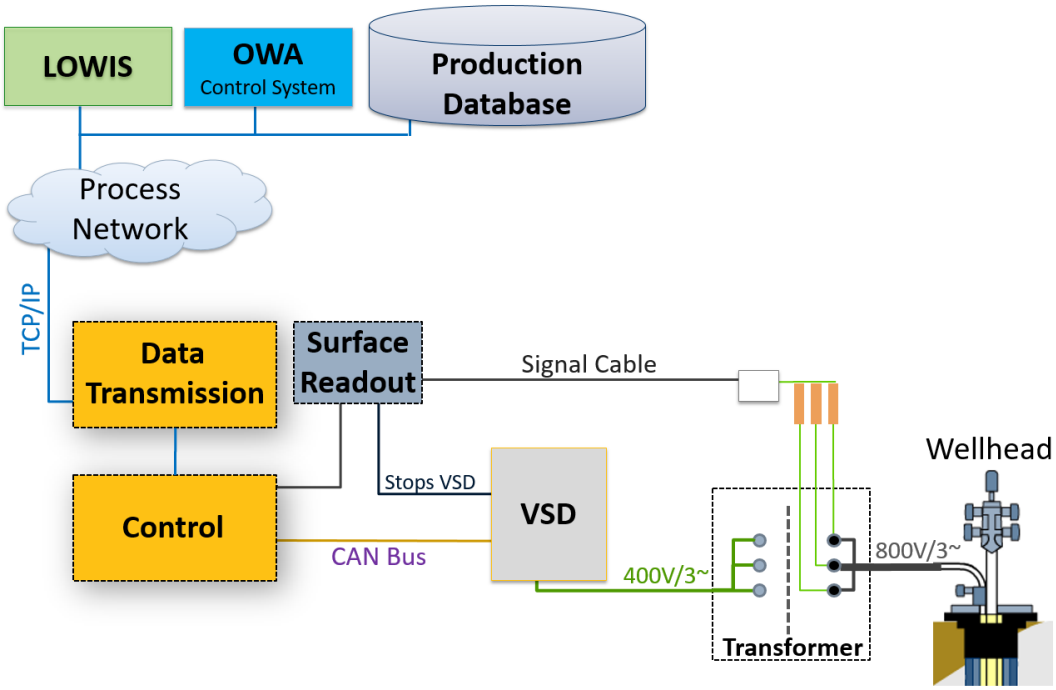


Figure 46 - Signal schematics and data flow

The monitoring tool LOWIS is not just storing the data in a database but also allows visualization of it. Since it was not possible to access the data by writing SQL queries, the data extraction was done with excel spreadsheets well by well. In total, data from 31 producing wells was extracted. Additionally, data from the production database, which contains production data measured at surface separators was extracted for the 31 ESP wells. The data was combined with downhole sensor data and surface data for production rate modelling.

## 6.2 Quality Control

After extracting the data from the databases, the data was screened for failure events which can be utilized for training of a neural network. Unfortunately only a few failure events were found in the stored data. The available failure events associated with the data trend in which the evenst are captured, can be found in Table 6 below. Column “Sampling” is related to the different data trends or sampling intervals current (10min), periodic (4h) and daily (24h).

Table 6 - Available failure events for machine learning

| Stored trend | Sampling | Shaft break | Pump wear | Seized pump |
|---|---|---|---|---|
| Current | 10min | 0 | 1 | 0 |
| Periodic | 4h | 3 | 1 | 1 |
| Daily | 24h | 3 | 1 | 1 |

In order to get a better overview about the data itself, statistics were applied and the different channels were cross-plotted against each other. This allowed finding dependencies between different data channels and revealed information regarding data quality and consistency.

Furthermore, similarities between wells have been identified. Figure 47 illustrates a matrix cross-plot of one production well.

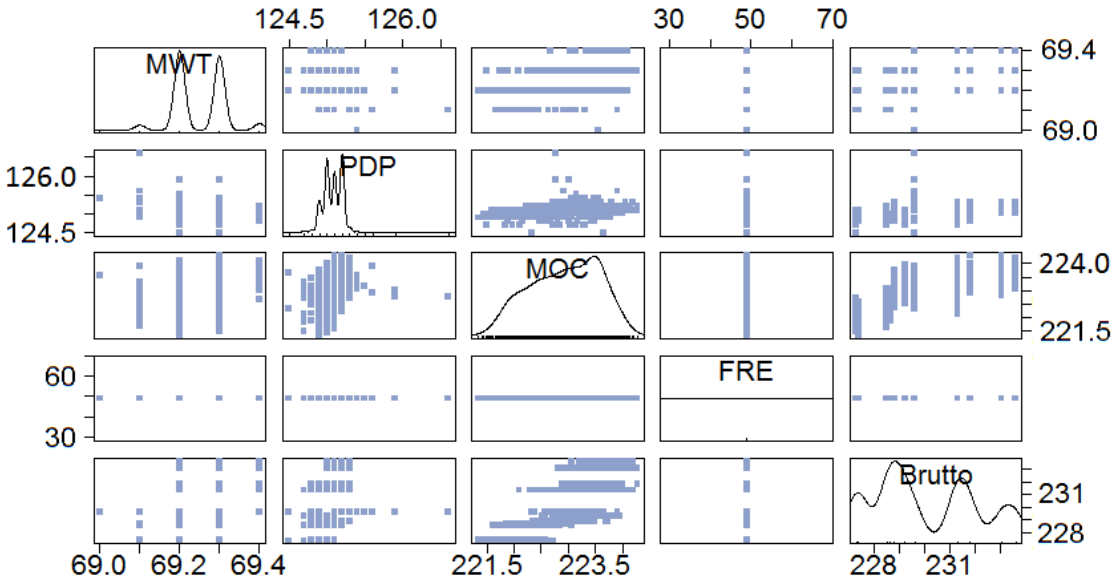


Figure 47 - Cross-plot matrix of different parameters from a single well

| | | |
|---|---|---|
| Where | MWT | Motor winding temperature [°C] |
| | PDP | Pump discharge pressure [bar] |
| | MOC | Motor current [A] |
| | FRE | Frequency [Hz] |
| | Brutto | Gross production rate [$m^3/d$] |

Additionally, well specific statistics were computed and exported to tables. Table 7 shows a reduced parameter list and the calculated statistical features. The data for plotting Figure 47 and computing Table 7 is originating from the same well. Hence, both are showing similar results.

Table 7 - Data statistics (reduced parameters) of a single well for QC

| Parameter | Motor winding temperature | Pump discharge pressure | Motor current | Frequency |
|---|---|---|---|---|
| Average | 69.3 °C | 123.8 bar | 223.14 A | 48.99 Hz |
| Minimum | 68.8 °C | 122.9 bar | 221.34 A | 48.99 Hz |
| Maximum | 69.5 °C | 126.6 bar | 226.16 A | 48.99 Hz |
| Standard Dev. | 0.08 °C | 0.58 bar | 0.63 A | 0.00 Hz |
| Variance | 0.01 $°C^2$ | 0.34 $bar^2$ | 0.40 $A^2$ | 0.00 $Hz^2$ |
| Nr. of values | 10000 | 10000 | 10000 | 10000 |
| Nr. of outliers | 0 | 0 | 0 | 0 |

## 6.3 Data Cleansing

In order to prepare the extracted data for later machine learning, data cleansing was necessary. By plotting the data in time series, it was possible to access the data visually. This gave a first idea about the data properties and allowed to write filters within R to get optimal results. Overall, four different filters were used: Outlier removal, time stamp handling, missing values treatment and plausibility check. Figure 48 illustrates a typical example of an outlier (upper left red circle), which can easily be removed by finding suitable limits for each channel. The limits were set in accordance with the sensor specifications. In case no measurement limitations were given, appropriate limits for each channel were chosen after analyzing the data with standard statistics such as average, minimum and maximum value.

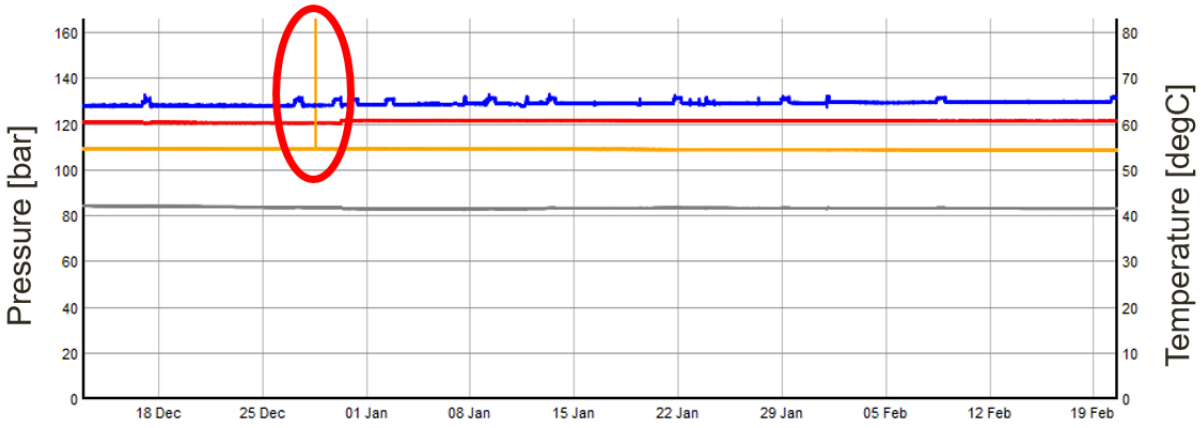


Figure 48 - Example for outlier removal

Additionally, inconsistent time stamps were handled in order to get a proper synchronized data set. Therefore, the time stamps of each channel were aligned with respect to the different sampling intervals.

In case of missing values, a moving window was used to detect and evaluate the size of the missing data. In case of small lacks, the last existing value was used to fill the gap. In case of too large sections, no data manipulating operation was performed to avoid possible distortion. Data statistics helped to monitor the effect of the treatment. The filling of missing values was carried out channel-wise.

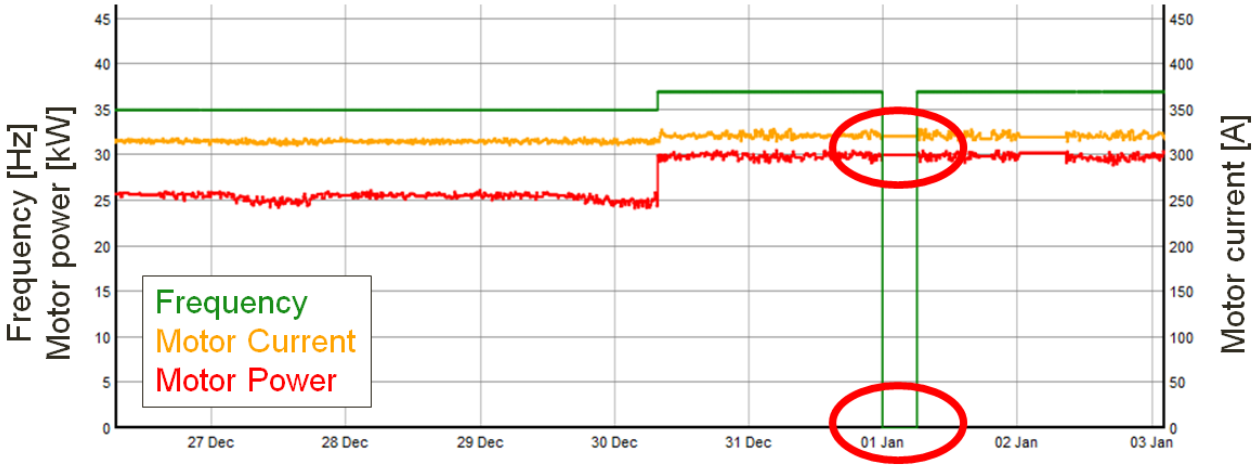


Figure 49 - Example for plausibility check

Figure 49 shows an example where a plausibility check was intended to interfere. Depending on system settings, data channels kept recording data even though the pump was switched off. The result of this misleading recording operation can be seen in the figure above, where the motor current and power should be zero when the frequency is zero. Since the frequency was given from the operator, it could be used to create a plausibility check. Therefore, channels such as motor current and power (Figure 49 – yellow and red line) were set to zero within the time period indicated within the red circles.

## 6.4 Data Preparation

Due to lack of different failure events and types, artificial data sets including shaft break and pump wear were modeled. The latter was created by using DesignRite, an artificial lift design and optimization software from Schlumberger. By changing head degradation within the software tool, different pumping efficiencies were simulated. The resulting pump curves were used to find proper settings for creating artificial pump wear trends. Therefore, real data channel trends of correctly working pumps were manipulated to show all characteristics of pump wear while maintaining measurement noise. Random variables were used to introduce different degrees of pump wear by influencing the various parameter gradients.

Secondly, shaft break failure sets were created by manual data manipulation. Since shaft break events are over within a few minutes to hours, data manipulation was done by hand using an old real life example of a shaft break as reference.

The artificially created data sets were built by manipulation of already cleaned data. Therefore, it was not necessary to perform data cleansing as described in Chapter 6.3 (Data Cleansing). In total, nine data sets including pump wear and nine data sets including shaft break have been prepared. On mixed case, including both failure types was created. All of those are referred to as artificial data sets.

In order to use the clean data sets for machine learning, the data had to be labeled. This process of data interpretation was carried out by the hand of visualized time series data.

Visualization was done with dygraph, a plotting package written in the programming language R. The labels for classification included three different states: Normal (normal operation), wear (pump wear) and break (shaft break).

## 6.5 Failure Classification

In this subchapter, all steps of failure classification are described.

### 6.5.1 Feature Preparation

Features are the elements of the input vectors, where each element is fed to an input neuron. After data extraction, fourteen features were available within each data set. Four of those fourteen features, the leakage measurements, were ignored, because they are not contributing to mechanical failure. Instead, two features were created by calculation of the first derivative of pump intake and pump discharge pressure. A sequential forward selection can be used to find a subset of features, which represents the data appropriately and results in accurate model. Due to too long computation times, complete SFS were carried out only for production rate modeling and shaft break classification. The features selected for model building are listed in Table 8. A green colored field indicates a used feature while a red colored field is indicating a not used one. For some data set arrangements, it was not possible to use all features as indicated, since a few were not available in all corresponding data sets. Hence, slight modifications of the failure classification features were done and are indicated when applicable.

Table 8 - Features and field of application

| Feature | Type | Failure Classification | Production Modeling |
|---|---|---|---|
| Motor winding temperature | Measured | Task 1, 2, 4, 5 | Selected by SFS |
| Bottom hole temperature | | Task 1, 2 | - |
| Pump intake pressure (PIP) | | Task 1, 2, 4, 5 | Selected by SFS |
| Pump discharge pressure (PDP) | | Task 1, 2, 4, 5 | Selected by SFS |
| Tubing pressure | | Task 1, 2 | - |
| Casing pressure | | Task 1, 2 | - |
| Motor current | | Task 1, 2, 4 | - |
| Motor power | | - | - |
| Frequency | | - | Selected by SFS |
| Vibrations | | Task 1, 2, 5 | - |
| 1st derivative of PIP | Calculated | Task 1, 2, 4 | - |
| 1st derivative of PDP | | Task 1, 2, 4 | - |

### 6.5.2 Feature Selection

When artificial data is used, all available features were selected for training since the SFS did not result in a clear selection in an appropriate period. Hence, different features were used for the various tasks described in Table 9.

The result of the SFS for failure classification is presented in Figure 50 below. The validation error during the SFS is only slightly decreasing, while the classification rates are showing an uptrend. Nevertheless, there is no significant improvement recognizable. However, the SFS was not completely run because of too long computation times as mentioned above.

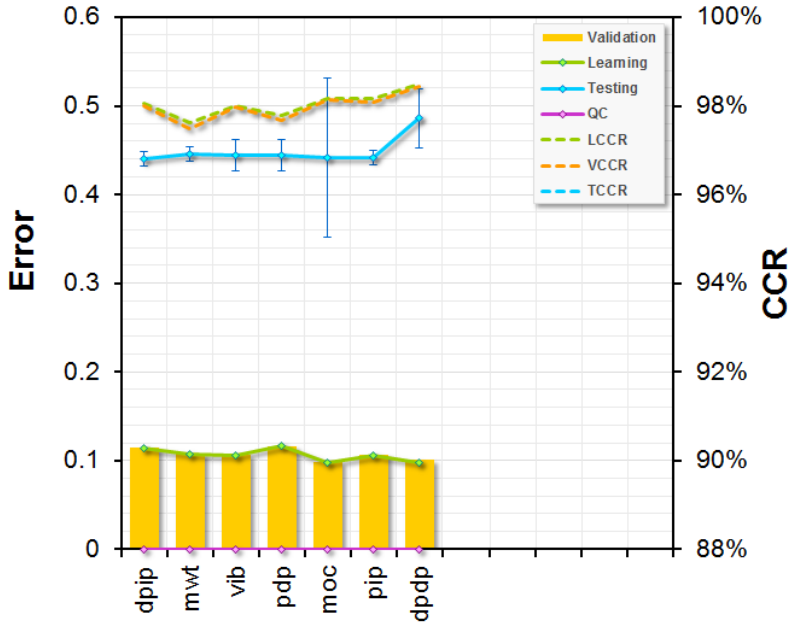


Figure 50 - Sequential forward selection for failure classification

| | | |
|---|---|---|
| Where | dpip | 1st Derivative of pump intake pressure |
| | mwt | Motor winding temperature |
| | vib | Vibrations |
| | pdp | Pump discharge pressure |
| | moc | Motor current |
| | pip | Pump intake pressure |
| | dpdp | 1st Derivative of pump discharge pressure |
| | CCR | Correct classification rate |

### 6.5.3 Methodology

Machine learning, which includes learning, validation and testing was performed in cVision (Version 4.0, Neuro Genetic Solutions), which automatically implements a softmax layer for output generation when using a categorical output. For data partitioning, the data was split in three parts for all tasks: 60% learning, 20% validation and 20% testing. This split varied, when

training arrangements such as leave-one-out or leave-two-out were used. Furthermore, a completely connected perceptron (FF neural network) was used for this time independent classification task. The architecture was varied from 0 (logistic regression) to a maximum of 15 hidden neurons depending on the task. The feed forward neural net used is completely connected. Hence, no other layers are in place.

In order to compare different models against each other, various combinations of data set arrangements were used for model building. Table 9 lists the different tasks roughly and shows the used training arrangements for each of them. Additionally, the available number of data sets is given. This number is equal to the number of wells, since each data set is obtained from another well. The different training arrangements are explained in the following:

- Single: Each set is used for learning, validation and testing.
- Leave one out: (LOO) All sets are used for learning and validation besides one. This left out is used for testing.
- Leave two out: (LTO) One set is used for training and two others are used for testing.
- All together: All sets are used for learning, validation and testing.

Table 9 - Task list and training arrangements

| Task | Description | Sampling | Nr. of sets | Training arrangements |
|---|---|---|---|---|
| 1 | Pump wear (ADS) | 10min | 9 | Single, LOO, all together |
| 2 | Shaft break (ADS) | 10min | 9 | Single, LOO, all together |
| 3 | Combination of 1 & 2 (ADS) | 10min | 1 | Single |
| 4 | Pump wear (RL + ADS) | 10min | 9 | Single, LOO, all together |
| 5 | Shaft break (RL) | 4h | 3 | Single, LOO, LTO, all together |

Where ADS Artificial data sets
RL Real life data/example

The results of the different tasks are presented in Chapter 6.5.4 (Results and Quality Control). Additionally, detailed information of all trained neural networks can be found in the appendix.

### Task 1 – Pump Wear (Artificial Data Sets)

This task includes training all nine artificial data sets with pump wear individually, as leave-one-out and all together. For model building, the features indicated in column “Failure Classification” of Table 8 were used.

### Task 2 – Shaft Break (Artificial Data Sets)

This task includes training all nine artificial data sets with shaft break individually, as leave-one-out and all together. For model building, the features indicated in column “Failure Classification” of Table 8 were used.

### Task 3 – Combination of Pump Wear and Shaft Break (Artificial Data Sets)

This case includes a combination of pump wear and shaft break in one artificial well data set. Furthermore, this is the only case that deals with an extended range of features than stated in Table 8. The training of the model was carried out by using all 9 artificial data sets of pump wear and all 9 of shaft break. The model was found to perform best with a network size including 10 hidden neurons. The data set with the failure combination was then used for testing. The used features for building the model are listed in Table 10:

Table 10 - Features for model building for pump wear and shaft break (Task 3)

| | |
|---|---|
| Measured | Motor winding temperature<br>Motor current<br>Tubing pressure<br>Pump intake pressure<br>Pump discharge pressure<br>Vibrations |
| Computed | 1st Derivative of motor winding temperature<br>1st Derivative of motor current<br>1st Derivative of tubing pressure<br>1st Derivative pump intake pressure<br>1st Derivative pump discharge pressure<br>Pressure ratio (intake pressure over discharge pressure) |

A visualization including an engineers data interpretation is illustrated in Figure 51. The shaded areas are related to the data interpretations, where the white are represents the operation range where no failure or malfunction occurs. The blue area indicates pump wear and the red area indicates shaft break. The arrows shall indicated the trend of the individual feature during pump wear, since the trend change is difficult to observe on the plotted scale. On the very left of Figure 51, the shaft break event can be found. The pump discharge pressure is rapidly dropping and equilibrating with the pump intake pressure, which is increasing due to loss of production. As a result of production loss, the motor is no longer cooled and an increase in motor winding temperature occurs.

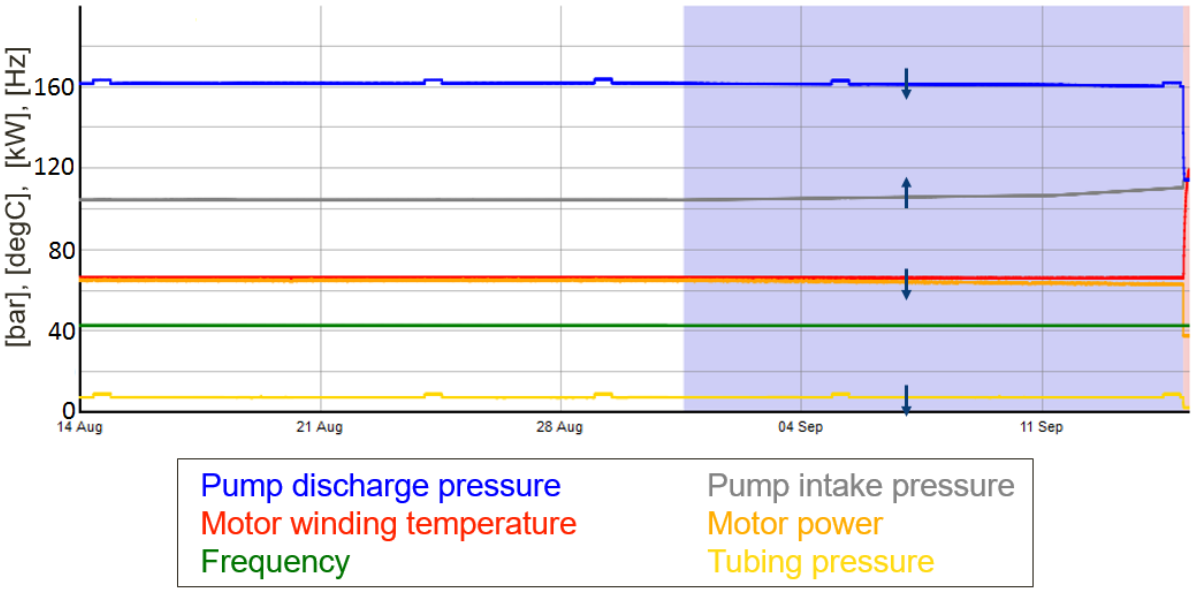


Figure 51 - Data visualization of an artificial data set including a combination of pump wear and shaft break

### Task 4 – Pump Wear (Real Life Example and Artificial Data Sets)

Task 4 combines real life data with artificially created data. The real life data is obtained by measurements taken at well 5, which was also used for creating an artificial case of pump wear. Therefore, the concerned artificial data set is replaced by the real life data of the same well. The training arrangements including eight artificial data sets and one real life example were “leave one out” and “all together”. Additionally, the real life data set is trained individually as well. For model building, the features indicated in column “Failure Classification” of Table 8 were used.

### Task 5 – Shaft Break (Real Life Examples)

This task includes training of three different real life examples with shaft break individually, in leave-one-out, leave-two-out and all-together training arrangement. For modeling, artificial neural networks with no hidden unit were used because a linear model was found to perform appropriately. Hence, these models are based on logistic regression. Additionally, a sequential forward selection was carried out while training with all wells together. The three data sets including shaft break events are available in four hour sampled intervals and consist of just a few observations each. The data of well 3 including data labels is illustrated in Figure 52.

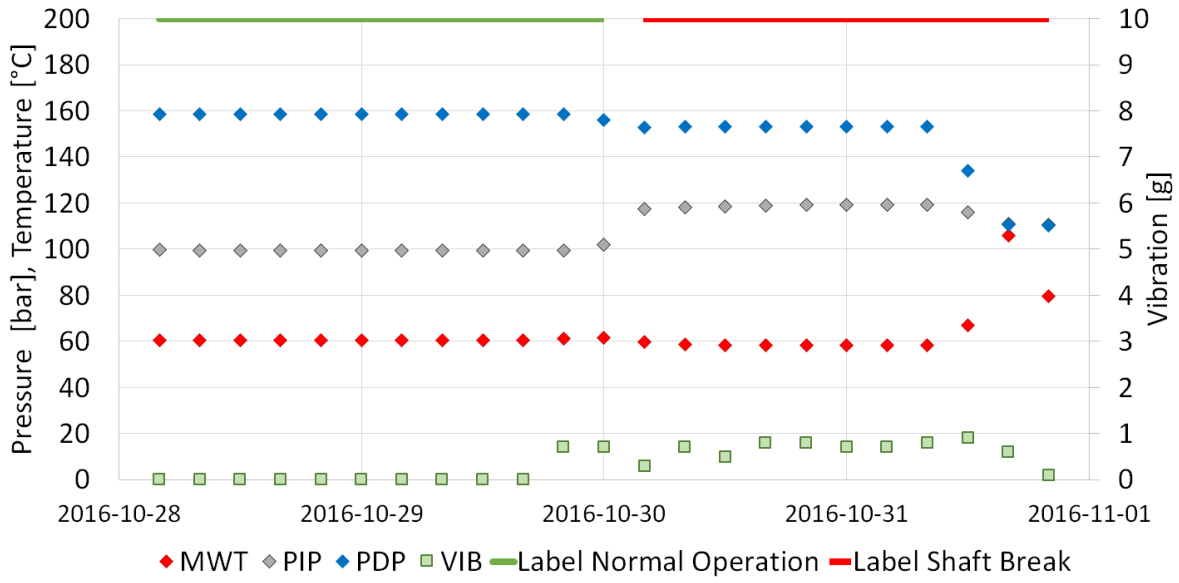


Figure 52 – Periodic shaft break data of well 3 including data labels

| | | |
|---|---|---|
| Where | MWT | Motor winding temperature |
| | PIP | Pump intake pressure |
| | PDP | Pump discharge pressure |
| | VIB | Vibration |

In order to obtain better statistical representation, the data was extended by using the existing mean values and standard deviations. This interpolation procedure added 15 observations to each interval. For model building, the features indicated in column “Failure Classification” of Table 8 were used.

### 6.5.4 Results and Quality Control

The results of failure classification are presented according to the different classification tasks listed in Table 9. Plots which are presenting model summaries or comparisons including the correct classification rate are always referring to the testing set in this regard (unless stated otherwise).

#### Task 1 - Pump Wear (Artificial Data Sets)

The result of the model building of task 1 is presented in Figure 53. For each individual artificial data set, the performance in terms of correct classification rate (CCR) of the test set is excellent. In all cases, 97% are exceeded. Well “1 – 9” represents the result of the training including all data sets. The correct classification rate for this training arrangement is 99%.

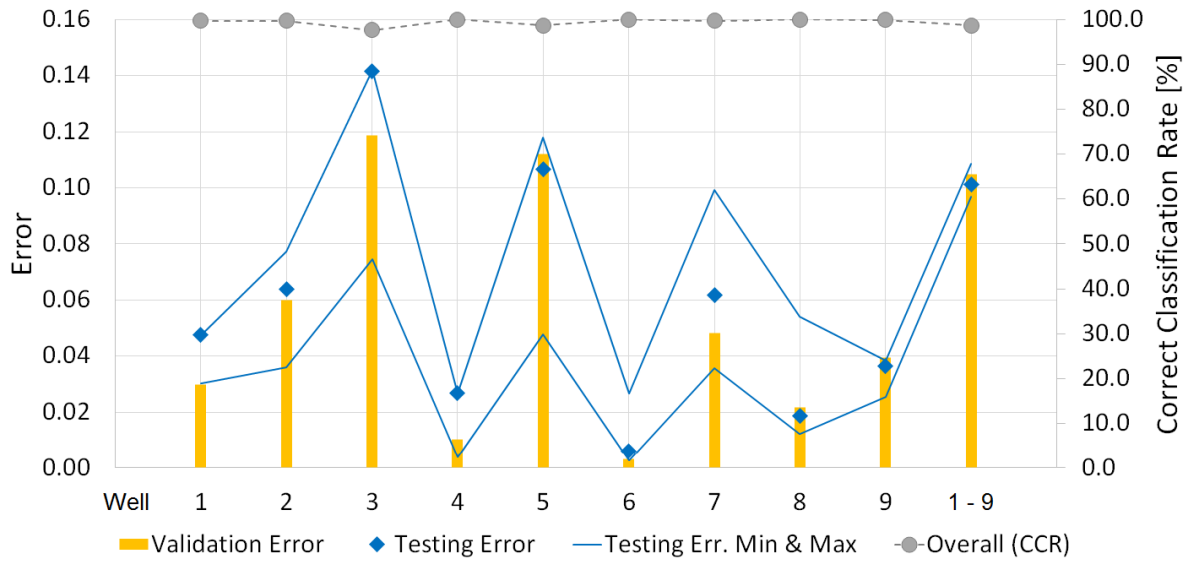


Figure 53 - Model evaluation of artificial data set based classifiers for pump wear: Task 1, Training arrangement “single” & “all together”

The confusion matrix of well 3 is presented in Table 11. The table is including the classification results of all three different data partitions. The green and red shaded cells are indicating the correct and incorrect classified observations respectively. There is no significant difference between the correct classification rates.

Table 11 - Confusion matrix of well 3 (Task 1)

| **Partition** | **Learning** | | **Validation** | | **Testing** | |
|---|---|---|---|---|---|---|
| Overall CCR | 98.1% | | 98.5% | | 97.6% | |
| Status | Normal | Wear | Normal | Wear | Normal | Wear |
| CCR | 98.8% | 97.7% | 99.0% | 98.2% | 98.3% | 97.1% |
| Normal | **2092** | 84 | **719** | 21 | **736** | 33 |
| Wear | 25 | **3497** | 7 | **1152** | 13 | **1117** |

The average network size including the best network generation of each case is 13 hidden neurons. The maximum network size during training was 15 neurons in the hidden layer.

Figure 54 illustrates the result of the leave-one-out arrangement. From special interest is well 5, which is classified with poor performance when tested. Low performances in classification occur most likely due to statistical differences of features between the training sets and testing set. No statistical analysis was performed to confirm this assumption.

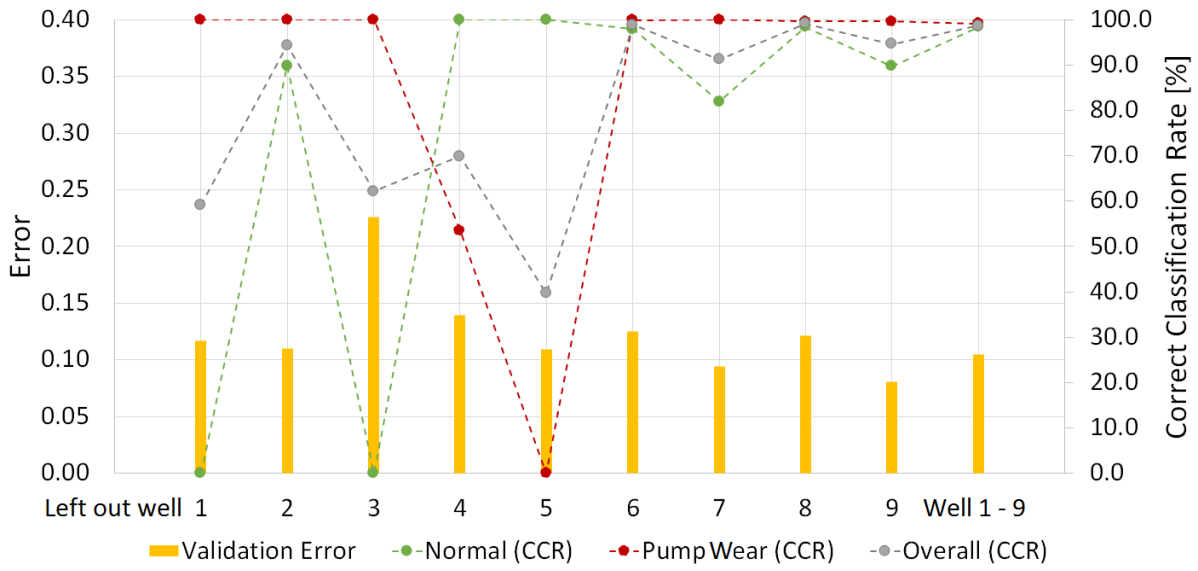


Figure 54 - Model evaluation of artificial data set based classifiers for pump wear: Task 1, Training arrangement “leave one out” & “all together”

More information regarding the models of the different well data sets can be found in the appendix.

### Task 2 – Shaft Break (Artificial Data Sets)

The result of the model building for single well training as well for all wells together is showing correct classification rates of greater 99% in all cases. Figure 55 is illustrating the outcome of this analysis. The overall network architecture is rather simple in terms of network size. The average network size including the best network generation of each case is 6 hidden neurons. The maximum network size during training was 15 neurons in the hidden layer.

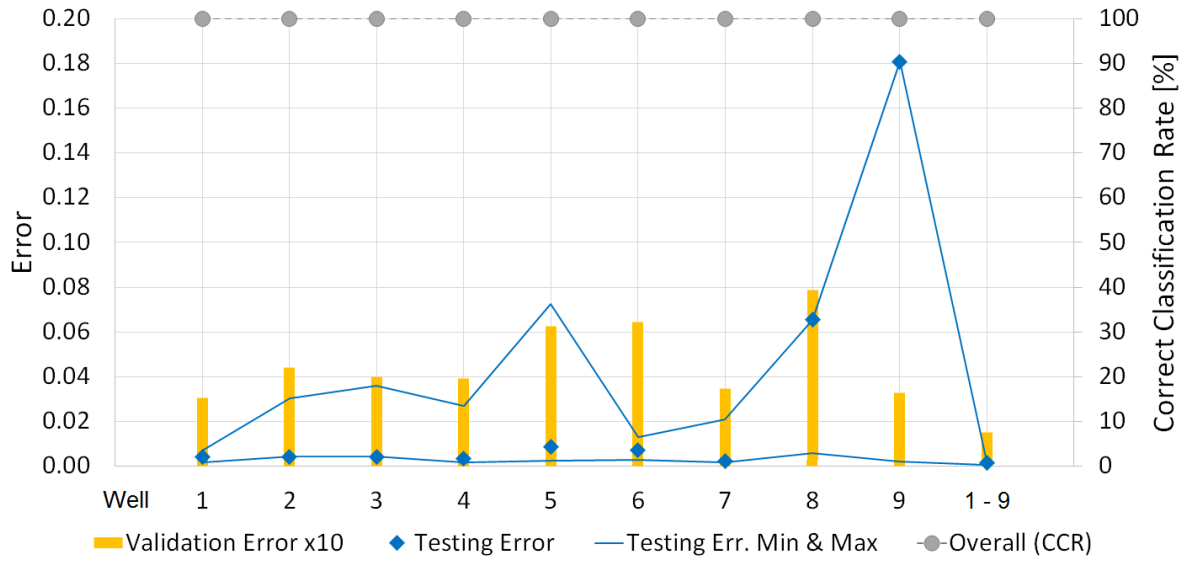


Figure 55 - Model evaluation of artificial data set based classifiers for shaft break: Task 2, Training arrangement “single” & “all together”

Figure 56 shows the model evaluation when applying the training arrangement “leave one out”. Additionally, the result of the training when all wells are included is shown for comparison. All classifiers perform above an overall correct classification rate of 90% (related to testing) beside well 1 and well 9. Both fail in classifying normal pumping conditions.


Figure 56 - Model evaluation of artificial data set based classifiers for shaft break: Task 2, Training arrangement “leave one out” & “all together”

Since the test sets are all of comparable size and the validation error of all models is in the same range, the reason for this high miss-interpretation is most likely a significant difference in features’ magnitudes and data consistency between training sets and testing set. No statistical analysis was performed to confirm this assumption.

More information regarding the models of the different well data sets can be found in the appendix.

### Task 3 – Combination of Pump Wear and Shaft Break (Artificial Data Sets)

The result of testing with the failure combination data set is visualized in Figure 57. The status with the highest probability is giving the by the model predicted status. Especially, the shaft break probability curve (red line) immediately peaks when the shaft break occurs. In the beginning of pump wear (blue shaded area), miss-classification occurs for a short period when pump wear is wrongly classified as normal operation (green line). It can be observed, that the blue pump wear curve is climbing belated.

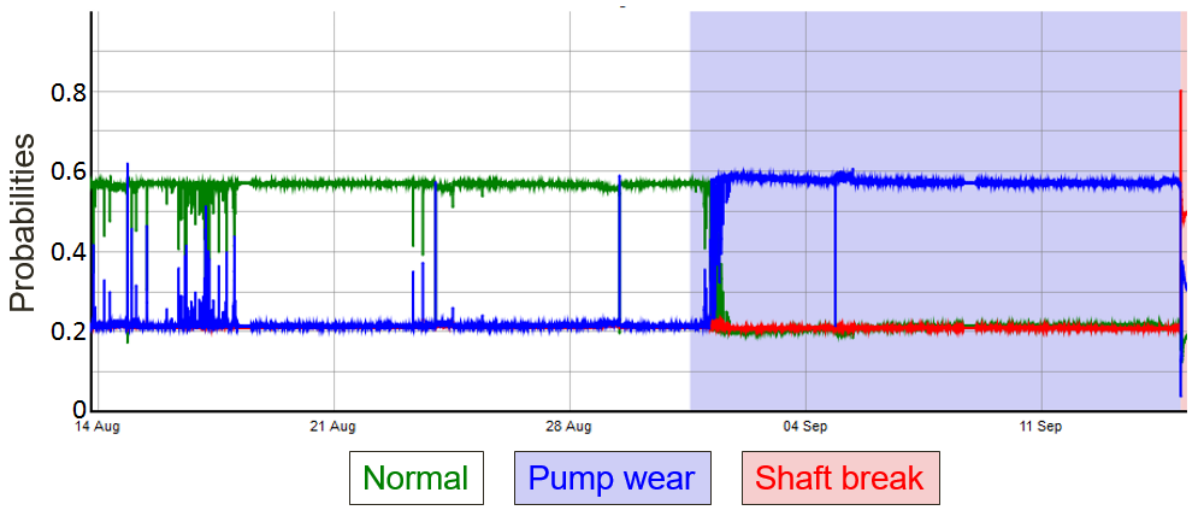


Figure 57 - Probability curves of the built predictive model for classifying pump wear and shaft break (Task 3)

A better quantitative representation is given in Table 12. The table is presenting the confusion matrix of the testing data set. The overall correct classification rate is 98.3 %, where no individual correct classification rate lies below 95 %. Only a minor number of observations is classified wrong. Hundred four as pump wear labeled observations were classified as pump wear. Vice versa, nineteen observations were classified wrongly.

Table 12 - Confusion matrix of the built predictive model for classifying pump wear and shaft break (Task 3)

| **Confusion Matrix** | Normal Operation | Pump wear | Shaft Break |
|---|---|---|---|
| Overall correct classification rate | 98.3 % | | |
| Correct classification Rate | 99.6 % | 95.0 % | 100.0 % |
| Normal operation | 4978 | 104 | 0 |
| Pump wear | 19 | 1991 | 0 |
| Shaft break | 0 | 0 | 28 |
| Wrong predicted observations | 19 | 104 | 0 |
| Nr. of observations | 4997 | 2095 | 28 |

The model for this task was created by a completely connected perceptron with 10 hidden units.

### Task 4 – Pump Wear (Real Life Example and Artificial Data Sets)

In this task, different training arrangements were tested. Artificial and real life data (well 5 RD) is used individually and in combination to classify normal operation and pump wear. In Figure 58, the result of the “single” and “all together” setup is presented. All models are predicting with a CCR of higher than 90%. Only well 3 and “1-9” (representing training of a model including all well data sets) are performing slightly below all the other classifiers. The result of

well 5 (real life data) shows that the model built with well-own data is capable of predicting pump conditions with an accuracy of about 99%.

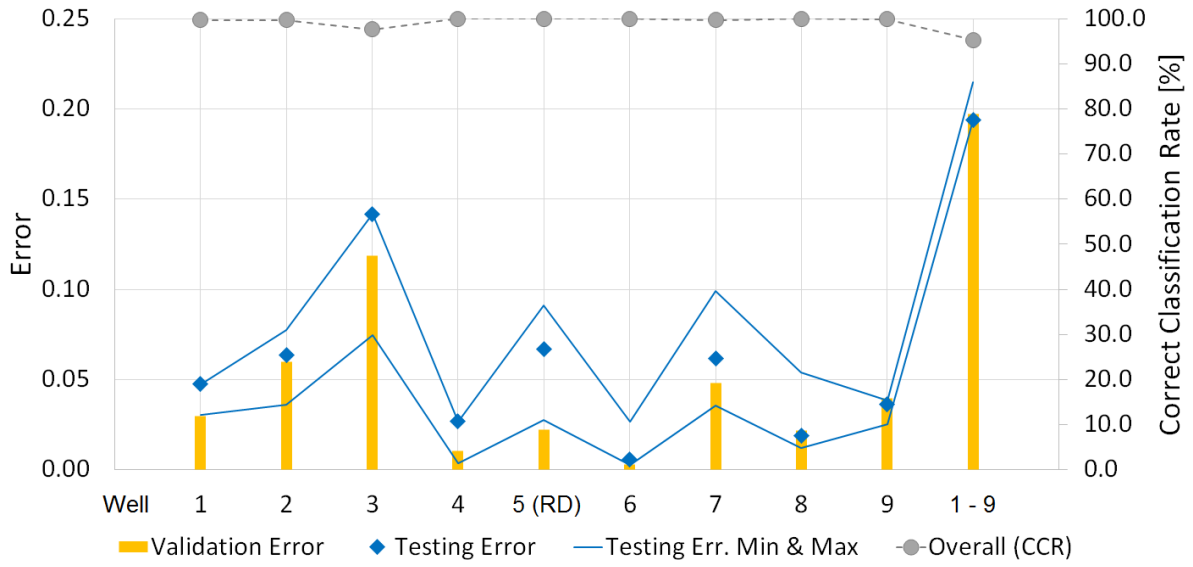


Figure 58 - Model evaluation of artificial and real data based classifiers for pump wear: Task 4, Training arrangement “single” & “all together”

In Figure 59, the results of the leave-one-out approach are presented. In order to highlight the miss-interpretation status-wise, the CCR of the test set for normal operation (green) and pump wear (red) are plotted. Almost all models show a very low CCR for one of the two states.

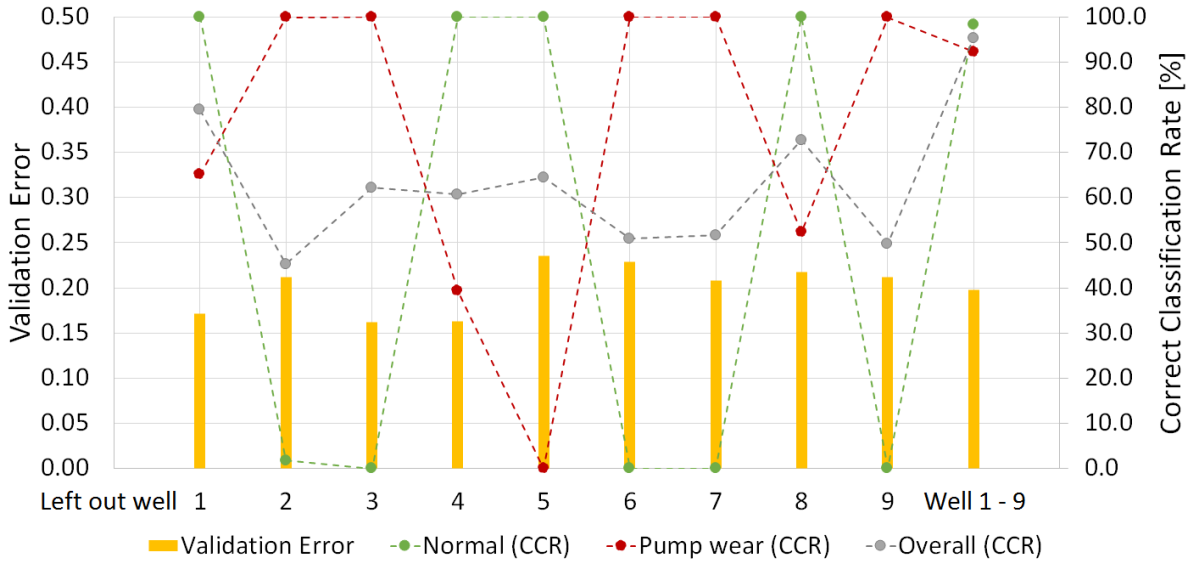


Figure 59 - Model evaluation of artificial and real data based classifiers for pump wear: Task 4, Training arrangement “leave one out” & “all together”

As stated in task 1, the leave-one-out training of these models also has been done by using artificial data of well 5 instead of the real life data. It can be said that the inclusion of well 5 (RD) in training data is influencing the model negatively in terms of testing performance, since the CCRs of models in Figure 54 are showing better results. The reason might be the large size of the real life example, which is about double the size of an artificial data set.

Moreover, the model which is built while leaving well 5 (RD) out performs low when tested. This indicates, that the training data (well 1 - 4 & 6 - 9) in this case might be significantly different from the test set well 5 (RD). Table 13 shall outline the data set size of well 5 (RD) as well as the fact, that also the artificial data set well 5 is failing when tested during task 1.

Table 13 - Comparison of the confusion matrices of the leave-one-out approach for real and artificial data of well 5 for testing

| Partition | Testing | | Testing | |
|---|---|---|---|---|
| Task | Task 1 | | Task 4 | |
| Data | Left out well 5 (AD) | | Left out well 5 (RD) | |
| Overall CCR | 39.7% | | 64.4% | |
| Status | Normal | Wear | Normal | Wear |
| CCR | 100.0% | 0.0% | 100.0% | 0.0% |
| Normal | 3895 | 5904 | 25370 | 14002 |
| Wear | 0 | 0 | 7 | 4 |

The ESP in well 5 is located around 200m above all other pumps which are investigated in this thesis. This difference might be the reason for high miss-interpretation. The significant gap in features' magnitudes between training sets and testing set is complicating model building.

More information regarding the models of the different well data sets can be found in the appendix.

### Task 5 – Shaft Break (Real Life Examples)

The results of the SFS are illustrated in Figure 60. The procedure was carried out with an arrangement of all wells together. The features pump discharge pressure and pump intake pressure are showing already very high CCRs and reduced validation and testing error.

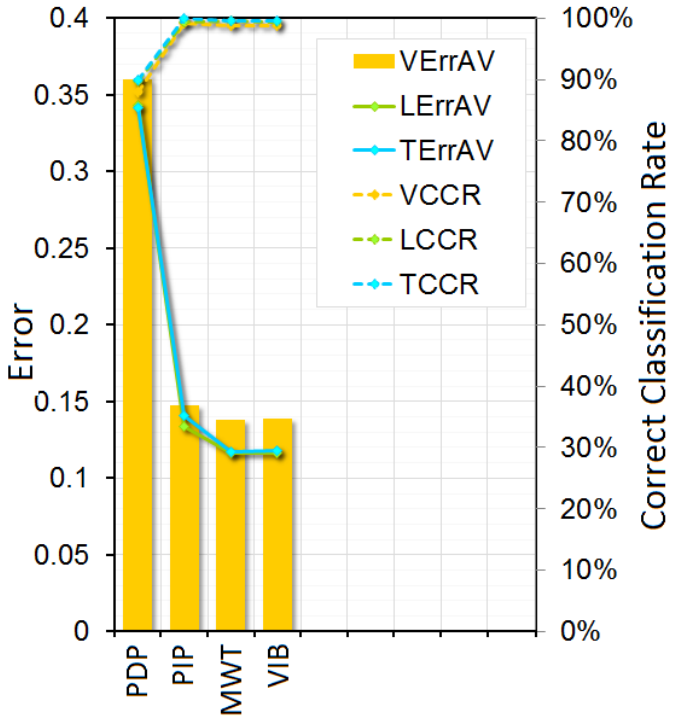


Figure 60 - Result of the sequential forward selection for task 5

| | | |
|---|---|---|
| Where | PDP | Pump discharge pressure |
| | PIP | Pump intake pressure |
| | MWT | Motor winding temperature |
| | VIB | Vibrations |
| | VErrAV | Averaged validation errors |
| | LErrAV | Averaged learning errors |
| | TErrAV | Averaged testing errors |
| | VCRR | Validation (overall) correct classification rate |
| | LCCR | Learning (overall) correct classification rate |
| | TCCR | Testing (overall) correct classification rate |

For the other presented results in this subchapter, all four features (as shown in Figure 60) are used.

To investigate on cross validation, different CV subsets were used to evaluate the influence of data partitioning. Figure 61 shows the comparison of five models which were built by including all wells for training and testing. Five different cross validations were applied, where the result of the different models is presented below. All five CVs are performing well and above 98% of the correct classification rate (testing overall). Considering validation and testing errors, there is only a small variance between the different models.

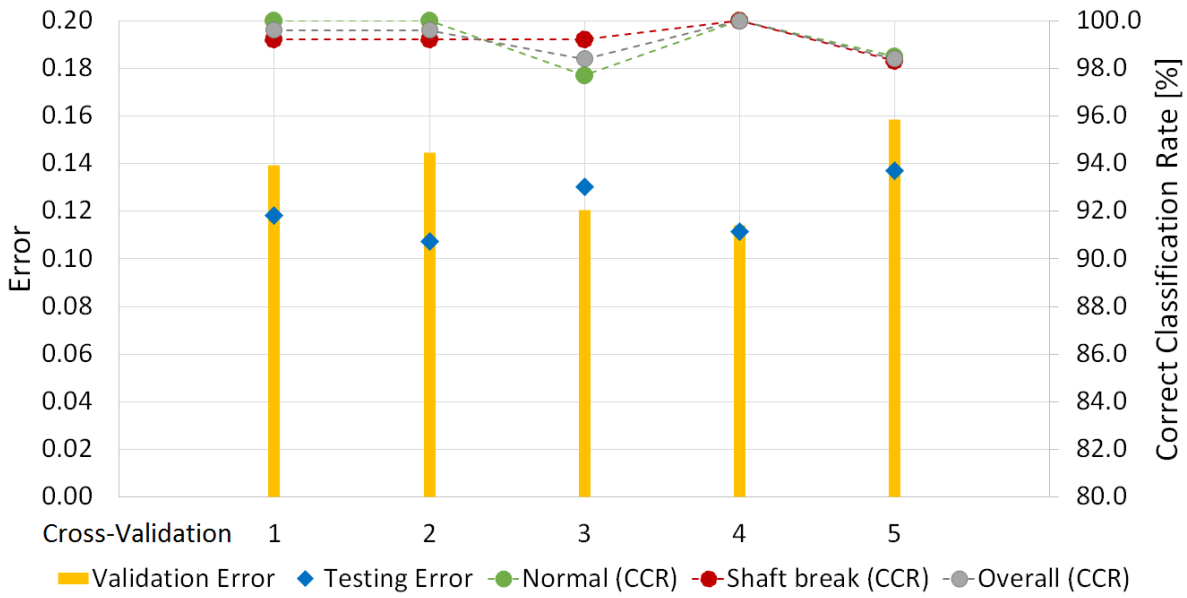


Figure 61 - Comparison of CCR of the test set of different cross validation families for training arrangement "all"

Table 14 shows the overall CCRs of all 5 different cross validations for learning, validation and testing. The fact, that almost no variance occurs in any CV set shows that the data is partitioned in a statistical representative manner. This analysis shows also that in this case a multilinear regression model performs successfully in failure classification of shaft break.

Table 14 - Overall correct classification rates of different cross validation families for training arrangement “all”

| CV | Learning | Validation | Testing |
|---|---|---|---|
| 1 | 99.3% | 98.8% | 99.6% |
| 2 | 99.7% | 98.0% | 99.6% |
| 3 | 99.3% | 100.0% | 98.4% |
| 4 | 99.1% | 99.6% | 100.0% |
| 5 | 99.6% | 99.2% | 98.4% |

The comparison of the models built by including each well individually is presented in Figure 62. The validation and testing errors are relatively low and the classification rates exceed 99% in all cases. For comparison, the result of the model built when including all wells for training is presented as well. This classifier shows slightly less performance in terms of CCR. But due to more used data sets during training, the model is more generalized. Nevertheless, all models are capable of classifying shaft break with a high accuracy.

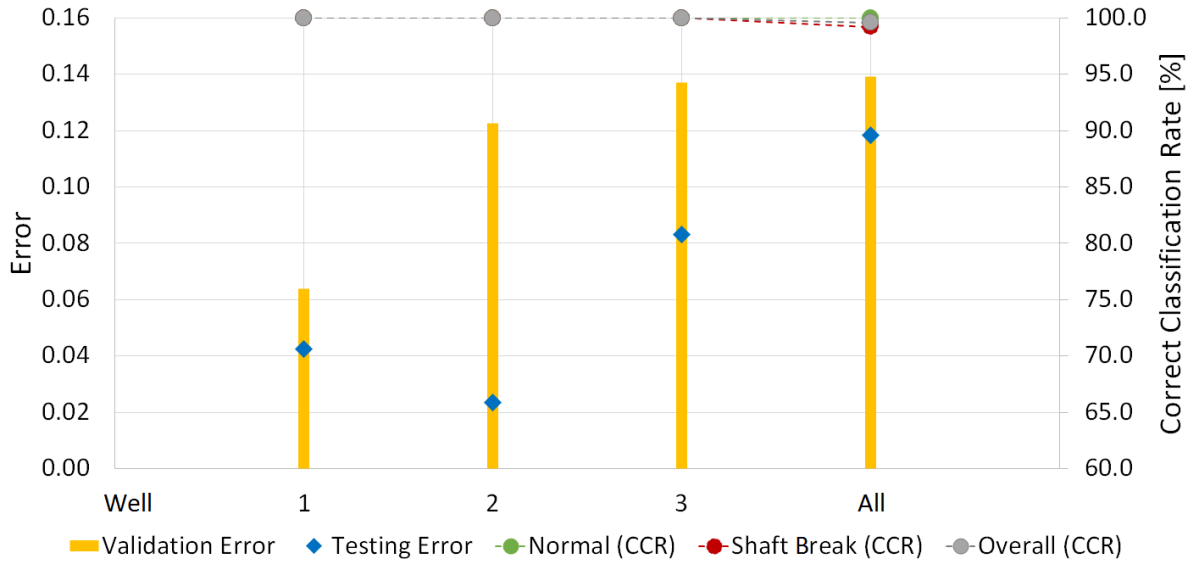


Figure 62 - Comparison of the single well based classifiers

Figure 63 shows the results of the leave-one-out arrangement. The validation and testing error refers to the wells, which are used for training the models. When well 3 is left out for training and used for testing, the CCR indicate low classification performance, even though the validation error of the model is rather low. A higher testing and validation error can be identified, when well 3 is included in training (Left out well 1 and 2).

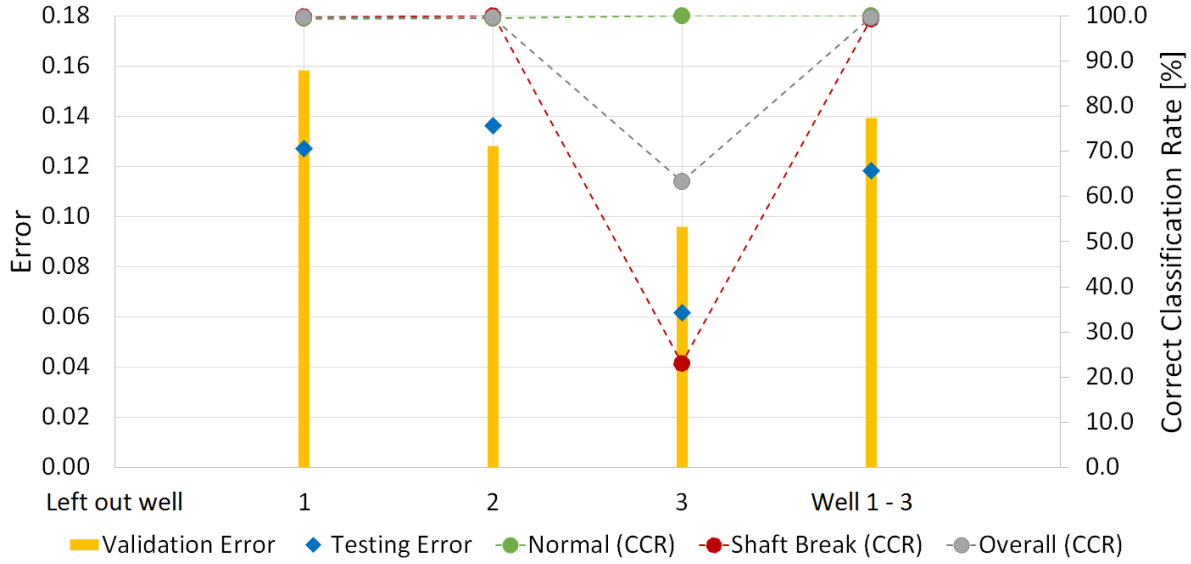


Figure 63 - Comparison of models built by the leave-one-out arrangement

The high miss-classification of the model built when well 3 is left out, as well as the increased validation and testing error of the three other models in Figure 63 occur due to wrong labelling of the data during data preparation. A pump-damaging event, which took place prior the actual shaft break was miss-interpreted. Since the model (Left out well 3) was trained with proper labeled data of well 1 and 2, the result is distorted.

Figure 64 shows the well data including interpolated values as well as the modeled probability curve for shaft break. The red line in the lower plot indicates the time range of shaft break labeled data. Further investigation regarding pump failure analysis showed, that the first pressure change on 30 October occurred most likely due to a hole in the pump's stage. Hence the result given by the probability curve is classifying the shaft break correctly. The wrong labeled data which is used for calculating correct classification rates explains the low performance illustrated in Figure 63 (Left out well 3).

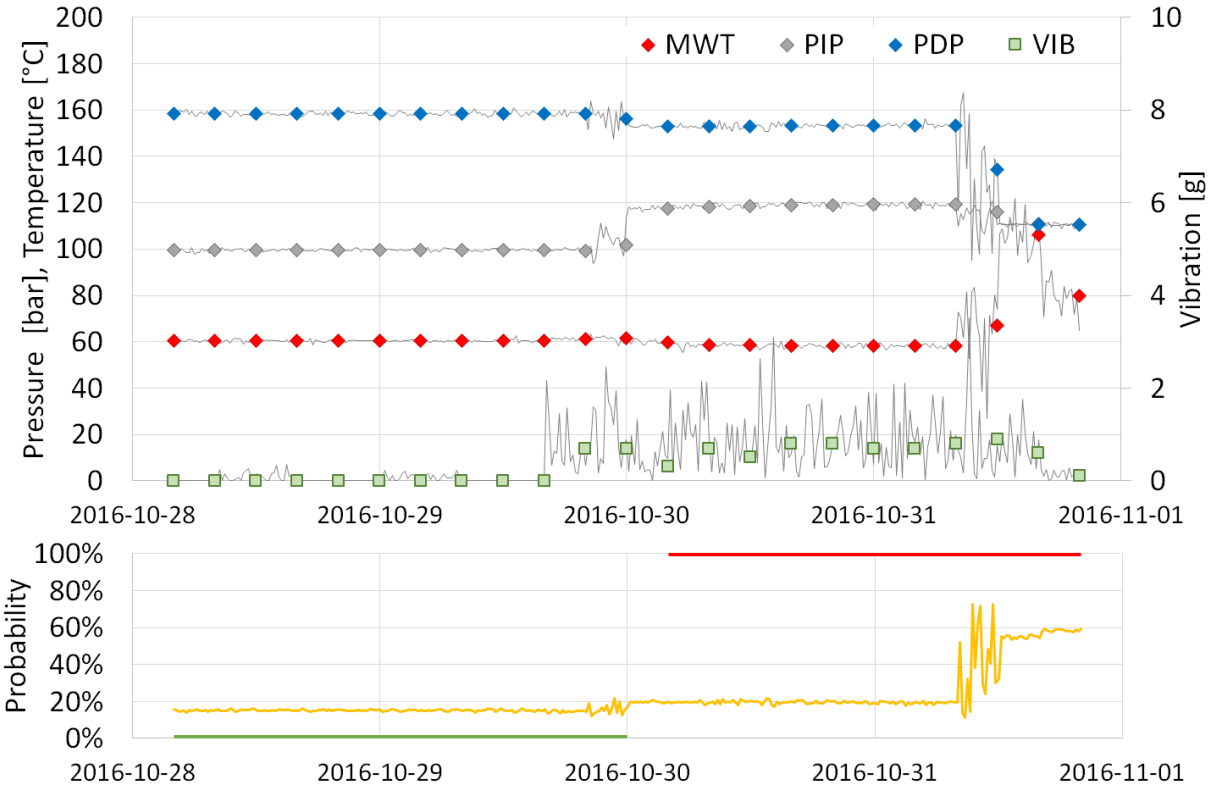


Figure 64 - Data and probability curves of the model "Left out well 3" (Task 5)

| | | |
|---|---|---|
| Where | MWT | Motor winding temperature |
| | PIP | Pump intake pressure |
| | PDP | Pump discharge pressure |
| | VIB | Vibration |

The results of training a model with only one well while testing it with two others is illustrated in Figure 65. The validation and testing error are referring to the training data, which was applied also for testing during the training. The correct classification rates are showing the result of the testing using the two left out wells. Again, the wrong labeled data of well 3 distorts the results. Especially when well 3 is used for training, the created classifier is not capable of interpreting shaft break when testing with well 1 and 2. When well 3 is included in testing, the result is negatively influenced although the models interpret the actual shaft break correctly according to probability curves. The probability curves are showing the same characteristics as the one depicted in Figure 64.

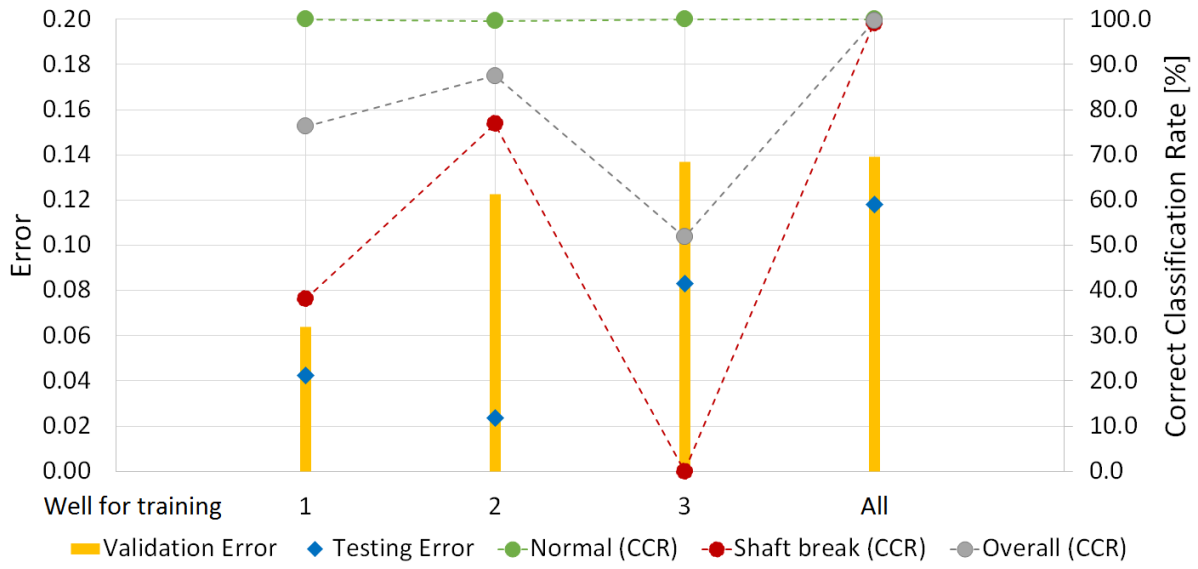


Figure 65 - Comparison of models built by the leave-two-out arrangement

More information regarding the models of the different well data sets can be found in the appendix.

## 6.6 Production Rate Modeling

In order to model gross production during measurement gaps, downhole and surface data were combined for model building. Therefore, measured production rates were assumed to be constant during the measurement interval of 12 hours. This assumption can be justified by a 12-hour pre-flush period of the separator and agreement of experienced field personnel.

Due to increased counter pressure during the measurement, the time when the well is connected to the separator can easily be identified. Tubing, Casing, pump intake and pump discharge pressure are showing a step in the measurement profile when the measurement starts and stops. By implementing a proper searching algorithm, gross production measurement can be allocated correctly time-wise. This procedure is necessary because of the inaccurate time stamp (only date) of separator data.

The separator measurement is causing a pressure increase upstream the metering station. Since the pumps are working dynamically, this change in pressure reduces production. This effect is also known as observer effect and occurs everywhere where the measurement influences the result of the measurement itself. Therefore, different data allocation methods were used to overcome and minimize this distorting effect:

- Production measurement is allocated exactly
- Production measurement is allocated partially outside of the true measurement period
- Production measurement is allocated fully outside of the true measurement period

### 6.6.1 Feature Selection

A sequential forward selection was performed to find the most important data channels for production rate modeling. Figure 66 illustrates the result of this statistical investigation and shows that only the four channels motor winding temperature, frequency, pump discharge pressure and pump intake pressure are necessary to find an appropriate model, since more channels are not improving the performance.

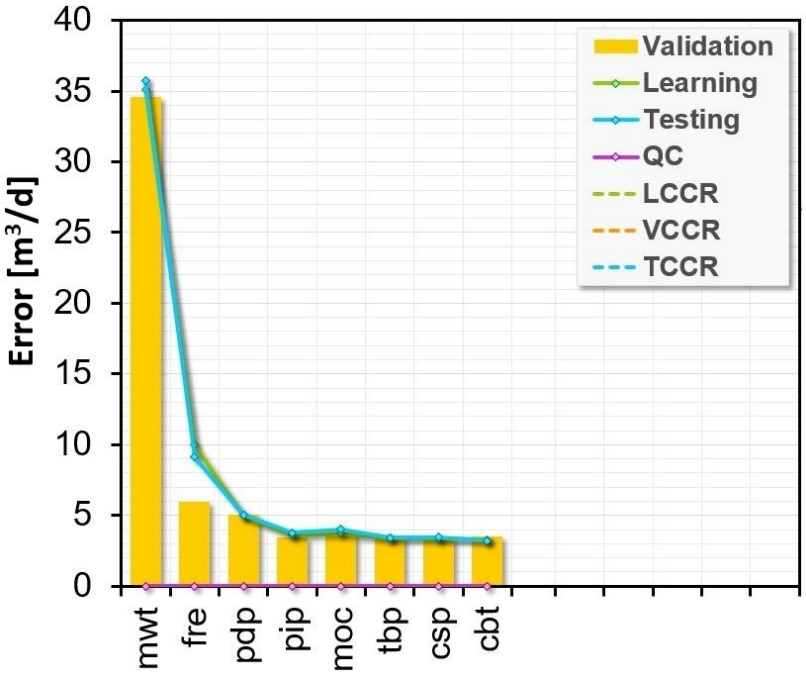


Figure 66 - Sequential forward selection for production rate modeling

| | | |
|---|---|---|
| Where | mwt | Motor winding temperature |
| | fre | Frequency |
| | pdp | Pump discharge pressure |
| | pip | Pump intake pressure |
| | moc | Motor current |
| | tbp | Tubing pressure |
| | csp | Casing pressure |
| | cbt | Bottom hole temperature |

### 6.6.2 Results

The first approach was carried out by aligning the separator measurement data exactly with the pressure increases observed in the pressure trends of pump intake and discharge pressure. The four features, which were selected by SFS as well as the measured gross production rate were applied for training. The results of the best model were presented in Figure 67. The completely connected FF neural network which was found to perform best with nine hidden neurons. This network size was applied for all three approaches.

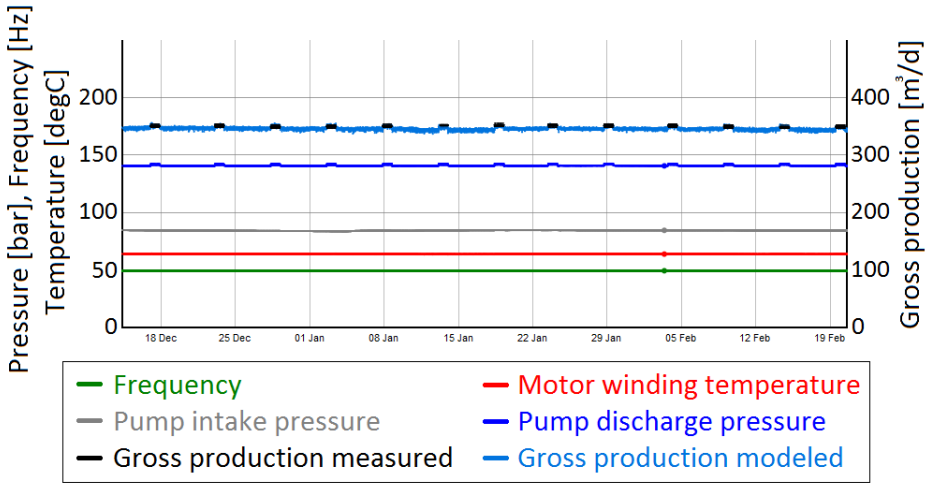


Figure 67 - Production rate modelling with exact separator data allocation

The measured gross production is always located at modeled production peaks, while outside of the measurement the production rate is decreased. This case highlights the difficulties coming from the observer effect and shows that this data arrangement is not resulting in a proper solution.

Figure 68 illustrates the result obtained by using a partial data shift between measured gross production data and downhole data. The separator data is shifted partially outside of the actual measurement period to enhance the performance and decrease the impact of the observer effect. Nevertheless, the solution results in a possibly overestimating model, since the modeled production rate is higher than the measured one. To evaluate this result in detail, a second measurement method, which is not influencing the production system would have to be implemented. This could proof that the higher production is reasonable due to reduced counter pressure in the flow line in case of a measurement gap.

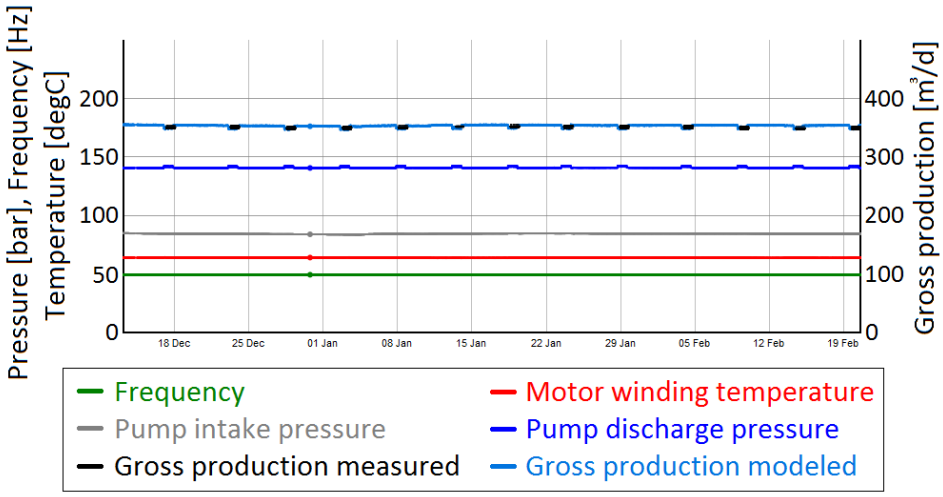


Figure 68 - Production rate modelling with partial separator data shift

In the last presented approach, the measured gross production is fully allocated outside of the actual measurement period. As it can be seen in Figure 69, the separator data is shifted backwards in time. The result is showing an accurate fit of measured and modeled gross production, especially in the right half of Figure 69. Although, a underestimated modeled production rate is obtained around the 1st of January.

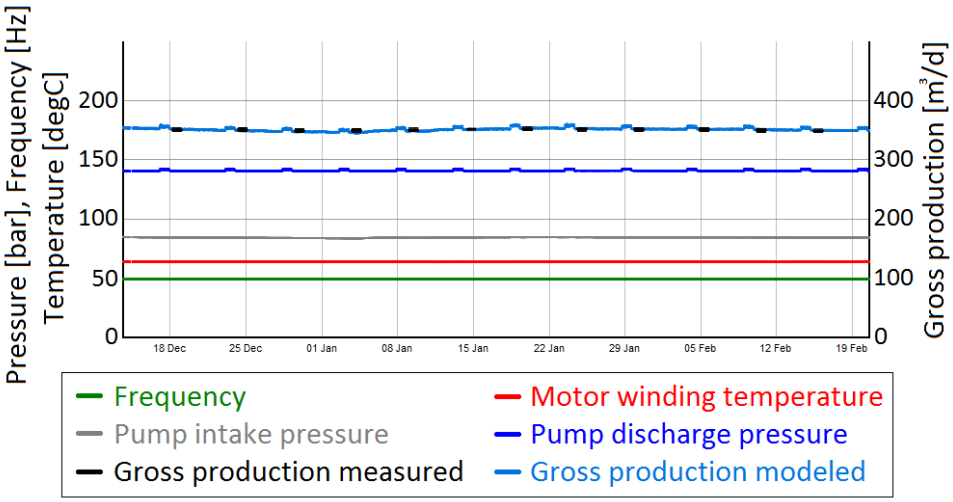


Figure 69 - Production rate modelling with total separator data shift

The approach of partial data shifting seems to be the most reasonable one regarding the elimination of the observer effect. The validation and testing errors of the models are in the range of 3 – 6 $m^3$/d and can be decreased further by individual well training. Since production rates of ESPs are typically higher than 200 $m^3$/d, this error is small and thus neglect able. To improve production rate modelling, improved measurement methods capable of measuring multiphase flow while not influencing the production system have to be implemented. This measure would eliminate the observer effect completely, but would add higher complexity in terms of maintenance and results in higher cost.

# 7 Conclusion

The thesis showed that models built with artificial neural networks are capable of classifying pump failure with a high accuracy. Generated artificial data and real life data sets were successfully applied for training and testing.

Pump wear and shaft break can be identified automatically after a model is trained and evaluated properly. Especially for single well training arrangements, the correct classification rates exceeded 95% in all cases. Models built by using the leave-one-out approach with different well data sets are resulting in a wider performance range. These differences occur because the wells are not identically completed and the pumps are not located in the same depth inside the wellbore.

Results of various training arrangements showed that quality control of created classification models is from high importance. Evaluation of proper data labelling, model network size, test set size in comparison to the training set size and data statistics of individual well data sets is crucial to exclude problems resulting in low correct classification rates from the very beginning.

The modeling of production rates during measurement gaps is resulting in an accurate prediction. The integration of separator data was successfully carried out under the assumption of constant production during the measurement. Data cleansing was implemented to ensure consistent and correct data sets for proper model building. Sequential forward selection was successfully used to reduce the dimensionality of the input data by identification of relevant features.

The impact of the observer effect caused by the separator was reduced by applying different separator data allocations concerning actual measurement periods. These time-shift approaches resulted in accurate production rates. Although further evaluation of the modeled gross production is necessary to confirm that, the result is correctly in terms of error quantification.

For future research, data including more failure events than presented in this thesis might significantly increase the outcome of the presented approaches. In case of combined training approaches, clustering of wells by using well data statistics might allow model building of group specific classifiers. However, the introduction of well independent features might increase the model performance when trained with different well data sets.

Gross production rate modeling can be further investigated by implementing additional measurement methods, which are not influencing the production system. This possibly allows more accurate modeling of true production rates during measurement gaps.

# 8 References

[1] I. Giden, B. Kometer, P. Buerssner and L. Lobianco, "Re-development of an onshore mature oil field to double gross production by the use of sensor-equipped electrical submersible pumps," SPE, Paris, France, 2017.

[2] G. Kienberger and R. Fuchs, "Case history of the Matzen field - Matzen sand (16th TH): A story of success; Where is the end?," SPE, Vienna, Austria, 2006.

[3] T. G. Farr, P. A. Rpsem, E. Caro, R. Crippen, R. Duren, S. Hensley, M. Kobrick, M. Paller, E. Rodriguez, L. Roth, D. Seal, S. Shaffer, J. Shimada, J. Umland, M. Werner, M. Oskin, D. Burbank and D. Alsdorf, "The shuttle radar topography mission," *Reviews of Geophysics,* vol. 45, no. 2, pp. 1-33, 2007.

[4] A. Kröll, I. Gnojek, H. Heinz, R. Jiricek, B. Meurers, W. Seiberl, P. Steinhauser, G. Wessely and D. Zych, "Wiener Becken und angrenzende Gebiete (mit Erläut., 1-22)," Geologische Bundesanstalt, Vienna, 1993.

[5] I. Giden, B. Kometer, P. Toth, H. Geier, T. Florian and M. Sieberer, "Technology driven rejuvenation of a mature field by doubling the gross production rate," SPE, Dubai, 2016.

[6] F. Reinweber, "Master thesis: ESPs in OMV Austria E&P - Performance analysis and benchmarking," 2015.

[7] S. Gupta, L. Saputelli and M. Nikolaou, "Big data analytics workflow to safeguard ESP operations in real time," Society of Petroleum Engineers, The Woodlands, Texas, 2016.

[8] M. El Gindy, H. Abdelmotaal, K. Botros, I. Ginawi, E. Sayed and T. Edris, "Monitoring & surveillance improve ESP operation and reduce workover frequency," Society of Petroleum Engineers, Abu Dhabi, 2015.

[9] G. Han, M. Chen, H. Zhang and K. Ling, "Real-time monitoring and diagnosis of electrical submersible pump," Society of Petroleum Engineers, Houston, Texas, 2015.

[10] G. Takacs, Electrical submersible pumps manual - Design, operations and maintenance, Burlington, USA: Gulf Professional Publishing, 2009.

[11] L. W. Lake, Petroleum Engineering Handbook Volume 4, Austin, Texas: Society of Petroleum Engineers, 2007.

[12] A. P. Institute, "Recommended practice for sizing and selection of electric submersible pump installations," API Publishing Services, Washington, D.C., 2002.

[13] "Demistifying Artificial Neural Networks," 22 September 2014. [Online]. Available: https://dmm613.wordpress.com/2014/09/22/artificial-neural-networks-part-1/. [Accessed 28 June 2017].

[14] S. Haykin, Neural networks and learning machines, Pearson, 2009.

[15] I. Giden, B. Kometer and M. Eschberger, "Deployment of sensor equipped ESPs in a mature oilfield - A case study," Celle, Germany, 2016.

[16] P. P. S. Ltd, "Phoenix troubleshooting aid," Phoenix Petroleum Services Ltd, 1998.

[17] L. Eriksson, T. Byrne, E. Johansson, J. Trygg and C. Vikström, "Multi- and megavariate data analysis basic principles and applications," Umetrics Academy, 2013.

[18] J. A. Westerhuis, S. P. Gurden and A. K. Smilde, "Generalized contribution plots in multivariate statistical process monitoring," Chemometrics and Intelligent Laboratory Systems, 2000.

# Appendices

## Appendix A

Table 15 - Training and testing results of task 1 - Training arrangement “single” and “all”

| Well Nr. | Normal operation CCR [%] | Pump wear CCR [%] | Overall CCR [%] | Validation Error | Testing Error | Best Network Size |
|---|---|---|---|---|---|---|
| 1 | 99.6 | 99.8 | 99.7 | 0.0298 | 0.0475 | 15 |
| 2 | 100.0 | 99.2 | 99.7 | 0.0598 | 0.0637 | 6 |
| 3 | 98.3 | 97.1 | 97.6 | 0.1185 | 0.1416 | 12 |
| 4 | 100.0 | 99.9 | 100.0 | 0.0102 | 0.0267 | 9 |
| 5 | 99.0 | 98.4 | 98.7 | 0.1120 | 0.1065 | 5 |
| 6 | 100.0 | 100.0 | 100.0 | 0.0031 | 0.0059 | 14 |
| 7 | 100.0 | 99.3 | 99.7 | 0.0481 | 0.0619 | 13 |
| 8 | 100.0 | 99.9 | 100.0 | 0.0217 | 0.0188 | 14 |
| 9 | 99.9 | 99.9 | 99.9 | 0.0396 | 0.0365 | 5 |
| All | 98.4 | 99.1 | 98.7 | 0.1047 | 0.1013 | 13 |

Table 16 - Training and testing results of task 1 - Training arrangement “leave-one-out” and “all”

| Well Nr. | Normal operation CCR [%] | Pump wear CCR [%] | Overall CCR [%] | Validation Error | Best Network Size |
|---|---|---|---|---|---|
| LOO 1 | 0.0 | 100.0 | 59.2 | 0.1169 | 13 |
| LOO 2 | 89.8 | 100.0 | 94.3 | 0.1102 | 15 |
| LOO 3 | 0.0 | 100.0 | 62.2 | 0.2259 | 7 |
| LOO 4 | 100.0 | 53.5 | 69.9 | 0.1392 | 9 |
| LOO 5 | 100.0 | 0.0 | 39.7 | 0.1095 | 11 |
| LOO 6 | 97.9 | 99.9 | 98.9 | 0.1251 | 15 |
| LOO 7 | 81.9 | 100.0 | 91.2 | 0.0939 | 15 |
| LOO 8 | 98.4 | 99.6 | 99.1 | 0.1214 | 11 |
| LOO 9 | 89.7 | 99.6 | 94.6 | 0.0803 | 12 |
| All | 98.4 | 99.1 | 98.7 | 0.1047 | 13 |

Table 17 - Training and testing results of task 2 - Training arrangement “single” and “all”

| Well Nr. | Normal operation CCR [%] | Shaft Break CCR [%] | Overall CCR [%] | Validation Error | Testing Error | Best Network Size |
|---|---|---|---|---|---|---|
| 1 | 100.0 | 100.0 | 100.0 | 0.0030 | 0.0042 | 7 |
| 2 | 100.0 | 100.0 | 100.0 | 0.0044 | 0.0042 | 0 |
| 3 | 100.0 | 100.0 | 100.0 | 0.0040 | 0.0043 | 15 |
| 4 | 100.0 | 100.0 | 100.0 | 0.0039 | 0.0035 | 5 |
| 5 | 100.0 | 100.0 | 100.0 | 0.0063 | 0.0086 | 6 |
| 6 | 100.0 | 100.0 | 100.0 | 0.0064 | 0.0073 | 0 |
| 7 | 100.0 | 100.0 | 100.0 | 0.0035 | 0.0023 | 9 |
| 8 | 100.0 | 100.0 | 100.0 | 0.0079 | 0.0655 | 3 |
| 9 | 100.0 | 100.0 | 100.0 | 0.0033 | 0.1808 | 11 |
| All | 100.0 | 100.0 | 100.0 | 0.0015 | 0.0016 | 2 |

Table 18 - Training and testing results of task 2 - Training arrangement “leave-one-out” and “all”

| Well Nr. | Normal operation CCR [%] | Shaft Break CCR [%] | Overall CCR [%] | Validation Error | Testing Error | Best Network Size |
|---|---|---|---|---|---|---|
| LOO 1 | 0.0 | 100.0 | 14.2 | 0.0014 | 0.8831 | 3 |
| LOO 2 | 100.0 | 100.0 | 100.0 | 0.0010 | 0.0017 | 3 |
| LOO 3 | 100.0 | 100.0 | 100.0 | 0.0006 | 0.0059 | 2 |
| LOO 4 | 100.0 | 73.9.0 | 96.6 | 0.0018 | 0.1257 | 3 |
| LOO 5 | 100.0 | 100.0 | 100.0 | 0.0006 | 0.0023 | 2 |
| LOO 6 | 100.0 | 100.0 | 100.0 | 0.0015 | 0.0078 | 1 |
| LOO 7 | 100.0 | 100.0 | 100.0 | 0.0009 | 0.0013 | 2 |
| LOO 8 | 100.0 | 69.0 | 91.4 | 0.0014 | 0.2862 | 3 |
| LOO 9 | 0.0 | 100.0 | 19.2 | 0.0007 | 0.8990 | 3 |
| All | 100.0 | 100.0 | 100.0 | 0.0015 | 0.0016 | 2 |

Table 19 - Training and testing results of task 4 - Training arrangement “single” and “all”

| Well Nr. | Normal operation CCR [%] | Pump wear CCR [%] | Overall CCR [%] | Validation Error | Testing Error | Best Network Size |
|---|---|---|---|---|---|---|
| 1 | 99.6 | 99.8 | 99.7 | 0.0298 | 0.0475 | 15 |
| 2 | 100.0 | 99.2 | 99.7 | 0.0598 | 0.0637 | 6 |
| 3 | 98.3 | 97.1 | 97.6 | 0.1185 | 0.1416 | 12 |
| 4 | 100.0 | 99.9 | 100.0 | 0.0102 | 0.0267 | 9 |
| 5 (RD) | 100.0 | 100.0 | 100.0 | 0.0223 | 0.0667 | 2 |
| 6 | 100.0 | 100.0 | 100.0 | 0.0031 | 0.0059 | 14 |
| 7 | 100.0 | 99.3 | 99.7 | 0.0481 | 0.0619 | 13 |
| 8 | 100.0 | 99.9 | 100.0 | 0.0217 | 0.0188 | 14 |
| 9 | 99.9 | 99.9 | 99.9 | 0.0396 | 0.0365 | 5 |
| All | 98.2 | 92.3 | 95.3 | 0.1973 | 0.1939 | 6 |

Table 20 - Training and testing results of task 4 - Training arrangement “leave-one-out” and “all”

| Well Nr. | Normal operation CCR [%] | Pump wear CCR [%] | Overall CCR [%] | Validation Error | Best Network Size |
|---|---|---|---|---|---|
| LOO 1 | 100.0 | 65.1 | 79.4 | 0.1713 | 7 |
| LOO 2 | 1.8 | 99.9 | 45.2 | 0.2119 | 4 |
| LOO 3 | 0.0 | 100.0 | 62.2 | 0.1623 | 5 |
| LOO 4 | 100.0 | 39.3 | 60.7 | 0.1630 | 8 |
| LOO 5 (RD) | 100.0 | 0.0 | 64.4 | 0.2349 | 5 |
| LOO 6 | 0.0 | 100.0 | 50.9 | 0.2287 | 5 |
| LOO 7 | 0.0 | 100.0 | 51.6 | 0.2077 | 5 |
| LOO 8 | 100.0 | 52.3 | 72.7 | 0.2176 | 5 |
| LOO 9 | 0.1 | 99.9 | 49.7 | 0.2116 | 5 |
| All | 98.2 | 92.3 | 95.3 | 0.1973 | 6 |

Table 21 - Training and testing results of task 5 - analysis on cross validation, multi-linear regression models, training arrangement “all”

| CV | Normal operation CCR [%] | Shaft Break CCR [%] | Overall CCR [%] | Validation Error | Testing Error |
|---|---|---|---|---|---|
| 1 | 100.0 | 99.2 | 99.6 | 0.1392 | 0.1183 |
| 2 | 100.0 | 99.2 | 99.6 | 0.1445 | 0.1072 |
| 3 | 97.7 | 99.2 | 98.4 | 0.1205 | 0.1302 |
| 4 | 100.0 | 100.0 | 100.0 | 0.1141 | 0.1113 |
| 5 | 98.5 | 98.3 | 98.4 | 0.1583 | 0.1369 |

Table 22 - Training and testing results of task 5 - multi-linear regression models, training arrangement “single” and “all”

| Well Nr. | Normal operation CCR [%] | Shaft Break CCR [%] | Overall CCR [%] | Validation Error | Testing Error |
|---|---|---|---|---|---|
| 1 | 100.0 | 100.0 | 100.0 | 0.0639 | 0.0424 |
| 2 | 100.0 | 100.0 | 100.0 | 0.1226 | 0.0235 |
| 3 | 100.0 | 100.0 | 100.0 | 0.1370 | 0.0832 |
| All | 100.0 | 99.2 | 99.6 | 0.1392 | 0.1183 |

Table 23 - Training and testing results of task 5 - multi-linear regression models, training arrangement “leave-one-out” and “all”

| Well Nr. | Normal operation CCR [%] | Shaft Break CCR [%] | Overall CCR [%] | Validation Error | Testing Error |
|---|---|---|---|---|---|
| LOO 1 | 99.3 | 99.7 | 99.6 | 0.1583 | 0.1270 |
| LOO 2 | 99.4 | 100.0 | 99.5 | 0.1279 | 0.1362 |
| LOO 3 | 100.0 | 23.0 | 63.3 | 0.0958 | 0.0618 |
| All | 100.0 | 99.2 | 99.6 | 0.1392 | 0.1183 |

Table 24 - Training and testing results of task 5 - multi-linear regression models, training arrangement “leave-two-out” and “all”

| Well Nr. | Normal operation CCR [%] | Shaft Break CCR [%] | Overall CCR [%] | Validation Error | Testing Error |
|---|---|---|---|---|---|
| LTO 1 | 100.0 | 38.1 | 76.3 | 0.0639 | 0.0424 |
| LTO 2 | 99.6 | 76.9 | 87.5 | 0.1226 | 0.0235 |
| LTO 3 | 100.0 | 0.0 | 51.8 | 0.1370 | 0.0832 |
| All | 100.0 | 99.2 | 99.6 | 0.1392 | 0.1183 |

(LTO X means well X was used for training)

# Appendix B

## Code (Programming language R) for data import and data cleansing

```
library(xts)
library(zoo)
library(padr)
library(lubridate)
library(tidyr)
library(readxl)
library(xlsx)

### Choose Wells (Welllist)

# single: Welllist <- c("[redacted]")
# working:
Welllist <-
c("[redacted]")
# not working: Welllist <- c("[redacted]")
# all: Welllist <-
c("[redacted]")

### Change Settings

Interval  <- "Current" # No Change possible here - use different
Source File
Timeframe <- "Adapted" # No change possible here - use older Version
to access 8/12/16h Timeframes
POffset   <- 0.7       # Comparison Value for Production Data
Association
setPFRE   <- T         # T or F to enable/disable: FRE = 0 & MOC < 3
-> BRU = 0
setPDIP   <- T         # T or F to enable/disable: DIP < 2 -> BRU =
0
Excel     <- F         # write to Excel
writeNA   <- T         # write NA values

### Initialization
```

```
VTS1   <- logical(length=500000)
VTS2   <- c(1:500000)
for (vts in 2:500000) {VTS2[vts] <- VTS2[vts-1]+10}
for (vts in VTS2) {VTS1[vts]<-T
                   if (vts > 500000){break}}

MLSets <- matrix(0, nrow = length(Welllist), ncol = 6)
colnames(MLSets) <- c("Well","all","no CSP/TBP","Top
5","PIP,PDP,FRE,MOC","PIP,PDP,FRE")
# Cols <- as.character(c(1:length(Welllist)))

CTime <- gsub(":","_",substring(as.character(Sys.time()),0,16))
DirectoryName <- paste("C:/Users/student/Dropbox/Montanuni/MT
MUL/R/Output/Current/",CTime)
dir.create(DirectoryName)
dir.create(paste(DirectoryName,"/Statistics",sep = ""))
if (writeNA) {writeNA1 <- "NA"} else {writeNA1 <- ""}

### Start of the Well Loop

for (z in 1:length(Welllist)) {

Sonde <- Welllist[z]

#### Load & extract Data

DALINK1 <- ".xlsx"
DALINK2 <- "C:/Users/student/Dropbox/Montanuni/MT MUL/R/Daten zum
Plotten/Mit Header/"
DAlink <- paste(DALINK2,Sonde,"/",Sonde,"_",Interval,DALINK1,sep =
"")
DA <- read_excel(DAlink)
AD <- read_excel("C:/Users/student/Dropbox/Montanuni/MT
MUL/Daten/Datum der Ausfälle und Restarts.xlsx")
PDAlink <- paste("C:/Users/student/Dropbox/Montanuni/MT
MUL/Daten/GDB/",Sonde,DALINK1, sep = "")
ProdDA <- read_excel(PDAlink)
TimeProd <- ProdDA[,6]
SOBGrund <- ProdDA[,19]
DataProd <- ProdDA[,21:28]
Production <- cbind(TimeProd,DataProd)
Production <- drop_na(Production)
Statistics <- matrix (0,nrow = 9,ncol = 14)
```

```
row.names(Statistics) <- c("Average","Min","Max","Values","Outlier <
Min","Outlier > Max","NA","Std.Dev","Variance")
colnames(Statistics) <-
c("CBT","MWT","FCL","ZCL","CSP","TBP","PIP","PDP","DCA","DCP","MOC",
"MOP","FRE","VIB")
ReadLinkFD <- paste("C:/Users/student/Dropbox/Montanuni/MT
MUL/R/Settings/Failure Dates/",Sonde,".xlsx",sep = "")
FDExists = F
Proceed  = F

### In case no Data is available, a TS is added to allow proper
running of the code, NULL values are filtered later again

for (ts in c(1,3,5,7,9,11,13,15,17,19,21,23,25,27,29)){
  if (!is.na(DA[1,ts])) {
    MissingTS <- DA[1,ts]
    break
  }
}
for (ts in c(1,3,5,7,9,11,13,15,17,19,21,23,25,27,29)){
  if (is.na(DA[1,ts])) {
    DA[1,ts]  <- MissingTS
    DA[1,(ts+1)] <- -999
  }
}

### CHOOSING COLUMNS ACCORDING TO THE INTERVAL TYPE

if (Interval == "Current") {
  dCBT<-DA[,1:2]
  dFCL<-DA[,3:4]
  dZCL<-DA[,5:6]
  dDIP<-DA[,7:8]
  dDCA<-DA[,9:10]
  dDCP<-DA[,11:12]
  dVIB<-DA[,13:14]
  dMWT<-DA[,15:16]
  dPDP<-DA[,17:18]
  dPIP<-DA[,19:20]
  dCSP<-DA[,21:22]
  dMOC<-DA[,23:24]
  dMOP<-DA[,25:26]
  dTBP<-DA[,27:28]
  dFRE<-DA[,29:30]
```

```
} else {
  dCBT<-DA[,1:5]
  dFCL<-DA[,6:10]
  dZCL<-DA[,11:15]
  dDIP<-DA[,16:20]
  dDCA<-DA[,21:25]
  dDCP<-DA[,26:30]
  dVIB<-DA[,31:35]
  dMWT<-DA[,36:40]
  dPDP<-DA[,41:45]
  dPIP<-DA[,46:50]
  dCSP<-DA[,51:55]
  dMOC<-DA[,56:60]
  dMOP<-DA[,61:65]
  dTBP<-DA[,66:70]
  dFRE<-DA[,71:75]
  }

### REMOVE ALL ROWS WITH NA VALUES

CBT<-drop_na(dCBT)
FCL<-drop_na(dFCL)
ZCL<-drop_na(dZCL)
DIP<-drop_na(dDIP)
DCA<-drop_na(dDCA)
DCP<-drop_na(dDCP)
VIB<-drop_na(dVIB)
MWT<-drop_na(dMWT)
PDP<-drop_na(dPDP)
PIP<-drop_na(dPIP)
CSP<-drop_na(dCSP)
MOC<-drop_na(dMOC)
MOP<-drop_na(dMOP)
TBP<-drop_na(dTBP)
FRE<-drop_na(dFRE)

rm(dCBT,dFCL,dZCL,dDIP,dDCA,dDCP,dVIB,dMWT,dPDP,dPIP,dCSP,dMOC,dMOP,
dTBP,dFRE)

### DEFINE FORMAT FOR TIME AND DATE

CBT$TS_CBT <-as.POSIXct(CBT$TS_CBT,format="%m/%d/%Y
%H:%M:%S",tz="GMT")
```

```
FCL$TS_FCL <-as.POSIXct(FCL$TS_FCL,format="%m/%d/%Y
%H:%M:%S",tz="GMT")
ZCL$TS_ZCL <-as.POSIXct(ZCL$TS_ZCL,format="%m/%d/%Y
%H:%M:%S",tz="GMT")
DIP$TS_DIP <-as.POSIXct(DIP$TS_DIP,format="%m/%d/%Y
%H:%M:%S",tz="GMT")
DCA$TS_DCA <-as.POSIXct(DCA$TS_DCA,format="%m/%d/%Y
%H:%M:%S",tz="GMT")
DCP$TS_TCP <-as.POSIXct(DCP$TS_TCP,format="%m/%d/%Y
%H:%M:%S",tz="GMT")
VIB$TS_VIB <-as.POSIXct(VIB$TS_VIB,format="%m/%d/%Y
%H:%M:%S",tz="GMT")
MWT$TS_MWT <-as.POSIXct(MWT$TS_MWT,format="%m/%d/%Y
%H:%M:%S",tz="GMT")
PDP$TS_PDP <-as.POSIXct(PDP$TS_PDP,format="%m/%d/%Y
%H:%M:%S",tz="GMT")
PIP$TS_PIP <-as.POSIXct(PIP$TS_PIP,format="%m/%d/%Y
%H:%M:%S",tz="GMT")
CSP$TS_CSP <-as.POSIXct(CSP$TS_CSP,format="%m/%d/%Y
%H:%M:%S",tz="GMT")
MOC$TS_MOC <-as.POSIXct(MOC$TS_MOC,format="%m/%d/%Y
%H:%M:%S",tz="GMT")
MOP$TS_MOP <-as.POSIXct(MOP$TS_MOP,format="%m/%d/%Y
%H:%M:%S",tz="GMT")
TBP$TS_TBP <-as.POSIXct(TBP$TS_TBP,format="%m/%d/%Y
%H:%M:%S",tz="GMT")
FRE$TS_FRE <-as.POSIXct(FRE$TS_FRE,format="%m/%d/%Y
%H:%M:%S",tz="GMT")


### GENERATE XTS

if (Interval == "Current"){
xtCBT<- xts(x=CBT$DA_CBT,order.by=CBT$TS_CBT)
xtFCL<- xts(x=FCL$DA_FCL,order.by=FCL$TS_FCL)
xtZCL<- xts(x=ZCL$DA_ZCL,order.by=ZCL$TS_ZCL)
xtDIP<- xts(x=DIP$DA_DIP,order.by=DIP$TS_DIP)
xtDCA<- xts(x=DCA$DA_DCA,order.by=DCA$TS_DCA)
xtDCP<- xts(x=DCP$DA_TCP,order.by=DCP$TS_TCP)
xtVIB<- xts(x=VIB$DA_VIB,order.by=VIB$TS_VIB)
xtMWT<- xts(x=MWT$DA_MWT,order.by=MWT$TS_MWT)
xtPDP<- xts(x=PDP$DA_PDP,order.by=PDP$TS_PDP)
xtPIP<- xts(x=PIP$DA_PIP,order.by=PIP$TS_PIP)
xtCSP<- xts(x=CSP$DA_CSP,order.by=CSP$TS_CSP)
```

```
xtMOC<- xts(x=MOC$DA_MOC,order.by=MOC$TS_MOC)
xtMOP<- xts(x=MOP$DA_MOP,order.by=MOP$TS_MOP)
xtTBP<- xts(x=TBP$DA_TBP,order.by=TBP$TS_TBP)
xtFRE<- xts(x=FRE$DA_FRE,order.by=FRE$TS_FRE)
} else {
xtCBT<- xts(x=CBT[2:5],order.by=CBT$TS_CBT)
xtFCL<- xts(x=FCL[2:5],order.by=FCL$TS_FCL)
xtZCL<- xts(x=ZCL[2:5],order.by=ZCL$TS_ZCL)
xtDIP<- xts(x=DIP[2:5],order.by=DIP$TS_DIP)
xtDCA<- xts(x=DCA[2:5],order.by=DCA$TS_DCA)
xtDCP<- xts(x=DCP[2:5],order.by=DCP$TS_TCP)
xtVIB<- xts(x=VIB[2:5],order.by=VIB$TS_VIB)
xtMWT<- xts(x=MWT[2:5],order.by=MWT$TS_MWT)
xtPDP<- xts(x=PDP[2:5],order.by=PDP$TS_PDP)
xtPIP<- xts(x=PIP[2:5],order.by=PIP$TS_PIP)
xtCSP<- xts(x=CSP[2:5],order.by=CSP$TS_CSP)
xtMOC<- xts(x=MOC[2:5],order.by=MOC$TS_MOC)
xtMOP<- xts(x=MOP[2:5],order.by=MOP$TS_MOP)
xtTBP<- xts(x=TBP[2:5],order.by=TBP$TS_TBP)
xtFRE<- xts(x=FRE[2:5],order.by=FRE$TS_FRE)
}
### ASSOCIATE XTS WITH NAMES

if (Interval == "Current"){
names(xtCBT)<-c("CBT")
names(xtFCL)<-c("FCL")
names(xtZCL)<-c("ZCL")
names(xtDIP)<-c("DIP")
names(xtDCA)<-c("DCA")
names(xtDCP)<-c("DCP")
names(xtVIB)<-c("VIB")
names(xtMWT)<-c("MWT")
names(xtPDP)<-c("PDP")
names(xtPIP)<-c("PIP")
names(xtCSP)<-c("CSP")
names(xtMOC)<-c("MOC")
names(xtMOP)<-c("MOP")
names(xtTBP)<-c("TBP")
names(xtFRE)<-c("FRE")
} else {
names(xtCBT)<-c("CBT","MaxCBT","MinCBT","StdCBT")
names(xtFCL)<-c("FCL","MaxFCL","MinFCL","StdFCL")
names(xtZCL)<-c("ZCL","MaxZCL","MinZCL","StdZCL")
names(xtDIP)<-c("DIP","MaxDIP","MinDIP","StdDIP")
```

```
names(xtDCA)<-c("DCA","MaxDCA","MinDCA","StdDCA")
names(xtDCP)<-c("DCP","MaxDCP","MinDCP","StdDCP")
names(xtVIB)<-c("VIB","MaxVIB","MinVIB","StdVIB")
names(xtMWT)<-c("MWT","MaxMWT","MinMWT","StdMWT")
names(xtPDP)<-c("PDP","MaxPDP","MinPDP","StdPDP")
names(xtPIP)<-c("PIP","MaxPIP","MinPIP","StdPIP")
names(xtCSP)<-c("CSP","MaxCSP","MinCSP","StdCSP")
names(xtMOC)<-c("MOC","MaxMOC","MinMOC","StdMOC")
names(xtMOP)<-c("MOP","MaxMOP","MinMOP","StdMOP")
names(xtTBP)<-c("TBP","MaxTBP","MinTBP","StdTBP")
names(xtFRE)<-c("FRE","MaxFRE","MinFRE","StdFRE")
}

### ALIGNING DATA TO ROUNDED INTERVALS

if (Interval == "Current"){
  xtCBTa <- align.time(xtCBT,600)
  xtFCLa <- align.time(xtFCL,600)
  xtZCLa <- align.time(xtZCL,600)
  xtDIPa <- align.time(xtDIP,600)
  xtDCAa <- align.time(xtDCA,600)
  xtDCPa <- align.time(xtDCP,600)
  xtVIBa <- align.time(xtVIB,600)
  xtMWTa <- align.time(xtMWT,600)
  xtPDPa <- align.time(xtPDP,600)
  xtPIPa <- align.time(xtPIP,600)
  xtCSPa <- align.time(xtCSP,600)
  xtMOCa <- align.time(xtMOC,600)
  xtMOPa <- align.time(xtMOP,600)
  xtTBPa <- align.time(xtTBP,600)
  xtFREa <- align.time(xtFRE,600)
}
if (Interval == "Periodic"){
  xtCBTa <- align.time(xtCBT,14400)
  xtFCLa <- align.time(xtFCL,14400)
  xtZCLa <- align.time(xtZCL,14400)
  xtDIPa <- align.time(xtDIP,14400)
  xtDCAa <- align.time(xtDCA,14400)
  xtDCPa <- align.time(xtDCP,14400)
  xtVIBa <- align.time(xtVIB,14400)
  xtMWTa <- align.time(xtMWT,14400)
  xtPDPa <- align.time(xtPDP,14400)
  xtPIPa <- align.time(xtPIP,14400)
  xtCSPa <- align.time(xtCSP,14400)
```

```
  xtMOCa <- align.time(xtMOC,14400)
  xtMOPa <- align.time(xtMOP,14400)
  xtTBPa <- align.time(xtTBP,14400)
  xtFREa <- align.time(xtFRE,14400)
}
if (Interval == "Daily"){
  xtCBTa <- align.time(xtCBT,86400)
  xtFCLa <- align.time(xtFCL,86400)
  xtZCLa <- align.time(xtZCL,86400)
  xtDIPa <- align.time(xtDIP,86400)
  xtDCAa <- align.time(xtDCA,86400)
  xtDCPa <- align.time(xtDCP,86400)
  xtVIBa <- align.time(xtVIB,86400)
  xtMWTa <- align.time(xtMWT,86400)
  xtPDPa <- align.time(xtPDP,86400)
  xtPIPa <- align.time(xtPIP,86400)
  xtCSPa <- align.time(xtCSP,86400)
  xtMOCa <- align.time(xtMOC,86400)
  xtMOPa <- align.time(xtMOP,86400)
  xtTBPa <- align.time(xtTBP,86400)
  xtFREa <- align.time(xtFRE,86400)
}

Temperatures <- cbind(xtCBTa,xtMWTa)
Leakages <- cbind(xtFCLa,xtZCLa)
SPressures <- cbind(xtCSPa,xtTBPa)
DPressures <- cbind(xtPIPa,xtPDPa)
Currents <- cbind(xtDCAa,xtDCPa)
Motor <- cbind(xtMOCa,xtMOPa)
FREVIB <-cbind(xtFREa,xtVIBa)

comb1 <- cbind(Temperatures,Leakages)
comb2 <- cbind(SPressures,DPressures)
comb3 <- cbind(Currents,Motor)
comb4 <- cbind(comb1,comb2)
comb5 <- cbind(comb3,FREVIB)
Allxts <- cbind(comb4,comb5)

#### Change Allxts storage mode

storage.mode(Allxts) <- "numeric"

### Production Data
```

```
Production <- xts(x=Production[,2:9],order.by=Production$DATUM)

FirstSensorData <- substring(as.character(index(Allxts[1])),0,10);
CutProduction <-
(which(substring(FirstSensorData,0,8)==substring(as.character(index(
Production)),0,8))[1]-5)
if (is.na(CutProduction)) {CutProduction <- 1}

Production <- Production [(CutProduction:dim(Production)[1]),]

prows <- c(1:dim(Production)[1]); prows[] <- NA

for(pi in 1:dim(Production)[1]) {prows[pi] <-
which(as.character(index(Production[pi])) ==
substring(as.character(index(Allxts)),0,10))[1]}

prows[which(prows < 101)] <- NA
prows[] <- prows[]-100
prows1  <- !is.na(prows)
prows   <- subset(prows,prows1)
prows1  <- subset(1:length(prows1),prows1)

AllxtsProd <- Allxts[,-c(9:500)]
names(AllxtsProd) <-
c("Brutto","Oil","WC","DensityBH","Density","GOR","Gas","Water")
AllxtsProd[,] <- NA

for (pi in 1:length(prows)) {

  if (prows[pi]-100 < 1) {paverage <- mean(Allxts[(1:500),8], na.rm
= T)} else {if (prows[pi]+400 > dim(Allxts)[1]) {paverage <-
mean(Allxts[((dim(Allxts)[1]-500):dim(Allxts)[1]),8], na.rm = T)}
else {paverage <- mean(Allxts[((prows[pi]-100):(prows[pi]+400)),8],
na.rm = T)}}

  if (is.nan(paverage)) {next}

  allow = F

  for(pii in (prows[pi]:(prows[pi]+300))) {

  if (is.na(Allxts[pii,8])) {next}
```

```
  if ((Allxts[pii,8] - paverage) > POffset) {AllxtsProd[pii,1:8] <-
Production[prows1[pi],1:8]; if (is.na(AllxtsProd[(pii-1),1])){if
(allow) {AllxtsProd[(pii-1),1:8] <- Production[prows1[pi],1:8]}};
allow = T}

  if (pii == dim(Allxts)[1]) {break}

}}

### Production in Case FRE = 0 & MOC < 3

if (setPFRE) {AllxtsProd[which(Allxts$FRE == 0 & Allxts$MOC < 3),1]
<- 0}

if (setPDIP) {AllxtsProd[which(abs(Allxts$PDP - Allxts$PIP) < 2),1]
<- 0}

### Filter Outliers and replace them

MinMaxValues <- matrix(0,nrow = 2,ncol = 14)
row.names(MinMaxValues) <- c("Min","Max")
colnames(MinMaxValues) <- colnames(Statistics)
NAValues <- c(0,0,0,0,0,0,0,0,0,0,0,0,0,0)
MinMax <- read_excel("C:/Users/student/Dropbox/Montanuni/MT
MUL/R/Daten zum Plotten/Mit Header/MinMax.xlsx")
MinMax <- as.matrix(MinMax)
storage.mode(MinMax) <- "numeric"

### Filter Outliers

for (f in 1:14) {
  for (u in 1: dim(Allxts)[1])   {
    if (is.na(Allxts[u,f])) {NAValues[f] <- NAValues[f] +1} else {
      check <- Allxts[u,f]
      if (check < MinMax[1,f]) {Allxts[u,f] <- NA
      MinMaxValues[1,f] <- (MinMaxValues[1,f]+1)}
      if (check > MinMax[2,f]) {Allxts[u,f] <- NA
      MinMaxValues[2,f] <- (MinMaxValues[2,f]+1)}
      Statistics[4,f] <- Statistics[4,f] +1
    }
  }}

### get Failure Dates and prepare for Classification
```

```
if (file.exists(ReadLinkFD)) {

FDExists = T

FD <- read_excel(ReadLinkFD, col_names = T)
FD$Date   <-as.POSIXct(FD$Date,format="%Y-%m-%d %H:%M:%S",tz= "GMT")

xtFD <- xts(x = FD$Failure,order.by = FD$Date)
if (Interval == "Current")  {xtFD <- align.time(xtFD,600)}
if (Interval == "Periodic") {xtFD <- align.time(xtFD,14400)}
names(xtFD) <- c("Failure")

if (index(Allxts[1]) < index(xtFD[1]) &
index(Allxts[dim(Allxts)[1]]) > index(xtFD[dim(xtFD)[1]])) {

Proceed = T

Failure <- as.character(xtFD$Failure)
Failure <- c("Normal",Failure)
FIntervals <- c(1:(length(Failure)+1))

for (fd in 2:(length(FIntervals)-1)) {FIntervals[fd] <-
which(index(xtFD[fd-1]) == index(Allxts))}
FIntervals[length(FIntervals)] <- dim(Allxts)[1]+1

}}

### add Columns for Classes

Classes   <- Allxts[,1:11]
colnames(Classes) <- c("Normal","Separator","Wear","Shaft
Break","Plugged Intake","Short Circuit","Low PI","Tbg
Leak","Mode","Measurement","Cut")
Classes[] <- 0
Classes[which(!is.na(AllxtsProd[,1])),2] <- 1

if (FDExists & Proceed) {

for(fd in 1:(length(FIntervals)-1)) {

  if (Failure[fd] == "Wear")
{Classes[(FIntervals[fd]:(FIntervals[(fd+1)]-1)),3]  <- 1}
  if (Failure[fd] == "Break")
{Classes[(FIntervals[fd]:(FIntervals[(fd+1)]-1)),4]  <- 1}
```

```
  if (Failure[fd] == "Plugged")
{Classes[(FIntervals[fd]:(FIntervals[(fd+1)]-1)),5]  <- 1}
  if (Failure[fd] ==
"SCircuit"){Classes[(FIntervals[fd]:(FIntervals[(fd+1)]-1)),6]  <-
1}
  if (Failure[fd] == "LowPI")
{Classes[(FIntervals[fd]:(FIntervals[(fd+1)]-1)),7]  <- 1}
  if (Failure[fd] == "Leak")
{Classes[(FIntervals[fd]:(FIntervals[(fd+1)]-1)),8]  <- 1}
  if (Failure[fd] == "Cut")
{Classes[(FIntervals[fd]:(FIntervals[(fd+1)]-1)),11] <- 1}
  if (Failure[fd] == "Normal")
{Classes[(FIntervals[fd]:(FIntervals[(fd+1)]-1)),1]  <- 1}

}} else {Classes[which(is.na(AllxtsProd[,1])),1]  <- 1}

### merge xts

Result <- cbind(Allxts,AllxtsProd,Classes)
ResultNA <- as.data.frame(Result)
ResultStats <- ResultNA

### add Measurement to ResultNA (Separator: On/Off)

ResultNA[which(!is.na(AllxtsProd[,1])),32] <- "On"
ResultNA[which(is.na(AllxtsProd[,1])),32]  <- "Off"

### Data Statistics

ResultStats = as.data.frame(ResultStats)
ResultStats1 <- ResultStats
ResultStats <- as.matrix(ResultStats)

# change to numeric for using function cor

storage.mode(ResultStats) <- "numeric"

# calculate Std Deviation

SDandVar <- matrix(nrow = 2,ncol = 14)
for(o in 1:14) {
  SDandVar[1,o] <- round(sd(Allxts[,o], na.rm = TRUE),3)
  SDandVar[2,o] <- round(var(Allxts[,o], na.rm = TRUE),3)
}
```

```
for (s in 1:dim(Statistics)[2]){
  Statistics[1,s] <- round(mean(ResultStats[,s], na.rm = TRUE),3)
  Statistics[2,s] <- min(ResultStats[,s], na.rm = TRUE)
  Statistics[3,s] <- max(ResultStats[,s], na.rm = TRUE)
  Statistics[5,s] <- MinMaxValues[1,s]
  Statistics[6,s] <- MinMaxValues[2,s]
  Statistics[7,s] <- NAValues[s]
  Statistics[8,s] <- SDandVar[1,s]
  Statistics[9,s] <- SDandVar[2,s]
}

### Machine Learning Sets

MLSets[z,1] <- Welllist[z]
MLSets[z,2] <- dim(drop_na(ResultStats1))[1]
MLSets[z,3] <- dim(drop_na(subset(ResultStats1, select =
c("CBT","MWT","PIP","PDP","FRE","MOC","MOP","FRE","VIB","Brutto"))))
[1]
MLSets[z,4] <- dim(drop_na(subset(ResultStats1, select =
c("MWT","PIP","PDP","FRE","MOC","Brutto"))))[1]
MLSets[z,5] <- dim(drop_na(subset(ResultStats1, select =
c("PIP","PDP","FRE","MOC","Brutto"))))[1]
MLSets[z,6] <- dim(drop_na(subset(ResultStats1, select =
c("PIP","PDP","FRE","Brutto"))))[1]

### Check if all time stamps are present

ResultNA <- cbind(rownames(ResultNA),ResultNA)
colnames(ResultNA)[1] <- "TS"
ResultNA <- subset(ResultNA,!duplicated(ResultNA$TS))
ResultNA$TS <- as.POSIXct(ResultNA$TS,format="%Y-%m-%d
%H:%M:%S",tz="GMT")
ResultNA <- pad(ResultNA)

VTS <- VTS1[(1:dim(ResultNA)[1])]
ResultNA <- subset(ResultNA,VTS)
rownames(ResultNA) <- NULL

### EXPORT TO CSV

write.csv(ResultNA, file = paste(DirectoryName,"/",Sonde,".csv", sep
= ""), row.names = F, na = writeNA1)
```

```
if (Excel) {write.xlsx(ResultNA, file =
paste(DirectoryName,"/",Sonde,".xlsx", sep = ""), row.names = F,
showNA = writeNA)}

write.csv(Statistics, file =
paste(DirectoryName,"/Statistics/",Sonde,"_Stats.csv", sep = ""))

} # end of the first for loop

### write final Files

write(c("Interval:",Interval,"Timeframe [h]:",Timeframe,"Production
Offset",POffset,"set FRE/BRU",setPFRE), file =
paste(DirectoryName,"/Settings.txt", sep = ""))
write.csv(MLSets,file =
paste(DirectoryName,"/Statistics/MLSets.csv", sep = ""))
```

### Code (Programming language R) for creating a Crossplot Matrix

```
library(car)
library(RColorBrewer)
library(tidyr)

### Read Data

data <- read.csv("C:/Users/student/Dropbox/Montanuni/MT
MUL/R/Output/Current/Adapted/[redacted].csv")
stats <- read.csv("C:/Users/student/Dropbox/Montanuni/MT
MUL/R/Output/Current/Adapted/Statistics/[redacted]_Stats.csv")

Data <- drop_na(data)

### Vector for choosing channels for cross-plotting

vector <- c(F, F, T, F, F, F, F, F, T, F, F, T, F, T, F, T, F, F, F,
F, F, F, F, F, F, F, F, F, F, F, F, F, F)

data <- Data[,vector]

### create Plot and safe as picture (format png)

png(file = paste("C:/Users/student/Dropbox/Montanuni/MT
MUL","Plot.jpg",sep = ""), width = 2000, height = 2000)

### create cross-plot matrix with histograms in diagonal windows
### factor could be used to color data according to data split
(RColorBrewer)

scatterplotMatrix(~MWT+PDP+MOC+FRE+Brutto, data = data, diagonal =
c("density"),reg.line = "", smoother = F, col=my_color,smoother.args
= list(col="grey"),cex = 1, cex.axis = 2, pch = c(15,16,17),
main="Scatter Plot", legend.plot = F)

dev.off()
```